# THE USE OF ELECTROPHYSIOLOGICAL TESTING PROCEDURES TO DETERMINE AUDITORY NERVE FIBRE DAMAGE

by

**Petra van Blerk**

Submitted in partial fulfilment of the requirements for the degree
Master of Engineering (Bioengineering)

in the

Department of Electrical, Electronic and Computer Engineering
Faculty of Engineering, Built Environment and Information Technology

UNIVERSITY OF PRETORIA

November 2022

# SUMMARY

---

## THE USE OF ELECTROPHYSIOLOGICAL TESTING PROCEDURES TO DETERMINE AUDITORY NERVE FIBRE DAMAGE

by

**Petra van Blerk**

| | |
|---|---|
| Supervisor: | Dr W. Badenhorst |
| Co-supervisor: | Prof T. Hanekom |
| Department: | Electrical, Electronic and Computer Engineering |
| University: | University of Pretoria |
| Degree: | Master of Engineering (Bioengineering) |
| Keywords: | Model-based diagnostics, auditory nerve damage, cochlear implant modelling, user-specific model, electrophysiological testing. |

Damage to a cochlear implant (CI) user's auditory nerve fibres (ANFs) is one of the factors that may contribute to poor performance with the implant, likely because neural propagation of the electrical signal from the cochlear implant to the brain is impaired. Various mechanisms have been identified in literature that can cause damage to the auditory nerve. These mechanisms include neural degeneration, demyelination and nerve fibre loss. There is no standardised testing procedure to identify the location or types of cochlear nerve damage in cochlear implant users. Research has been conducted to investigate if the results of electrophysiological measurements could be used to identity auditory nerve fibre damage.

The aim of this study is to develop a procedure to identify potential neural damage using electrophysiological measurements. Two different clinical electrophysiological tests were identified for use in this procedure, namely electrically evoked compound action potential (eCAPs) and electrically evoked auditory brainstem responses (eABRs). First, indicators of distinct neural damage mechanisms reported in the literature for both electrophysiological tests were consolidated. The neural model used in this study was then verified against the expected eCAP responses from literature.

A population of auditory neural fibres was integrated with a three-dimensional volume conduction model to allow investigation of eCAP responses to the application of different damage mechanisms. ECAP and eABR measures were recorded for a specific CI recipient. These electrophysiological data were used to determine a neural damage profile. The identified damage was applied to a user-specific model of the CI recipients cochlea and implant electrode, and the effects on the predicted eCAP responses were analysed. The procedure developed in this study to identify potential neural damage proved promising, suggesting that neural damage could be identified using electrophysiological measures.

# LIST OF ABBREVIATIONS

| | |
|---|---|
| 3D | Three-dimensional |
| ABI | Auditory brainstem implant |
| ABR | Auditory brainstem response |
| AGF | Amplitude growth function |
| AN | Auditory nerve |
| ANF | Auditory nerve fibre |
| AP | Action potential |
| ASSR | Auditory steady-state responses |
| CI | Cochlear implant |
| CL | Current level |
| CN | Cochlear nerve |
| CND | Cochlear nerve deficiency |
| CT | Computerised tomography |
| eABR | Electrically evoked auditory brain stem response |
| eCAP | Electrically evoked compound action potential |
| eCochG | Electrocochleography |
| FEM | Finite element method |
| HC | Hair cells |
| HH | Hodgkin-Huxley |
| HHL | Hidden hearing loss |
| IHC | Inner hair cells |
| IPG | Interphase gap |
| MBD | Model-based diagnostics |
| MRI | Magnetic resonance imaging |
| NIHL | Noise-induced hearing loss |
| NRT | Neural response telemetry |
| OAE | Otoacoustic emissions |
| OHC | Outer hair cells |
| PD | Pulse duration |
| PW | Pulse width |

| | |
|---|---|
| RE | Recording electrode |
| RRP | Relative refractory periods |
| SE | Stimulation electrode |
| SFAP | Single fibre action potential |
| SGC | Spiral ganglion cell |
| SGN | Spiral ganglion neurons |
| TP | Tripolar |
| VC | Volume conduction |

# TABLE OF CONTENTS

**CHAPTER 1 INTRODUCTION** . . . . . **1**

1.1 PROBLEM STATEMENT . . . . . 1

1.1.1 Context of the problem . . . . . 1

1.1.2 Research gap . . . . . 3

1.2 RESEARCH OBJECTIVE AND QUESTIONS . . . . . 5

1.3 APPROACH . . . . . 6

1.4 RESEARCH GOALS . . . . . 6

1.5 RESEARCH CONTRIBUTION . . . . . 7

1.6 RESEARCH OUTPUTS . . . . . 7

1.7 OVERVIEW OF STUDY . . . . . 7

**CHAPTER 2 LITERATURE STUDY** . . . . . **10**

2.1 CHAPTER OVERVIEW . . . . . 10

2.2 INTRODUCTION . . . . . 10

2.3 FACTORS WHICH INFLUENCE THE INCIDENCE OF AUDITORY NERVE DAMAGE . . . . . 12

2.4 ANF DAMAGE MECHANISMS . . . . . 13

2.4.1 ANF degeneration . . . . . 14

2.4.2 ANF demyelination . . . . . 14

2.4.3 ANF loss . . . . . 15

2.5 EXISTING APPROACHES TO DETERMINING ANF DAMAGE . . . . . 15

2.6 PRESENT ELECTROPHYSIOLOGICAL NEURAL TESTING PROCEDURES . . 17

2.6.1 ECAP testing procedures . . . . . 17

2.6.2 ECAP response to degeneration . . . . . 19

2.6.3 ECAP response to demyelination . . . . . 21

2.6.4 ECAP response to fibre loss . . . 22
2.6.5 EABR testing procedures . . . 22
2.6.6 EABR response to degeneration . . . 23
2.6.7 EABR response to demyelination . . . 24
2.6.8 EABR response to fibre loss . . . 25
2.7 ANF MODELS . . . 25
2.8 ELECTRODE POSITION . . . 26
2.9 CHAPTER SUMMARY . . . 27

**CHAPTER 3 METHODS: ANF MODELLING . . . 28**
3.1 CHAPTER OVERVIEW . . . 28
3.2 MODELLING AUDITORY NERVE FIBRES . . . 28
3.2.1 ANF model . . . 28
3.2.2 Population ANF model . . . 30
3.2.3 Models setup . . . 30
3.3 MODELLING NEURAL DAMAGE . . . 31
3.3.1 Damage parameters . . . 31
3.3.2 Applying ANF damage to models . . . 37
3.4 EVALUATING THE SINGLE FIBRE NERVE MODEL AS A PREDICTOR OF NEURAL RESPONSE TO ANF DAMAGE. . . . 38
3.4.1 Demyelination: single fibre . . . 38
3.4.2 Degeneration . . . 39
3.5 EVALUATING THE NEURAL POPULATION MODEL AS A PREDICTOR OF NEURAL RESPONSE TO ANF DAMAGE . . . 40
3.5.1 Modelling ANF population damage . . . 41
3.6 DISCUSSION . . . 46
3.6.1 Factors which influence model accuracy . . . 47
3.6.2 ECAP response to damage . . . 47
3.6.3 Application of the findings . . . 48
3.7 CHAPTER OVERVIEW . . . 48

**CHAPTER 4 METHODS: ELECTROPHYSIOLOGICAL TESTING AND PERSON-SPECIFIC MODELLING . . . 50**
4.1 CHAPTER OVERVIEW . . . 50

4.2 EXPERIMENTAL DESIGN: ECAPS AND EABRS . . . . . 51
4.2.1 ECAP measurements . . . . . 51
4.2.2 EABR measurements . . . . . 53
4.3 DEVELOPMENT OF A PERSON-SPECIFIC AUDITORY NERVE MODEL . . . . 55
4.3.1 Person-specific model generation . . . . . 56
4.3.2 Application of person-specific model: ANF model input . . . . . 59
4.4 ECAP SIMULATION . . . . . 66
4.5 ELECTRODE-TO-MODIOLUS DISTANCE CALCULATION . . . . . 66
4.6 CHAPTER SUMMARY . . . . . 67

**CHAPTER 5 RESULTS . . . . . 68**
5.1 CHAPTER OVERVIEW . . . . . 68
5.2 CLINICAL ECAP MEASUREMENTS . . . . . 68
5.2.1 AutoNRT measurements at various stimulation CLs. . . . . 69
5.3 DATA ANALYSIS . . . . . 79
5.3.1 ECAP measurements at 5.5dB above T level . . . . . 79
5.3.2 ECAP measurements at 5.5dB above C level . . . . . 82
5.4 EABR MEASUREMENTS . . . . . 85
5.5 MODELLING NEURON FIRING RESPONSE FOR EACH ELECTRODE AT T LEVEL. . . . . 87
5.6 MODEL PREDICTED ECAPS . . . . . 89
5.6.1 Damage profile . . . . . 90
5.6.2 Damage on nerve fibres contributing to individual electrodes . . . . . 91
5.6.3 Compiled model responses . . . . . 98
5.6.4 Comparison of clinical responses and model prediction . . . . . 100
5.6.5 Electrode-to-modiolus distance measurements . . . . . 101
5.7 CHAPTER SUMMARY . . . . . 103

**CHAPTER 6 DISCUSSION . . . . . 104**
6.1 CHAPTER OVERVIEW . . . . . 104
6.2 CLINICAL ELECTROPHYSIOLOGICAL MEASUREMENTS . . . . . 104
6.2.1 AutoNRT (eCAP) measurements . . . . . 104
6.2.2 Clinical eABR measurements . . . . . 106
6.3 DAMAGE SIMULATION IN PERSON-SPECIFIC NEURAL MODELS. . . . . 106

6.3.1 Predicted eCAPs . . . . . 107
6.4 PROPOSED PROCEDURAL IMPROVEMENTS . . . . . 108
6.5 DISCUSSION OF RESEARCH QUESTIONS . . . . . 108
6.6 FUTURE WORK . . . . . 110

**CHAPTER 7 CONCLUSION . . . . . 112**
7.1 SUMMARY OF STUDY . . . . . 112
7.2 FINAL CONCLUSION . . . . . 114

**ADDENDUM A ADDENDUM: ADDITIONAL DATA . . . . . 130**
A.1 COMPLETE INTERPOLATED DATA SETS . . . . . 130
A.2 ADDITIONAL EABR MEASUREMENTS . . . . . 135
A.3 ADDITIONAL COMPILED ECAP SIMULATION RESULTS . . . . . 138
A.4 COMPARISON OF ECAP RESPONSES TO DAMAGED AND HEALTHY NEURAL MODELS USING COMPILED FIGURES . . . . . 144

# LIST OF FIGURES

1.1 Contextualisation of this study (shaded blocks) within the broader field of cochlear implant research. . . . . 8

2.1 Diagram illustrating sensorineural hearing loss mechanisms. . . . . 11
2.2 An illustration of the effect of various hearing loss mechanisms on the ANF: Demyelination, Fibre loss and Degeneration. . . . . 11
2.3 A basic eCAP waveform. . . . . 17
2.4 A basic eABR waveform. . . . . 23

3.1 Illustration of the single ANF model used for simulations, taken from Badenhorst, Hanekom and Hanekom 2017 with permission. . . . . 29
3.2 Electrode placement relative to single nerve fibre in the simulation. . . . . 29
3.3 Example of a biphasic, cathodic-first stimulus with a 100 $\mu$s pulse width. . . . . 29
3.4 Illustration of the ANF population model and electrode placement used in simulation. 30
3.5 Template of SFAP and eCAP responses to (a) degeneration (b) demyelination and (c) fibre loss. . . . . 33
3.6 Template of eABR responses to (a) degeneration (b) demyelination and (c) fibre loss. 36
3.7 Demyelination of the (a) dendrite and (b) axon of a single ANF, illustrating varying degrees of increased latencies and RRPs, and reduced amplitudes of the SFAP response. 38
3.8 Demyelination of the full neural length of a single neural fibre, also illustrating increased latencies and RRPs and reduced amplitudes of the SFAP response. . . . . 39
3.9 Figure illustrating the effect of degeneration in a single fibre's AP response. . . . . 39
3.10 Total single fibre degeneration and demyelination. . . . . 40
3.11 Electrode placement along nerve fibres. . . . . 41
3.12 Electrode placement across nerve fibres. . . . . 41
3.13 The effect of electrode placement on neural population eCAP responses to degeneration. 42

3.14 The eCAP response of a population of nerve fibres after various levels of demyelination were applied to the nerves' (a) dendrites and (b) axons, demonstrating increasing latencies and RRPs and decreasing amplitudes as demyelination increased. . . . . 43
3.15 The eCAP response of a population of nerve fibres after various levels of demyelination were applied to the full neural length, demonstrating increasing latencies and RRPs and decreasing amplitudes as demyelination increased. . . . . 43
3.16 Figure illustrating the effect of degeneration in a ANF population's eCAP response. . 44
3.17 Fibre loss population. . . . . 45
3.18 Total population degeneration and demyelination. . . . . 45

4.1 CustomSound EP AutoNRT eCAP outputs for electrode 22. . . . . 52
4.2 Electrode placement for eABR measurements of neural response to stimulation by a CI implanted in the user's right ear. . . . . 54
4.3 Hardware setup for eABR measurements. . . . . 55
4.4 Landmark point measurements taken at every 5° of the CT scans. . . . . 56
4.5 Overlay of the trajectories of the auditory nerve and cochlear channels on the CT scan. 57
4.6 Placement of the neural plane in relation to the cochlear structure with open spaces indicating the trajectory of the electrode array. The image illustrates the electric potential across the cochlear structure and neural surface when a stimulation current is applied through electrode 6. . . . . 58
4.7 The auditory neural surface generated in the COMSOL model illustrating calculated potentials used as input to the neural model. This image illustrates the electric potential across the neural plane when a stimulation current is applied through electrode 6 as well as the fibre trajectories. . . . . 58
4.8 Figure illustrating voltages for 1 A stimulation with electrode 1 at discrete coordinates from COMSOL output. The colour bar is used to indicate the relation between colour and voltage. . . . . 59
4.9 Original points at coordinates exported by COMSOL with (a) showing the side view of the coordinates and (b) showing the top view. . . . . 60
4.10 Original coordinate points differentiated into individual fibre trajectories at every 5°, with (a) showing the side view of the trajectories and (b) showing the top view. . . . 61
4.11 Placement of somas on the fibre trajectories. . . . . 62
4.12 Coordinates of the centres of compartments on all 105 fibres. . . . . 63

4.13 A visual representation of the voltage values at the centre of each compartment in response to stimulus by electrode 1, which is located at the most basal end of the cochlea. . . . . 64
4.14 A contour plot of the voltage distribution, indicating compartment positions to stimulus by electrode 16 . . . . . 65
4.15 Measurement of electrode to modiolus distance for electrode 1. . . . . 67

5.1 Measured eCAP (a) graphs and (b) latency and amplitude values for all electrodes at 199 CL stimulation. . . . . 70
5.2 Measured eCAP (a) graphs and (b) latency and amplitude values for all electrodes at 202 CL stimulation. . . . . 71
5.3 Measured eCAP (a) graphs and (b) latency and amplitude values for all electrodes at 208 CL stimulation. . . . . 72
5.4 Measured eCAP (a) graphs and (b) latency and amplitude values for all electrodes at 211 CL stimulation. . . . . 73
5.5 Measured eCAP (a) graphs and (b) latency and amplitude values for all electrodes at 178 CL stimulation. . . . . 74
5.6 Measured eCAP (a) graphs and (b) latency and amplitude values for all electrodes at 190 CL stimulation. . . . . 74
5.7 Measured eCAP (a) graphs and (b) latency and amplitude values for all electrodes at 193 CL stimulation. . . . . 75
5.8 Measured eCAP (a) graphs and (b) peak values for all electrodes at 145 CL stimulation. 76
5.9 Measured eCAP (a) graphs and (b) latency and amplitude values for all electrodes at 181 CL stimulation. . . . . 76
5.10 Measured eCAP (a) graphs and (b) latency and amplitude values for all electrodes at 184 CL stimulation. . . . . 77
5.11 Measured eCAP (a) graphs and (b) latency and amplitude values for all electrodes at 187 CL stimulation. . . . . 77
5.12 Measured eCAP (a) graphs and (b) latency and amplitude values for all electrodes at 205 CL stimulation. . . . . 78
5.13 N1 (a) amplitude and (b) latency above T level with 90% confidence band. . . . . 80
5.14 N1 (a) amplitude and (b) latency above T level with 75% confidence band. . . . . 81
5.15 N1 (a) amplitude and (b) latency above C level with 90% confidence band. . . . . 83

5.16 N1 (a) amplitude and (b) latency above C level with 75% confidence band. . . . . 84
5.17 eABR response to stimulation on electrode 6 with the peak values recorded in the table on the left. . . . . 85
5.18 eABR response to stimulation on electrode 7 with the peak values recorded in the table on the left. The CR trace values are the values of cursor-selected points on the grey trace. 86
5.19 eABR response to stimulation on electrode 21 with the peak values recorded in the table on the left. . . . . 86
5.20 Figure depicting the firing pattern of ANFs in the person-specific model, with red dots indicating the ANFs that fire and black dots indicating those that do not. . . . . 88
5.21 Figure illustrating overlap of the inner (red) and outer (blue) layer of nerve fibre dendrites. 89
5.22 Degenerated and healthy population population eCAP responses measured on electrode 4. Electrode 4 was the stimulation electrode (SE) and electrode 6 was the recording electrode (RE) for this simulation. . . . . 92
5.23 Degenerated and healthy population eCAP responses measured on electrode 5. Electrode 5 was the SE and electrode 7 was the RE for this simulation. . . . . 92
5.24 Degenerated and healthy population population eCAP responses measured on electrode 6. Electrode 6 was the SE and electrode 8 was the RE for this simulation. . . . . 93
5.25 Degenerated and healthy population eCAP responses measured on electrode 15. Electrode 15 was the SE and electrode 17 was the RE for this simulation. . . . . 93
5.26 Degenerated and healthy population eCAP responses measured on electrode 21. Electrode 21 was the was the SE and electrode 19 was the RE for this simulation. . . . . 94
5.27 Degenerated and healthy population population eCAP responses measured on electrode 22. Electrode 22 was the SE and electrode 20 was the RE for this simulation. . . . . 94
5.28 Healthy and demyelinated population eCAP responses measured on electrode 8. Electrode 8 was the stimulation electrode (SE) and electrode 10 was the recording electrode (RE) for this simulation. . . . . 95
5.29 Healthy and demyelinated population eCAP responses measured on electrode 17. Electrode 17 was the stimulation electrode (SE) and electrode 19 was the recording electrode (RE) for this simulation. . . . . 96
5.30 eCAP responses generated by a healthy population and population with fibre loss measured on electrode 5. Electrode 5 was the SE and electrode 7 was the RE for this simulation. . . . . 97

5.31 eCAP responses generated by a healthy population, a population with fibre loss and a population with combined fibre loss and fibre degeneration measured on electrode 5. Electrode 5 was the SE and electrode 7 was the RE for this simulation. . . . . 98
5.32 eCAPs of Electrodes 20, 21 and 22 with healthy neural population. . . . . 99
5.33 eCAPs of Electrodes 20, 21 and 22 with damage applied to the neural population in accordance with the damage profile. . . . . 99
5.34 N1 values of clinically measured eCAPs. . . . . 100
5.35 N1 Values of modelled eCAPs from healthy (green) and damaged (blue) neural populations. . . . . 101
5.36 Placement of electrodes relative to fibre trajectories in person-specific ANF model. . 102
5.37 Electrode-to-modiolus distance measurements. . . . . 102

A.1 (a) N1 and (b) P1 latency above threshold. . . . . 131
A.2 (a) N1 and (b) P1 amplitude above threshold. . . . . 132
A.3 (a) N1 and (b) P1 amplitude above comfort level. . . . . 133
A.4 (a) N1 and (b) P1 latency above comfort level. . . . . 134
A.5 eABR response to stimulation on electrode 1 with the peak values recorded in the table on the left. . . . . 135
A.6 eABR response to stimulation on electrode 12 with the peak values recorded in the table on the left. . . . . 136
A.7 eABR response to stimulation on electrode 13 with the peak values recorded in the table on the left. . . . . 136
A.8 eABR response to stimulation on electrode 16 with the peak values recorded in the table on the left. . . . . 137
A.9 eABR response to stimulation on electrode 20 with the peak values recorded in the table on the left. . . . . 137
A.10 eABR response to stimulation on electrode 22 with the peak values recorded in the table on the left. . . . . 138
A.11 eCAPs of electrodes 4, 5, 6 and 15 with healthy neural population. . . . . 139
A.12 eCAPs of electrodes 5, 14 and 15 with healthy neural population. . . . . 139
A.13 eCAPs of electrodes 4, 6 and 14 with with a healthy neural population. . . . . 140
A.14 eCAPs of electrodes 5, 13 and 14 with with a healthy neural population. . . . . 141
A.15 eCAPs of electrodes 3, 4, 8, 10, 11 and 13 with with a healthy neural population. . . 141

A.16 eCAPs of electrodes 7 through 12 with with a healthy neural population. . . . . 142
A.17 eCAPs of electrodes 3, 7 and 12 with with a healthy neural population. . . . . 142
A.18 eCAPs of electrodes 3, 8, 9, 10 and 11 with with a healthy neural population. . . . . 143
A.19 eCAPs of electrodes 3, 8, 9, 10 and 11 with a healthy neural population. . . . . 143
A.20 eCAPs of electrodes 4, 5, 6 and 13 with a healthy neural population. . . . . 144
A.21 eCAPs of electrodes 4, 5, 6 and 13 with damage applied to neural population. . . . . 145
A.22 eCAPs of electrodes 3, 5, 6 and 12 with a healthy neural population. . . . . 145
A.23 eCAPs of electrodes 3, 5, 6 and 12 with damage applied to neural population. . . . . 146

# LIST OF TABLES

3.1 A summary of the qualitative eCAP responses to neural damage in comparison to normal eCAP waveform responses. . . . . 32

3.2 A summary of the qualitative eABR responses to neural damage in comparison to normal eABR waveform responses. . . . . 34

3.3 Comparison of population model eCAP N1 Latency: Degeneration vs Demyelination. 46

4.1 Table Of AutoNRT Parameters. . . . . 53

5.1 Damage profile used in this study. . . . . 91

6.1 N1 and P1 coordinates at (left) 208 and (right) 211 CL stimulation. Each column contains the latency ($\mu$s) and amplitude ($\mu$V) values for the specified peak, separated by a comma. . . . . 105

# CHAPTER 1 INTRODUCTION

## 1.1 PROBLEM STATEMENT

### 1.1.1 Context of the problem

Over 466 million people, or 6.1% of the world's population, suffer from disabling hearing loss, making it the most prevalent sensory impairment found in humans (Mathers, Smith and Concha 2000; Olusanya, Davis and Hoffman 2019). Cochlear implants (CIs) are used to provide a sense of sound to people with severe hearing loss, who would not benefit form a standard hearing aid. Hearing aids only amplify sound signals to allow better acoustic stimulation of the auditory periphery of someone with hearing loss (Leuwer and Müller 2005). A cochlear implant is an electronic device which delivers electrical stimulation directly to the auditory nerve in the inner ear, bypassing any damaged or missing structures in the ear. The device detects sound signals using an external microphone, encodes the signals digitally and transmits the encoded signals to the implanted electrode array (Wolfe 2020).

The first attempts to restore hearing by using electrical stimulation date back to the late 1700s and early 1800s when physicists like Benjamin Wilson and Allesandro Volta attempted to stimulate the auditory system with electrical current (Wolfe 2020). In 1957 Andre Djourno and Charles Eyries were the first to develop and implant a device which successfully stimulated the auditory nerve directly. This device was not implanted in the cochlea but rather at the stump of the severely damaged auditory nerve (Eshraghi et al. 2012). The user was only able to distinguish changes in the stimulus intensity and to differentiate broad stimulation frequency changes (Wilson and Dorman 2008). In 1985 William F House read a newspaper article describing the work of Djourno and Eyries, which prompted him to explore the development of implantable hearing technology. In 1961 Dr. House collaborated with John Doyle, a neurosurgeon, to implant the first true CI. A single gold wire electrode was implanted in the scala tympani through an opening anterior to the round window. In January of 1961 two people received such implants, after which both users were able to perceive a sensation of sound. Both

implants were removed after a short period of time because possible infection or edema was suspected (Mudry and Mills 2013). This sparked the development of cochlear implants with single- and eventually multi-channel devices (Wolfe 2020). In recent years the advance in CI development have included improved surgical practices and the development of advanced speech coding strategies (Eshraghi et al. 2012). Despite the considerable progress in CI development, these implants still fall short of truly restoring the user's speech perception, and methods of improving cochlear implants are continuously being researched (Eshraghi et al. 2012).

With the continued advancement of cochlear implants, various modelling processes have also developed. Cochlear models provide a possible diagnostic tool by allowing the emulation of experiments which cannot be performed physically due to technical and ethical limitations. Some of the first cochlear models were lumped-parameter models developed by Johnstone, Johnstone and Pugsley (1966) and Honrubia, Strelioff and Sitko (1976). Strelioff (1973) developed a model which described the electrical properties of cochlear structures within a guinea pig cochlea. Soon after, another three-dimensional discrete resistance model was developed by Black and Clark (1980). These models show the current spread in the cochlea and could be used to evaluate various electrode configurations. These lumped models were limited to examining only the electric potentials and current distributions inside the cochlea, as the models were not yet coupled to auditory nerve models. The development of three-dimensional (3D) volume conduction cochlear models made it possible to investigate the distributions of electric potential and current density in the human cochlea in response to electrical stimulation (Tong et al. 1990), as well as to examine how neuroprosthetic devices will function under various conditions for specific users (Mangado et al. 2015).

Computational models of electrically stimulated auditory nerve fibres were being developed concurrently. In 1987 Colombo and Parkins developed the first electrical cable biophysical model of the mammalian auditory-nerve neuron (Kalkman, Briaire and Frijns 2016). The model was based on the original Hodgkin and Huxley nerve model (Hodgkin and Huxley 1952), but included modifications to better incorporate physiological data obtained from single auditory nerve fibre (ANF) experiments in squirrel monkeys (Parkins and Colombo 1987). Electrical auditory nerve models have been improved over time by including data from various electrophysiological mammalian neuron studies (Kalkman, Briaire and Frijns 2016). Improved knowledge of the morphology of the human auditory nerve has also contributed to the improvement of ANF models (Rattay, Lutter and Felix 2001; Dekker, Briaire and Frijns 2014).

As computational power increased, more complex cochlear models could be implemented (Agrawal and Newbold 2012). The integration of cochlear models with computational ANF models started around 1990, when Finley et al. were the first to publish simulations of a three-dimensional volume conduction model coupled with a model of the auditory nerve (Finley, Wilson and White 1990). Several integrated models soon followed (Frijns, Snoo and Schoonhoven 1995; Hanekom 2001; Dang et al. 2015).

Cochlear implant users experience different levels of restored sound and speech perception. One of the factors which influences the efficacy of the implant is auditory neural health, as damage to the auditory nerve may alter the conduction parameters of electrically excited neural activity. The understanding of the specific effects of partial auditory nerve degeneration on cochlear implant function is limited at present (Pfingst, Zhou et al. 2015). However, severe spiral ganglion neuron (SGN) degeneration appears to limit the efficacy of hearing restoration by a cochlear implant (Landry et al. 2011), as severe SGN degeneration reduces the neural targets for cochlear implant stimulation (Shibata et al. 2011). A correlation between the degree of preservation of SGN and the level of speech recognition after cochlear implantation has also been established (Nadol 1997). Determining the health of the auditory nerve through a non-invasive method would be a valuable tool in the pursuit of cochlear implant improvement.

Correctly identifying specific ANF damage has proved problematic, as there is no one established testing method (Earl and Chertoff 2009). There have been calls for a distinct hypothesis explaining how each psychophysical or electrophysiological measure may be affected by a specific aspect of neuronal health or survival (Carlyon et al. 2021).

If a subject has severe auditory nerve (AN) damage or a completely absent AN, they may not benefit from a cochlear implant, in which case an auditory brainstem implant (ABI) may be an alternative method of treatment (Colletti et al. 2005). The ABI bypasses the AN by stimulating the second order neurons in the cochlear nucleus using a multichannel surface array (Wong et al. 2019).

### 1.1.2 Research gap

Various physiological, electrophysiological and psychophysical measurements have been implemented to determine the amount of sensory and neural damage to the auditory system (Zhou and Pfingst 2014). Physical means of determining auditory neural health include CT scans, magnetic resonance

imaging (MRI) scans and histopathological examinations. Histopathological analysis of the auditory periphery during autopsy allows better understanding of the mechanisms underlying auditory nerve pathology. Cochlear histopathologic examinations only provide post-mortem insight (Viana et al. 2015), and the findings highlight the need for non-invasive clinical diagnostic tools (Sagers et al. 2017). Imaging of the inner ear has also been used to evaluate hearing loss and to determine if tumours, congenital, inflammatory or infectious diseases are present (Verbist 2012). Cochlear imaging techniques still have very poor quality (Włodarczyk and Skarżyński 2020). Computed tomography (CT) scans allow imaging of the bony details of the sound conduction pathway and evaluating otospongiosis. They are subsequently indicated for cases of conductive or mixed hearing loss (Chen, Phillips and D. 2015; Verbist 2012). For sensorineural hearing loss, MRI scans are preferable, as they provide a better view of the vestibulocochlear nerve. Both types of physiological scans may also be used complementarily.

Electrophysiological measurements that may be performed on CI users include electrically evoked compound action potentials (eCAPs), electrically evoked auditory brainstem responses (eABRs), auditory steady-state responses (ASSRs) and otoacoustic emissions (OAEs) (Ramekers et al. 2014; Shinn and Musiek 2007). ECAPs reflect the electrically evoked synchronized response of a population of auditory nerve fibres (He, Teagle and Buchman 2017). EABRs indicate the responsiveness of the peripheral auditory nerve fibres up to the brainstem, allowing measurement of the transmission of signals between the cochlea and the brain (Di Stadio et al. 2019). ASSR is used to objectively measure hearing thresholds and may be used to monitor the condition of the auditory nerve (Rampp et al. 2017). OAEs are generated in the cochlea by the outer hair cells and provide a simple, non-invasive indicator of cochlear function (Kemp 2002). Electrocochleography (eCochG) is another electrophysiological test, which is used to measure sound induced electrical potentials along the auditory pathway. ECochG can distinguish between sensory and neural damage by the distinct level- and frequency-dependent characteristics (Meenderink, Lin and Dong 2021). The use of tripolar (TP) electrode configurations have also been proposed as a possible means of determining auditory neural health. Regions with poor neural survival in the cochlea may be identified by abnormally high TP thresholds (Bierer and Faulkner 2010).

Furthermore, reduced psychophysical thresholds, as well as the shapes and levels of threshold-versus-stimulus-duration functions have been correlated with better neural survival (Tejani, Abbas and Brown 2017; Pfingst, De Haan and Holloway 1991). Physiologically, the number and density of spiral ganglion

cells have also been used as a measure of auditory neural health (Dhanasingh et al. 2020). Many of the studies in which these measurements were implemented have aimed to address the problem of determining the health and survival of the auditory nerve. Thus far, these measurements have not provided a reliable and consistent method with which to determine auditory neural health. Due to the limitations of physiological testing procedures and the incomplete information obtained from any single electrophysiological or psychophysical procedure, this study aims to add to the existing knowledge base by considering the combination of two electrophysiological procedures as an improvement to present methods for determining the type and extent of AN damage.

## 1.2 RESEARCH OBJECTIVE AND QUESTIONS

Cochlear implants aim to induce excitation of the AN using electrical stimulation, which means that the health and survival of the AN is crucial to good CI performance. CI functionality depends on a wide array of factors, one of which is the condition of the ANF. Even under ideal circumstances CIs do not completely restore normal hearing and many users still have poor speech recognition (Pisoni et al. 2017). Research into improving cochlear implants is complicated by the limitations of human in vivo studies. Many of these limitations can be overcome by implementing detailed cochlear models as a means to investigate non-invasive intervention outcomes (Heshmat et al. 2020). Incorporating auditory nerve fibre models into the cochlear volume conduction models provides a tool for predicting neural excitation patterns. Various person-specific cochlear models have been constructed using CT-scan data (Malherbe, Hanekom and Hanekom 2015; Cakir, Dwyer and Noble 2017; Gee et al. 2021). Using person-specific information regarding the health of nerve fibres throughout the cochlea to construct the integrated auditory nerve model will allow a more accurate model to be generated for each user, which incorporates their unique neural survival pattern (Nogueira et al. 2016). The research objective for this study is to find an improved in vivo method of determining ANF health for a specific user using electrophysiological tests.

The study's research objective has prompted investigation into the following research questions.

- Is it possible to evaluate a single AN model as well as an elementary population AN model as predictors of neural response to ANF damage by using expected characteristics of SFAP and eCAP responses to damage as reported in the literature?
- Can electrophysiological responses be used to identify or differentiate between damage mechanisms affecting ANFs?

- How successful is the person-specific compound volume conduction (VC) and computational ANF model in predicting the amplitude and latency characteristics of measured outcomes?
- Can a compound ANF model, which incorporates ANF damage provide insight on how the placement of electrodes in the cochlea influences the characteristics of eCAPs?

## 1.3 APPROACH

Since cochlear neural survival affects the effectiveness of CIs, it is important to develop models which reflect the characteristics of person-specific cochlear anatomy, neural survival profiles and electrode array placement.

To date, several 3D CI models have been developed for research purposes, but very few have been employed for diagnostic purposes (Hanekom and Hanekom, 2016). Computational cochlear models are ideally suited to inform the diagnosis and possible treatments of cochlear neural damage. To achieve this, the models must include the neural survival information specific to the CI user.

Various methods of determining neural damage will be investigated and the most promising methods will be compiled into a testing procedure. This proposed neural testing procedure will provide information regarding the condition of the auditory nerve fibres. This information can then be incorporated into the implementation of the person-specific ANF model.

Once the proposed method for determining neural health has been established in simulation, it will be evaluated in a clinical experiment. The experiment will be designed to determine the type and location of neural damage within the cochlea, allocated into sections neighbouring the electrode contacts of the implanted array. The damage will be determined by examining the effect that the degree, and different types of neural damage have on measured electrophysiological test responses. The eCAP and eABR electrophysiological tests will be used to identify the neural damage to an individual's cochlear nerve fibres.

## 1.4 RESEARCH GOALS

The first goal of this study is to determine a neural testing procedure, which aims to determine the health of a person's auditory nerve fibres. A further goal of this study is to develop a method for applying the different types and levels of determined neural damage to the nerve fibres in the three-dimensional

cochlear model. A clinical application of the testing procedure and the subsequent application of neural damage to a three-dimensional model will be conducted.

## 1.5 RESEARCH CONTRIBUTION

The information obtained using the testing procedure developed in this study may improve subsequent models, as more accurate person-specific neural models would complement the anatomically accurate person-specific 3D models. Additionally, this information may also provide a means to determine cochlear nerve damage and allow possible treatments or alternative stimulation procedures to be investigated in simulation. Degeneration of the AN may progress with time, necessitating a consistent method for monitoring this progression using non-invasive electrophysiological responses.

## 1.6 RESEARCH OUTPUTS

Journal and conference outputs:

- A journal article from work presented in this dissertation has been submitted to an accredited international journal: Swanepoel P, Badenhorst W and Hanekom T "Electrophysiological assessment of ANF damage.", Submitted to Ear and Hearing.
- A poster and video presentation at the Conference on Implantable Auditory Prostheses (CIAP): Swanepoel P, Badenhorst W, Hanekom T & Hanekom JJ, "Can the effects of auditory nerve damage be accounted for in a computational ECAP model?", 2021 Conference on Implantable Auditory Prostheses, Online, July 2021, p. 78

Research tools and methods:

- A standardised protocol for determining the type and extent of ANF damage using established electrophysiological tests.
- Two ANF configuration models evaluated against expected eCAP measurements from literature.
- A person specific cochlear model which includes auditory nerve fibres with the option of implementing various damage mechanisms.

## 1.7 OVERVIEW OF STUDY

This study examined methods for assessing auditory neural health and incorporating an individual's neural health profile into a computational person-specific ANF model. Figure 1.1 contextualises the research conducted for this study within the broader field of cochlear implant research.

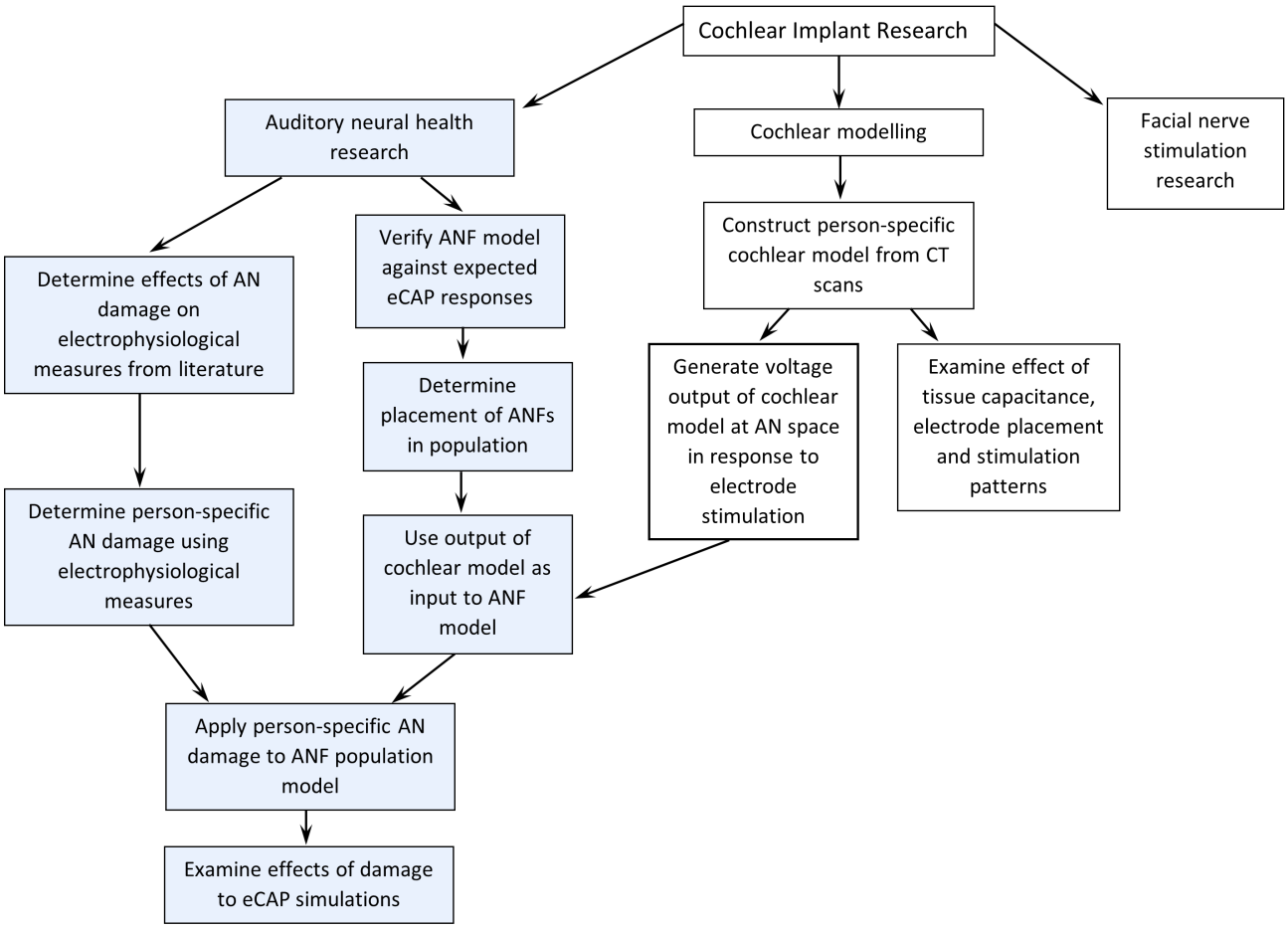


**Figure 1.1.** Contextualisation of this study (shaded blocks) within the broader field of cochlear implant research.

This dissertation is divided into six chapters. **Chapter 1** (this chapter) outlines the background, specific research problem and the research questions addressed by this study. **Chapter 2** presents a literature review of electrophysiological testing procedures and how the measurements relate to various auditory nerve damage configurations. The aetiology of ANF damage and the various damage mechanisms are also discussed. **Chapter 3** describes the configuration and evaluation of two ANF damage models used to demonstrate the electrophysiological responses to neural damage. **Chapter 4** reports the experimental setup for obtaining clinical eCAP and eABR measurements, as well as the method for determining a neural damage profile from electrophysiological responses. The process of integrating the ANF model with a user-specific 3D cochlear model is also described in this chapter. **Chapter 5** summarizes the results obtained from the clinical electrophysiological responses, the neural damage estimation, and the subsequent person-specific cochlear model outputs. **Chapter 6** presents a

discussion of the clinical results, the effect of the damage applied to the user-specific neural model outputs and the significance of all results in relation to the research questions. **Chapter 7** offers a conclusion to results discussed in this dissertation as well as a review of all findings obtained during the course of this study.

# CHAPTER 2 LITERATURE STUDY

## 2.1 CHAPTER OVERVIEW

This chapter aims to provide an overview of the literature that constitutes the framework for the present auditory neural health study. Section 2.2 presents an introduction to electrophysiological testing methods, types of hearing loss and the responsible damage mechanisms. In Section 2.3 the possible factors which influence the incidence of ANF damage are discussed. Section 2.4 describes three ANF damage mechanisms investigated in this study. In Section 2.5 the existing methods of determining ANF damage are discussed. Section 2.6 focuses specifically on the electophysiological methods which are currently used to determine auditory nerve health. Section 2.7 gives background regarding the history and development of ANF models.

## 2.2 INTRODUCTION

Cochlear implants, which restore a sense of hearing, are the standard treatment for people with profound sensorineural hearing loss. The implants bypass the normal auditory process and electrically stimulate the auditory nerve (AN) via electrodes implanted in the cochlea, leading to CI users experiencing different levels of restored speech understanding. The efficacy of the implants relies on neural health, as damage to the auditory nerve will limit or completely inhibit the conduction of electrically excited neural activity. This study provides an overview of electrophysiological methods for determining the health and survival of ANFs and the extent to which damage to ANFs can be accounted for in a computational model.

Auditory neural health depends on various hearing loss aetiologies. In order to use a modelling approach to disentangle the effect of neural health on CI performance, these aetiologies need to be qualified according to their primary neural damage mechanisms. Hearing loss can be categorised as either *conductive* or *sensorineural* hearing loss. *Conductive* hearing loss occurs when the conduction

of sound waves through the outer or middle ear to the inner ear is impeded (Isaacson and Vora 2003). *Sensorineural* hearing loss occurs when some combination of the outer hair cells (OHCs), inner hair cells (IHCs) and spiral ganglion neurons (SGNs) are damaged, dysfunctional or lost (Kohrman et al. 2020). In this study, only sensorineural hearing loss will be considered. Figure 2.1 shows the qualification of the aetiologies according to damage mechanisms implemented as distinct modelling elements in this study, namely ANF degeneration, ANF demyelination and ANF loss. Cochlear implantation is commonly indicated as treatment for moderate-to-profound sensorineural hearing loss (Buss et al. 2018), which encompasses all three of the damage mechanisms depicted in figure 2.2.

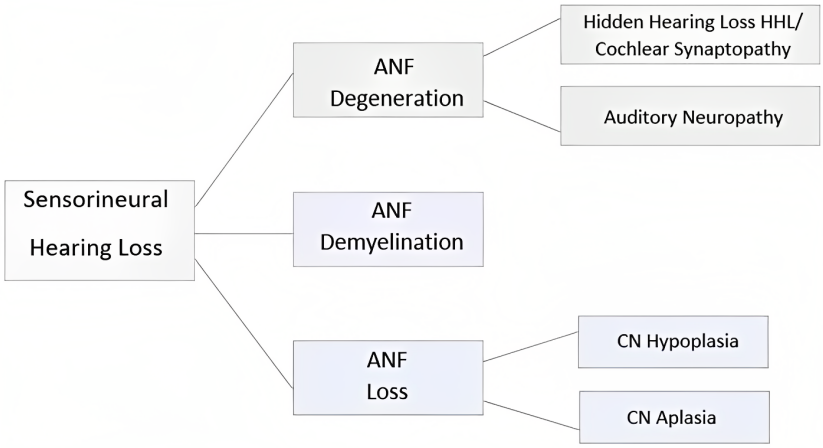


**Figure 2.1.** Diagram illustrating sensorineural hearing loss mechanisms.

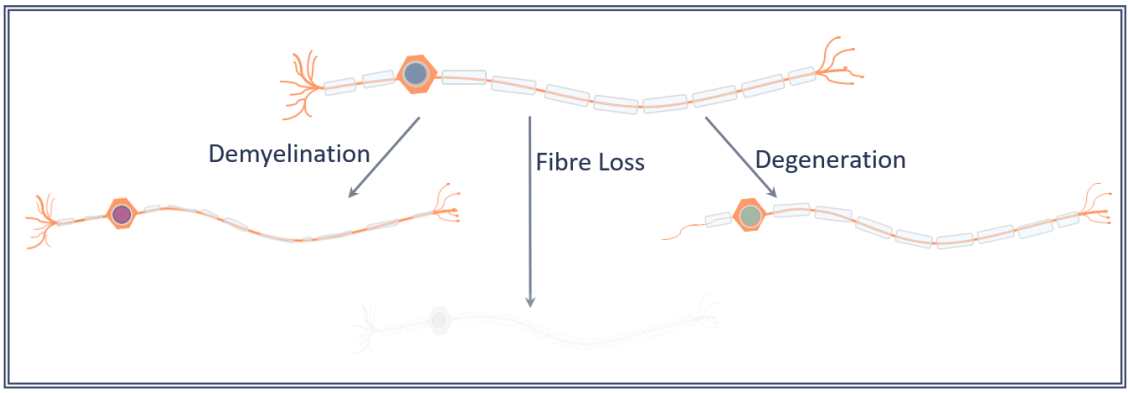


**Figure 2.2.** An illustration of the effect of various hearing loss mechanisms on the ANF: Demyelination, Fibre loss and Degeneration.

## 2.3 FACTORS WHICH INFLUENCE THE INCIDENCE OF AUDITORY NERVE DAMAGE

Noise-induced hearing loss (NIHL) is one of the most common causes of deafness. The Centers for Disease Control and Prevention estimates that approximately 17% of adults have suffered permanent noise-induced damage to their hearing (CDC 2021). Exposure to intense sound levels can be a result of recreational, occupational or military environments. NIHL is the result of noise damage to the sensory hair cells (HCs), synapses and primary auditory neurons (Kurabi et al. 2017).

Presbycusis, also known as age-related hearing loss, is the most common sensory impairment seen in the elderly and refers to hearing loss caused by the ageing process. This kind of hearing loss is generally bilaterally symmetrical (Lee 2013). The ageing process generally results in reduced hearing ability and a greater risk of cochlear sensory-neural cell degeneration. Presbycusis can result from either cochlear degeneration or loss of ANFs during cochlear ageing. Hearing loss generally starts in the high-frequency section of the auditory spectrum and spreads towards the low-frequency section with age (Wang and Puel 2020).

Hearing loss can occasionally be caused by traumatic brain injuries which have been shown to result in damage to either the central or peripheral auditory system (Emerson et al. 2011). The possible types of damage include degeneration of the spiral ganglion and organ of Corti, damage to the auditory and vestibular nerves and subsequent intralabyrinthine connective tissue formation (Bartholomew et al. 2020).

Hereditary hearing loss can be classified as syndromic, which is associated with malformations of the external ear in combination with abnormalities in other organs, or nonsyndromic, which displays no visible external abnormalities but can be associated with abnormalities of the middle and/or inner ear (Shearer, Hildebrand and Smith 1993). Over 400 types of genetic deafness and 60 genes for syndromic and nonsyndromic hearing loss have been identified (Kochhar, Hildebrand and Smith 2007). Many of these hereditary conditions cause sensorineural hearing loss, which is often the result of auditory nerve damage. These conditions include Stickler syndrome, Pendred syndrome, Neurofibromatosis 2 and various other diseases and gene mutations (Kochhar, Hildebrand and Smith 2007). Malformation of the inner ear has also been associated with sensorineural hearing loss (Kazahaya and Singh 2007). Inner ear malformations are generally a congenital condition which likely cause cochlear nerve deficiency (CND) combined with cochlear aperture stenosis. Studies have found that individuals with congenital

unilateral sensorineural hearing loss are more likely to have inner ear malformations than those with bilateral hearing loss (Orzan et al. 2021).

Meniere's disease is a progressive disorder that affects the inner ear. The disorder is characterized by recurrent episodes of vertigo, tinnitus, a feeling of aural fullness and fluctuating sensorineural hearing loss (Alonso et al. 2021). The aetiology of the disease is not known; it is however thought to occur due to the accumulation of endolymphatic fluid in the cochlea. Hearing loss as a result of Meniere's disease usually presents unilaterally (Sharma 2017).

Benign tumours originating from the Schwann cells of the cochleovestibular nerve may result in gradually worsening sensorineural hearing loss in the ipsilateral ear (Gan et al. 2021). These tumours are referred to as acoustic neuroma and may also be called vestibular schwannoma, acoustic neurinoma, acoustic neurofibroma or vestibular neuroma (Greene and Al-Dhahir 2022).

Ototoxicity is the impairment of inner ear tissues caused by pharmacological treatments and is characterized by vestibular or cochlear dysfunction (Ganesan et al. 2018). If cochlear cells are exposed to aminoglycoside antibiotics, which are used to treat several diseases like tuberculosis and bacterial pneumonia, for an extended period of time it may result in the death of outer hair cells in the organ of Corti. Cochlear hair cell (HC) damage caused by ototoxic medication leads to retrograde AN damage which progresses from the base of the cochlea to the apex. The degree of hearing loss is directly proportional to the dose of the ototoxic drug and repeated exposure leads to additive damage. As a common cause of acquired hearing loss, bacterial meningitis can result in permanent sensorineural hearing loss and, in rare cases, profound bilateral hearing loss (Kutz et al. 2006). The exact site of physiological damage caused by meningitis has not been established. Outer hair cell damage, severe loss of spiral ganglion cells and lesions of central neural pathways have all been suggested. Suppurative labyrinthitis and ossification of the cochlea may also result from meningitis (Du, Wu and Li 2006).

## 2.4 ANF DAMAGE MECHANISMS

The damage mechanisms identified from literature which are examined in this study are discussed in this section.

### 2.4.1 ANF degeneration

*ANF degeneration* as a hearing loss mechanism encompasses various hearing loss aetiologies. Hidden hearing loss (HHL), also known as cochlear synaptopathy, refers to degeneration of cochlear synapses without the loss of HCs and SGNs (Kohrman et al. 2020). Auditory neuropathy refers to hearing loss as a result of auditory nerve dysfunction, which is distinct from impairment because of HC loss. This condition presents with normal objective measurements of HC activity, such as otoacoustic emissions, but abnormal measurements of auditory nerve functions, such as auditory brainstem responses (ABRs) (Rance and Starr 2015). ANF degeneration can be caused by a number of factors such as infections, ageing, dementia, ototoxic medications, metabolic disorders, neural diseases and prolonged exposure to dangerously loud sounds (Zahnert 2011). Several of these pathologies involve degeneration of ANFs over a period of time (Shibata et al. 2011). One such pathology is NIHL as a result of damage to either the inner HCs or synaptic connections between HCs and cochlear neurons (Bohne and Harding 2000; Liberman 2017). A second example is the degeneration of the spinal ganglion over time which may be caused by trauma from electrode implantation that could lead to new bone formation and perielectrode fibrosis (Nadol 1997). This suggests that degeneration of the AN may progress over time, making it necessary to have a consistent approach for monitoring this progression through non-invasive, electrophysiological responses.

### 2.4.2 ANF demyelination

*ANF demyelination* is considered a separate hearing loss mechanism in this study, as it can be applied as a separate modelling element. Neural demyelination is the term used to describe any damage to a nerve fibre's myelin sheath. Another myelin disorder, neural dysmyelination, which refers to any condition that results in abnormal myelin synthesis, is also considered under this modelling element. Demyelination can be caused by various environmental, genetic and age-related factors. These factors include acoustic overexposure (Tagoe et al. 2014) and ototoxic medication such as carboplatin (Ding, McFadden and Salvi 2002). Iron-deficiency anaemia in infancy could also alter AN myelination and have long lasting effects on auditory signal transmission (Algarín et al. 2003), while hyperbilirubinemia has been linked to ANF damage as a result of damage to the IHC synapses and myelin sheaths (Ye et al. 2012). Certain cases of the rare autoimmune disorder Guillain–Barré syndrome have, in turn, been shown to result in acoustic nerve conduction abnormalities from demyelination, indicated by abnormal brainstem auditory evoked potentials (Nelson, Gilmore and Massey 1988). The perikaryal demyelination of ANF myelin sheaths appears to be symptomatic of age-related hearing loss (Cohen,

Park and Grasso 1990), which may contribute to the loss of SGNs and the ensuing decline of the AN function (Xing et al. 2012).

### 2.4.3 ANF loss

*ANF loss* is the third mechanism of hearing loss implemented as a modelling element in this study. Cochlear nerve deficiency (CND), defined as a small or absent cochlear nerve, is a common cause of unilateral sensorineural hearing loss, particularly in cases where the deafness is congenital (Clemmens et al. 2013). CND is a general term used to describe both cochlear nerve hypoplasia which is a significant narrowing of the cochlear nerve (CN), and cochlear nerve aplasia which refers to the absence of the CN (Cinar et al. 2019). People with CN hypoplasia may benefit from cochlear implantation, whereas cochlear implantation is contra-indicated for CN aplasia (Buchman et al. 2006). This study will consequently only consider CN hypoplasia.

## 2.5 EXISTING APPROACHES TO DETERMINING ANF DAMAGE

Damage to the AN has several detrimental effects on neural activation, such as elevated thresholds and reduced suprathreshold amplitudes in electrophysiological responses (Kujawa and Liberman 2009), as well as changes in the pattern of neural excitation in the cochlea (Cohen, Richardson et al. 2003). For example, higher stimulation currents are required to stimulate damaged ANFs relative to intact ANFs, which in turn leads to a wider spread of neural excitation in the cochlea. The increased spread of excitation could result in overlapping excitation regions, which may reduce the user's speech perception (Shibata et al. 2011). Moreover, severe ANF degeneration can reduce the neural targets for electrical stimulation by the CI, diminishing its efficacy (Goehring et al. 2019). The peripheral excitation behaviour of neurons as observed in electrophysiological responses is intrinsically linked to the perceptual outcomes of a CI user (Brochier, Guérit et al. 2021). The unique neural damage profiles of CI users may explain the widely varying speech understanding performance observed (Guedes et al. 2007). Consequently, information regarding the condition of an individual's AN may allow optimal programming of the device for the user (Carvalho et al. 2020).

Person-specific computational models of the auditory periphery attempt to predict neural excitation behaviour as a result of electrical stimulation (Malherbe, Hanekom and Hanekom 2015). These models may be applied to investigate and probe a variety of phenomena in CI users, among others the effect of neural health on the neurophysiological outcomes that may be expected for a specific CI recipient. A

VC model that describes the cochlear morphology and electrical characteristics of the tissue is used to predict the spread of current as a result of electrical stimulation. The current distribution predicted by the VC model can subsequently be translated to neural excitation characteristics by a neural model. However, the effects of degeneration and demyelination are often not taken into account in the neural component of the existing computational models. This is primarily because there is presently no established method for the quantification of auditory neural survival profiles to inform the models. Including information about neural damage could improve the accuracy of a model's predictions for a specific user.

Despite the lack of standardised auditory neural testing procedures, attempts have been made to include varying degrees of auditory nerve damage when modelling the auditory periphery. Goldwyn, Bierer and Bierer (2010) developed a computational model of simplified cochlear geometry which can simulate variations in spiral ganglion density and illustrate how these affect the simulated neural activation patterns. Verhulst, Altoè and Vasilkov (2018) simulated cochlear synaptopathy by altering the number and types of ANF that connect to each inner HC in the cochlear model. Another study implemented a cochlear model for which either intact or degenerate nerve fibres could be used to investigate whether neural degeneration affects the optimal position in which the electrode should be placed (Briaire and Frijns 2006). A later study by Snel-Bongers et al. (2013) implemented three sets of nerve fibres with different stages of degeneration in their cochlear model to account for possible neural damage. This study suggested that inconsistencies in the results may reflect the assumption that only one degeneration morphology was implemented at a time and that a combination of the different morphologies may provide more accurate predictions. None of these modelling approaches, however, represent a user-specific neural survival profile, but rather a general level of AN damage.

Several studies have been conducted to examine the plausibility of using either eCAP or eABR measurements to determine the survival rate and health of the auditory nerve (Pourjavid et al. 2011; Starr, Picton, Sininger et al. 1996). Many of these studies have focused on a single type of electrophysical test (either eCAP or eABR) and have investigated responses specific to either nerve degeneration or demyelination or have not specified the type of neural damage. In this study, degeneration, demyelination and fibre loss are investigated as separate mechanisms of neural damage that may occur independently or concurrently.

## 2.6 PRESENT ELECTROPHYSIOLOGICAL NEURAL TESTING PROCEDURES

At present there is no standardised in vivo protocol for determining the extent of auditory nerve damage, as no single objective procedure provides a complete and accurate measure of neural health. Furthermore, the electrophysiological waveforms which are typically used to probe neural health need expert interpretation. A standardised interpretation protocol may allow more consistent assessment of surviving spiral ganglion ANFs among different researchers and clinicians.

### 2.6.1 ECAP testing procedures

The first electrophysiological testing approach evaluated for this study was eCAP measurement.

ECAPs offer a possible test procedure to determine the health of the AN (Hughes, Castioni et al. 2012). The use of eCAPs to determine CI stimulus levels for individual electrodes has been established in various studies, while more recent studies have examined the possibility of using eCAP measurements to determine the physiological condition of the AN (He, Teagle and Buchman 2017). An eCAP is a synchronous response that is generated by a large number of ANFs. The waveform consists of a positive peak P0, followed by a negative peak N1, followed by another positive peak P1, as shown in figure 2.3. Some publications refer to the positive peaks as P1 and P2 with the negative peak N1 (Abbas and Brown 2015).

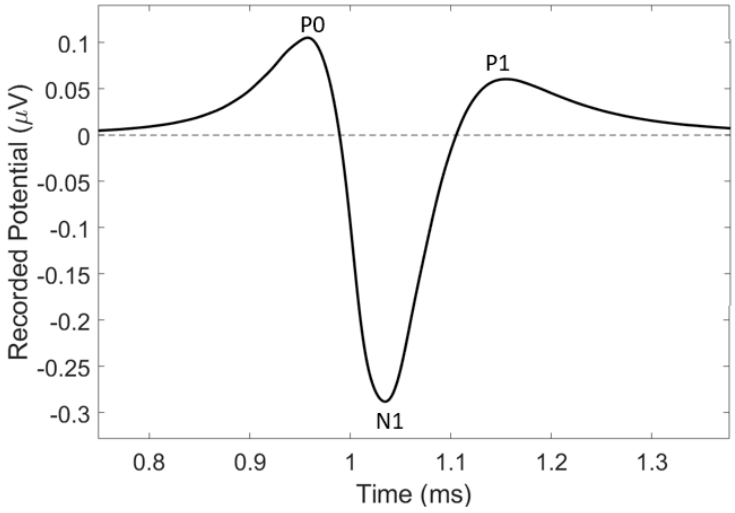


**Figure 2.3.** A basic eCAP waveform.

#### 2.6.1.1 Stimulus artefact rejection paradigms

Stimulus artefacts often contaminate the recorded eCAP response, obscuring important information (Deprez et al. 2017). Forward masking, alternating polarity and subthreshold template subtraction are the three most common, artefact-reduction methods (Baudhuin, Hughes and Goehring 2016; He, Teagle and Buchman 2017).

Brown, Abbas and Gantz (1990) developed the forward-masking paradigm which minimises the stimulus artefact and allows artefact-free eCAPS to be recorded using an intracochlear electrode. The forward-masking paradigm, also referred to as the masker-probe paradigm, is one of the most popular techniques used to reduce stimulus artefacts in eCAPs and is the default method used by Cochlear's Custom Sound EP software (*Custom sound® EP* 2021; Alvarez et al. 2008; Baudhuin, Hughes and Goehring 2016). Two biphasic current pulses are presented in this method. This first pulse is referred to as the 'masker' and the second as the 'probe'. The procedure for the forward-masking paradigm is (Brown, Abbas and Gantz 1990; He, Teagle and Buchman 2017):

1. A probe-only stimulus (A) is applied as a single biphasic current pulse. This stimulus elicits an eCAP and a substantial stimulus artefact.
2. A masker-plus-probe stimulus (B) is applied which consists of a masker biphasic pulse, followed by a probe biphasic pulse. The pulses are presented with a masker probe interval (MPI) that will ensure that the probe stimulus occurs in the ANF refractory period which will result in a combination of the two stimulus artefacts and an absent or reduced neural response.
3. A masker-only stimulus (C) is presented which consists of another single biphasic pulse. This response will consist of the masker artefact and associated eCAP.
4. Extraction of the eCAP from the stimulus artefact is achieved by subtraction. The artefact evoked by the probe can be identified by subtracting the masker-only response from the masker-plus-probe response (B-C). This artefact is then subtracted from the entire response evoked by the probe to obtain the artefact-free eCAP response (A-(B-C)) .

The limitation of this method is that it requires that the masker-plus-probe response should only have one evoked eCAP response and two stimulus artefacts. If the masker-to-probe intervals or masker stimulus is chosen incorrectly an unintended neural response may be elicited, resulting in an unsuccessful artefact removal (He, Teagle and Buchman 2017).

The alternating polarity method is used exclusively as the artefact reduction method used by Advanced Bionics' SoundWave and MED-EL's Maestro software (Baudhuin, Hughes and Goehring 2016). The procedure for this method is :

1. A cathodic-leading stimulus (A) is applied, inducing an eCAP and artefact.
2. An anodic-leading stimulus (B) is then applied, inducing another eCAP and artefact.
3. Because of the alternating polarity of the stimulation, the artefacts elicited by the two stimuli have reverse polarity. The eCAP polarity stays the same. This allows the stimulus artefacts to be removed by averaging both responses, leaving an artefact-free eCAP ((A+B)/2).

This method relies on the assumption that reversing the polarity does not affect the eCAP latencies or amplitudes. It has been shown that the latency of the evoked eCAPs differ for cathodic and anodic leading stimuli, which means that this method may result in distorted eCAP measurements (Undurraga, Wieringen et al. 2010; He, Teagle and Buchman 2017).

Miller et al. (1998) developed the subthreshold template subtraction method. The steps for this method are as follows:

1. A response is evoked using a biphasic stimulation pulse (A) that is below the neural threshold, which will consist of only the stimulus artefact.
2. A second response is evoked using a supra-threshold biphasic stimulation pulse (B), which will contain both the stimulus artefact and the evoked eCAP.
3. The artefact response (A) is scaled up to correspond to the size of the stimulus artefact in (B).
4. The scaled artefact response is then subtracted from response B, leaving only the eCAP.

This artefact removal paradigm is the least prevalent as it requires a very accurate recording system and low ambient noise level (He, Teagle and Buchman 2017).

### 2.6.2 ECAP response to degeneration

#### 2.6.2.1 Amplitude

Multiple studies have shown that suprathreshold eCAP amplitudes reflect the sum of auditory neuronal activities and can consequently be used to indicate the level of preservation of the AN (Caldas et al.

2016; Scheperle 2017; He, Shahsavarani et al. 2018). This was verified by a study which showed that suppressed amplitudes of eCAP waveform peaks seem to reflect the degeneration of the AN (Kujawa and Liberman 2009).

#### 2.6.2.2 N1 latency

Increased nerve degeneration has been shown to result in reduced N1 peak latency (Strahl et al. 2016). It has been theorised that the latency of the eCAP peaks (especially N1) elicited at high-intensity levels reflects the site of excitation along the neuron. In the event of dendrite degeneration, the site of excitation moves to the central axon of the nerve. This results in shorter N1 latencies at high stimulation levels for degenerated ANFs (Stypulkowski and van den Honert 1984).

#### 2.6.2.3 Relative refractory periods (RRPs)

Studies examining the effects of ANF damage on the RRPs of eCAPs have reported varying results. For example, a study by Botros and Psarros (2010) suggested that longer RRPs are associated with better neural survival in CI users. Similarly an AN model also predicted a decrease in RRPs as progressive retrograde nerve fibre degeneration is implemented (Smit, Hanekom and Hanekom 2008). Conversely, another study found that CN deficiency caused no significant difference in the relative refractory period (He, Shahsavarani et al. 2018).

#### 2.6.2.4 Functions

Various functions derived from eCAP measurements have been investigated for possible use in determining auditory neural health (Biesheuvel, Briaire and Frijns 2018). For example, the slope of the eCAP amplitude growth function (AGF) has been shown to be predictive of spiral ganglion neural density (Pfingst, Zhou et al. 2015). A negative correlation between the AGF slope and the duration of deafness and cochlear implantation age suggests that ANF damage will result in reduced AGF slopes (Gärtner et al. 2021). AN damage also appears to result in a steeper eCAP amplitude-intensity function (Legatt 2018). Steep input-output functions (also known as eCAP growth functions) may indicate better survival of spiral ganglion populations, which are an indication of better auditory neural health (He, Shahsavarani et al. 2018; Xu et al. 2020). This assumption has been substantiated by studies which found that the slopes of eCAP input-output functions in users with CND were significantly smaller than users with normal-size CNs (He, Shahsavarani et al. 2018).

#### 2.6.2.5 Pulse duration (PD) and Inter-phase gap (IPG)

The effect of changes in the PD and IPG on both eABR and eCAP responses have been examined to determine the health of the AN. Subjects with CND have showed more profound IPG effects in their

maximum eCAP amplitude and the slope of the eCAP input-output function and smaller effects on the eCAP thresholds than subjects with normal CNs (He, Xu et al. 2020). There is also evidence that the stimulation current level required to evoke an eABR or eCAP response of a specific amplitude decreases with increasing PD and IPG. Neural loss or damage reduces the magnitude of this decrease in the required stimulation current (Prado-Guitierrez et al. 2006; Ramekers et al. 2014). Poorer eCAP discrimination also appears to indicate the loss of spiral ganglion nerve fibres, as well as a reduction in AN synchronization (Ji et al. 2014).

#### 2.6.2.6 Cathodic versus anodic stimulus

Polarity sensitivity studies have shown ANFs to have a higher sensitivity to anodic compared to cathodic polarity suprathreshold stimulation levels (Hughes, Choi and Glickman 2018; Undurraga, Carlyon et al. 2013). Recent studies have indicated that this polarity sensitivity could correlate to neural degeneration (Jahn and Arenberg 2019). Biophysical modelling data indicate that cathodic stimulation likely excites the peripheral processes, whereas anodic stimulation could potentially initiate action potentials at the central axon (Joshi, Dau and Epp 2017). Consequently, cathodic stimulation may be less effective than anodic stimulation in degenerated ANFs, as degeneration generally progresses from the peripheral processes to the central axon (Herrmann et al. 2021).

### 2.6.3 ECAP response to demyelination

#### 2.6.3.1 Amplitude

Mild myelin damage has been shown to result in slightly reduced eCAP amplitudes. These reductions have also shown the possibility of recovery over time. Severe myelin damage, however, results in reduced amplitudes, elevated thresholds and prolonged peak latencies (El-Badry and McFadden 2009). A study has suggested demyelination as a mechanism for hidden hearing loss, which presents with reduced suprathreshold amplitude of the sound-evoked compound action potential (Wan and Corfas 2017).

#### 2.6.3.2 Latency

The latency of the eCAP waveform is also affected by ANF demyelination. Prolonged N1 latencies in eCAP responses indicate demyelination. The N1 latency also seems to correlate with wave I, III and V eABR latencies. An increase of these latencies indicate a reduction in the ANF's myelin layer (Ito et al. 2004; Zhang et al. 2017).

#### 2.6.3.3 RRP

It has been established that demyelinated fibres have longer eCAP refractory periods than healthy fibres (Kaji 2003). Simulations have also shown that axonal demyelination of the auditory nerve results in an increase in the refractory period due to a reduction in the rate of repolarization of the AP (Quandt and Davis 1992). Both the absolute and relative refractory periods seem to be prolonged when demyelination is present (Low and McLeod 1977).

### 2.6.4 ECAP response to fibre loss

#### 2.6.4.1 Amplitude

Subjects with auditory neuropathy display smaller eCAP amplitudes and significantly higher eCAP thresholds than normal hearing individuals (He, Abbas et al. 2016). Multiple participants demonstrated a statistically significant correlation between maximum eCAP amplitude and spiral ganglion cell (SGC) density (Ramekers et al. 2014).

#### 2.6.4.2 Latency

AN deficiency has been shown to prolong the eCAP N1 latency (Xu et al. 2020). One study showed that CND results in prolonged peak latency and increased response width (He, Chao et al. 2020). Another study indicated that subjects with auditory neuropathy spectrum disorder have longer averaged P1 latencies and greater response widths than subjects who only have sensorineural hearing loss.

#### 2.6.4.3 Interphase gap

Subjects with CND have exhibited a smaller IPG effect on the eCAP threshold and a larger IPG effect on the maximum eCAP amplitude than subjects with normal-sized cochlear nerves (He, Chao et al. 2020). This may be explained by the greater probability of spike initiation near the threshold level in people with normal cochlear nerves, resulting in increased sensitivity to changes in the IPG.

### 2.6.5 EABR testing procedures

The second electrophysiological measure evaluated for this study was eABR waveforms. ABR measurements provide another potential tool for identifying ANF damage (Kujawa and Liberman 2009). ABRs are typically measured by presenting either clicks or tone stimuli and recording electric potentials using surface electrodes placed on the forehead and mastoid (Gorga, Johnson et al. 2006). Instead of directly evaluating a subject's hearing ability, ABR tests evaluate the synchronous auditory neural function (Winston 2013). The ABR measurements present as a series of individual potentials or

waves, that are thought to correspond to the serial processing of the auditory pathway (Eliades and Tsunada 2019). The waveforms consist of approximately seven vertex positive waves, as illustrated by figure 2.4. The ABR wave peaks originate from various auditory structures. Wave I and II are generated by auditory nerve pathways, wave III originates in the cochlear nucleus and wave IV in the superior olivary complex. Wave V is attributed to the lateral lemniscus (S. Abdelsalam and Omar 2015).

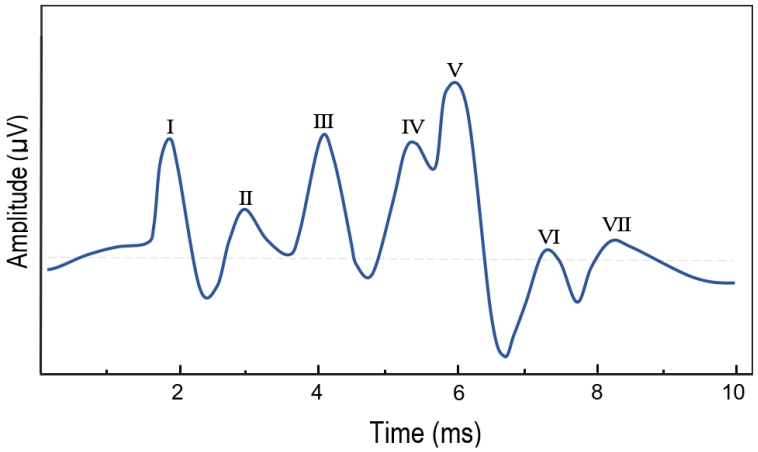


**Figure 2.4.** A basic eABR waveform.

Only waves I to V are generally assessed for neural diagnostic purposes. For CI users eABRs are measured using the implanted electrode array and surface electrodes. These eABR waveforms can be used to distinguish between the various neural damage mechanisms: neural degeneration, demyelination and fibre loss. The wave delays or latencies, amplitudes and wave functions are all characteristics that could contribute to the identification of the type and level of damage to the AN.

### 2.6.6 EABR response to degeneration

#### 2.6.6.1 Amplitude

Abnormalities in the amplitudes of the various waves of the eABR waveform appear to correspond to the amount of damage to, or loss of, ANFs. Damage to the ANFs appears to result in reduced supra-threshold eABR amplitudes (Furman, Kujawa and Liberman 2013). Studies specifically examining the amplitudes of eABR wave I or wave V showed a significant correlation between reduction of these amplitudes and the level of auditory neuropathy (Stamper and Johnson 2015; Verhulst, Bharadwaj

et al. 2015; Rance and Starr 2015; Barbee et al. 2018; Buran et al. 2020; Liberman and Kujawa 2017).

#### 2.6.6.2 Latency

In eABR measurements, an increase in latency of the waves has been identified as a means of determining auditory nerve damage (Kasbekar et al. 2019). Various encephalomyopathies and neural disorders, as well as vestibular schwannomas, have been shown to affect auditory neural conduction, resulting in increased eABR interwave latencies (Eggermont 2019).

#### 2.6.6.3 Functions

Various functions derived from recorded eABR waveforms offer possible tools for analysing AN damage. For example, steeper slopes in the latency-intensity functions of an eABR wave V seem to indicate sensorineural hearing loss (Gorga, Worthington et al. 1985). The slopes of the eABR input-output functions also appear to correlate with AN survival (Pfingst, Zhou et al. 2015). The amplitude ratio of wave V to wave I has also been examined for possible use in identifying AN dysfunction (Rance and Starr 2015).

### 2.6.7 EABR response to demyelination

#### 2.6.7.1 Amplitude

Studies have shown that poor auditory nerve myelination may result in decreased wave I amplitudes and elevated wave I thresholds (Zhou, Abbas and Assouline 1995). Demyelination disorders have been shown to result in abnormal ABRs with reduced amplitudes (Rance and Starr 2015).

#### 2.6.7.2 Latency

Demyelination of ANFs results in diminished functionality of a CI, as the conductivity of the AN is affected. Studies have shown that myelin deficits may cause increased eABR wave I latencies, as well as increases in the interval latencies between wave II-IV and wave III-IV (Ito et al. 2004; Zhang et al. 2017). These suprathreshold latencies seem to reflect the importance of myelination for the AN's conduction velocity (Long et al. 2018). Some studies offer the loss of Schwann cells as an explanation for the prolonged latency and increased width of eABR wave I (Wan and Corfas 2017).

#### 2.6.7.3 Threshold

Demyelination also seems to result in elevated eABR thresholds (Zhang et al. 2017; Long et al. 2018). In cases of severe myelin damage, eABR readings may be completely absent (El-Badry and McFadden 2009).

### 2.6.8 EABR response to fibre loss

#### 2.6.8.1 Amplitude

Patients with CND, which usually refers to a small or absent auditory nerve, have been shown to display decreased wave V amplitude (Wang, Guo et al. 2022). Cochlear malformations, which often include hypoplasia, may result in reduced wave III amplitudes (Di Stadio et al. 2019)

#### 2.6.8.2 Latency

Patients with CND have additionally been shown to exhibit delayed wave V latency (Wang, Guo et al. 2022). Another study also found that cochlear nerve hypoplasia results in an evoked eABR wave with delayed latency (Yamazaki et al. 2015)

## 2.7 ANF MODELS

Many of the first ANF models were based on animal morphology, such as the unmyelinated giant squid-based model from Hodgkin and Huxley (1952), the myelinated frog-based model from Frankenhaeuser and Huxley (1964) and the rat-based model from Schwarz and Eikhof (1987). The animal morphology was used, as detailed anatomical information can be obtained from animal experiments, which cannot be gained from human studies. Developing ANF models which more closely reflect human morphology may allow more accurate model predictions of physiologically measured data. For this reason, the conductance-based model presented in Hodgkin and Huxley (1952) has since been adjusted to take into account that human neurons function at higher temperatures than squid neurons, which accelerate several of the gating processes. Another model adjustment of conductance values is required to accommodate higher channel density (Macherey et al. 2007).

Three such adapted models are briefly discussed. Smit, Hanekom and Hanekom (2009) developed a modified HH compartmental model which was based on the original nerve morphology by Rattay, Lutter and Felix (2001). This model included a human Ranvier node which was achieved by slowing down the fast activating potassium current kinetics and modifying several parameters including resting membrane potential, membrane capacitance, ionic and leakage conductances and corresponding equilibrium potentials to better reflect corresponding human parameter values. The model was then further improved by adding a persistent sodium current which was integrated into a generalised single cable human sensory ANF model (Smit, Hanekom and Hanekom 2009).

Another adapted model was developed by Briaire and Frijns (2005), which is based on the Schwarz-Eikhof-Frijns model (Frijns, Snoo and Schoonhoven 1995). The modifications included a 10 $\mu$m soma diameter and a 2 $\mu$m pre-somatic compartment as implemented by by Rattay, Lutter and Felix (2001) which required nodes of Ranvier with corresponding diameters to be added to that segment (Briaire and Frijns 2005). The internodal distances of the dendrite was also scaled to ensure the correct anatomical position of the dendritic terminal nodes and soma when the nerve model was integrated with the cochlear VC model (Briaire and Frijns 2005).

A third adapted model is a compartmental ANF model which is based on the Hodgkin-Huxley model and was developed by Rattay, Lutter and Felix (2001). In this compartmental model each sub-unit is modelled separately. This HH squid-based model was adjusted for the increased temperatures at which human nerves function by multiplying the right side of the differential equations for the gating variables ($m$, $n$ and $h$) by 12 in order to accelerate the gating processes. The model also accounted for 10-fold channel density by multiplying the potassium, sodium and leakage conductance values by 10. This model aimed to reflect human morphology by including alternating unmyelinated dendritic nodes and dendritic internodes, unmyelinated compartments around the soma, an unmyelinated soma and alternating unmyelinated and myelinated central axon internodes (Rattay, Lutter and Felix 2001).

## 2.8 ELECTRODE POSITION

The electrode-to-modiolar distances of the implanted CIs have to be taken into account when analysing electrophysiological responses, as they may affect these responses. Studies have found that electrode-to-modiolar distances may contribute to the current level required for suprathreshold stimulation. This also means that increased neural responses can be generated at the same stimulation level by decreasing modiolar distance (Davis et al. 2016).

Different electrode array designs affect the electrode-to-modiolar distances. Pre-curved arrays, such as the perimodiolar arrays, have been shown to have significantly reduced electrode-to-modiolar distances compared to straight arrays (Davis et al. 2016). Perimodiolar electrodes correlate to lower eCAP threshold values as a result of closer nerve–electrode interaction (Christov et al. 2016).

Studies examining the correlation between eCAP parameters and SGN survival have also noted that non-neural factors, such as electrode-modiolus distance must be taken into account when analysing eCAP results to determine neural survival (Brochier, McKay and Carlyon 2021). This supposition

is supported by another study which cites significant correlation between eCAPs and electrode-to-modiolar distances (Wermeskerken, Olphen and Graamans 2009). Increased modiolus-electrode distance appears to correlate with higher eCAP thresholds (Lee et al. 2020).

The correspondence between eABRs and electrode-to-modiolar distances have also been investigated. Moving the electrode from the cochlear outer wall towards the modiolus has shown significant reductions in eABR thresholds as well as a general decrease in the gradient of the eABR input-output function (Shepherd, Hatsushika and Clark 1993). This was corroborated by a study that showed a reduction in the eABR threshold when the electrode array was moved from a lateral to a medial position in the cochlea (Risi 2018).

## 2.9 CHAPTER SUMMARY

Existing electrophysiological measurements, various types of hearing loss, and the underlying mechanisms of ANF damage were investigated for this literature study. From the literature it was determined that eCAPS and eABRS are the most promising measurements for use in determining ANF damage in this study. This chapter reviewed the information available in the literature about the effect of degeneration, demyelination and fibre loss on the prominent characteristics such as the amplitude and latency of eCAP and eABR waveforms. The available data was compiled into a comprehensive table for reference purposes when analysing electrophysiological response characteristics for indicators of several damage mechanisms.

The information compiled from the literature is then utilized in this study to propose a method for parameterizing the mechanisms that define various neural damage types (ANF degeneration, demyelination, and fibre loss). These mechanisms can then be identified in clinical eCAP and eABR responses. The clinical damage profiles can then be used to add another layer of user-specificity to their model. These models can be used to investigate the health of a CI user's auditory nerve and allow for model-based diagnostics.

# CHAPTER 3 METHODS: ANF MODELLING

## 3.1 CHAPTER OVERVIEW

In section 3.2 the single fibre and population models used in this study are described. Section 3.3 outlines the expected effects of ANF damage on eCAP responses, and describes the process of applying ANF damage to the neural models. The evaluation of the single fibre and ANF population models as predictors of eCAP responses to ANF damage as anticipated from the literature is shown in sections 3.4 and 3.5, respectively. Section 3.6 provides a discussion of the eCAP responses to damage. A chapter overview is presented in section 3.7.

## 3.2 MODELLING AUDITORY NERVE FIBRES

### 3.2.1 ANF model

Elementary computational auditory neural models were constructed in MATLAB[1] to examine the effects of degeneration and demyelination of the ANF on eCAP amplitude and latency. The morphology used for the construction of the single human auditory neuron model is based on the neural model developed by Badenhorst, Hanekom and Hanekom (2017). The model is rooted in the Hodgkin-Huxley-based human compartmental ANF model of Rattay, Lutter and Felix (2001). The ANF has 26 active nodes and 47 compartments in total. Additionally, the dendrite's inter-nodal distances were scaled in accordance with the model by Kalkman, Briaire, Dekker et al. (2014). This scaling was done to compensate for the temperature constraints of the Rattay model and to increase the anatomical accuracy regarding the dendritic terminal nodes at the lateral edge of the spiral lamina and of the soma in Rosenthal's canal. The neural model is illustrated in figure 3.1.

[1] MATLAB 2018a, The MathWorks, Inc., Natick, Massachusetts, United States

The first simulation of the eCAP measurement was set up using a single neuron model with two monopolar point electrodes. The electrodes are aligned along the fibre as seen figure 3.2. The single fibre response is technically not an eCAP response as the response is not *compound* and should be called a single fibre action potential (SFAP). The single fibre response should still give some indication of the expected responses to neural damage as eCAPs represent a synchronous response of multiple electrically stimulated nerve fibres. A biphasic, cathodic-first stimulus with a 100 $\mu$s pulse width was used in this simulation (figure 3.3). Both the stimulating and recording electrodes were located 0.75 mm above the straight fibre within an infinite homogeneous medium. The stimulating electrode was placed above node 1 and the recording electrode was placed 20 mm further along the fibre. The modelling temperature was set at 37°C for all simulations.

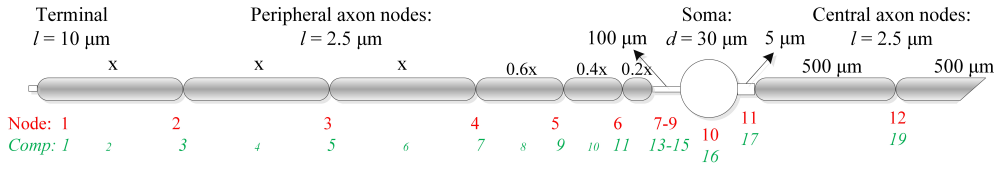


**Figure 3.1.** Illustration of the single ANF model used for simulations, taken from Badenhorst, Hanekom and Hanekom 2017 with permission.

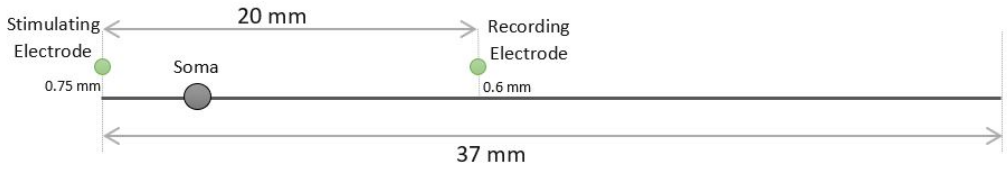


**Figure 3.2.** Electrode placement relative to single nerve fibre in the simulation.

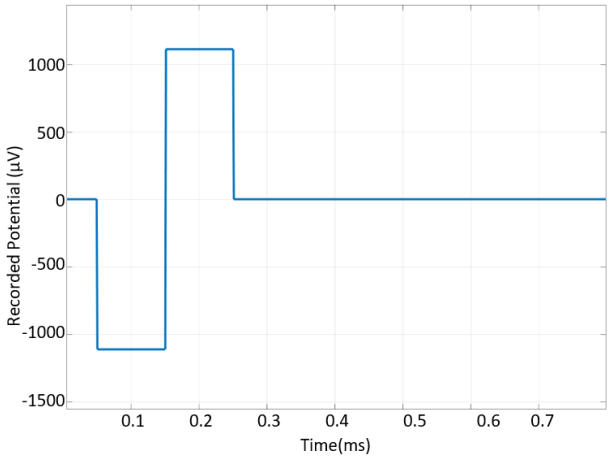


**Figure 3.3.** Example of a biphasic, cathodic-first stimulus with a 100 $\mu$s pulse width.

### 3.2.2 Population ANF model

An elementary ANF population model was created that contains a population of 101 straight ANFs (figure. 3.4). The ANFs are uniformly spaced around a semicircle with a diameter of 6 mm that mimics the curve of the organ of Corti in the basal turn of the cochlea. While this model was not intended to serve as an anatomically accurate population model, it allowed transverse alignment of electrode contacts with different fibres in the population instead of the electrodes being aligned along the fibre as seen in the single fibre model (figure. 3.2).

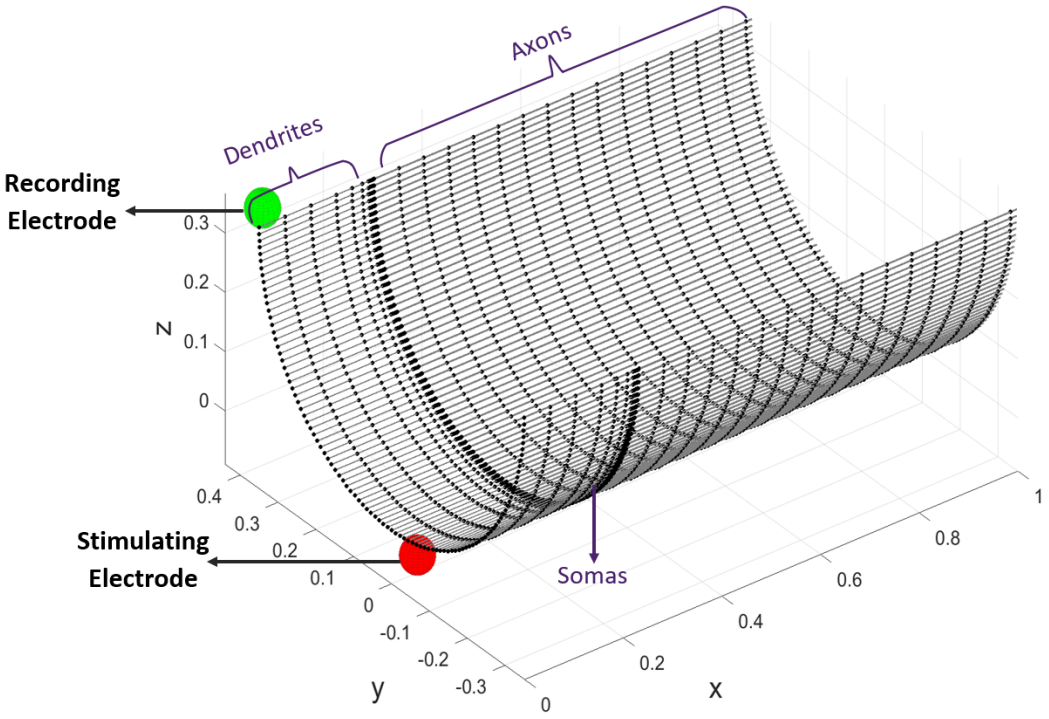


**Figure 3.4.** Illustration of the ANF population model and electrode placement used in simulation.

### 3.2.3 Models setup

The computational models are based on a system of transmembrane voltage dependent HH-based differential equations (Hodgkin and Huxley 1952). The computational ANF model includes adjustable parameters that can used to simulate different types and levels of ANF damage in the model, specifically the number of myelin layers and compartments to be removed from the modelled nerve fibres.

## 3.3 MODELLING NEURAL DAMAGE

Neural damage parameters can be established using either eCAP or eABR measurements, or both as complimentary measurements. These parameters inform the type and level of damage to the nerve fibres in a peripheral auditory model. In this study parameters for damage mechanisms were applied to ANF models, after which electrophysiological measurements of the auditory periphery (eCAPs) were simulated to evaluate the predicted output from the neural damage model against the expected eCAP responses.

### 3.3.1 Damage parameters

The information obtained from a review of available literature concerning eCAP and eABR responses was consolidated to produce a tabled inventory of the electrophysiological responses that are associated with each type of neural damage. The combination of these tables and the eCAP damage templates allow the prediction of eCAP responses to various types and degrees of neural damage.

Table 3.1 shows the effect of neural damage on eCAP responses as reported in the literature. The effects of ANF demyelination, ANF degeneration and ANF loss on an eCAP response are illustrated in figure 3.5 a to c.

**Table 3.1.** A summary of the qualitative eCAP responses to neural damage in comparison to normal eCAP waveform responses.

| Observed response | References | Damage Mechanism |
|---|---|---|
| Prolonged N1 latency. | Ito et al. 2004<br>Zhang et al. 2017<br>El-Badry, Ding et al. 2007 | Demyelination |
| Increased eCAP relative refractory periods. (Slower recovery) | Quandt and Davis 1992<br>Kaji 2003<br>Low and McLeod 1977 | |
| Reduced suprathreshold amplitude | El-Badry, Ding et al. 2007<br>Wan and Corfas 2017 | |
| Reduced N1 latency at stimulation levels near saturation. | Schvartz-Leyzac and Pfingst 2016<br>Stypulkowski and van den Honert 1984<br>Lai and Dillier 2000 | Degeneration |
| Shorter eCAP relative refractory periods. (Faster recovery) | Botros and Psarros 2010<br>Smit, Hanekom and Hanekom 2008* | |
| Significantly higher eCAP thresholds | He, Shahsavarani et al. 2018; He, Xu et al. 2020 and Shepherd, Roberts and Paolini 2004 cited in Skidmore et al. 2020 | Fibre Loss |
| Smaller maximum eCAP amplitudes | He, Xu et al. 2020 | |
| Flatter slopes of input-output functions | He, Shahsavarani et al. 2018 | |

(* Based on simulated data)

The template below illustrates the expected eCAP responses to demyelination, degeneration and fibre loss. The three figures in the template illustrate the expected change of eCAP characteristics such as latency and amplitude when various ANF damage mechanisms are applied. The solid black waveforms represent the eCAP response of a healthy nerve, while the coloured lines represent the expected eCAP response of a damaged nerve.

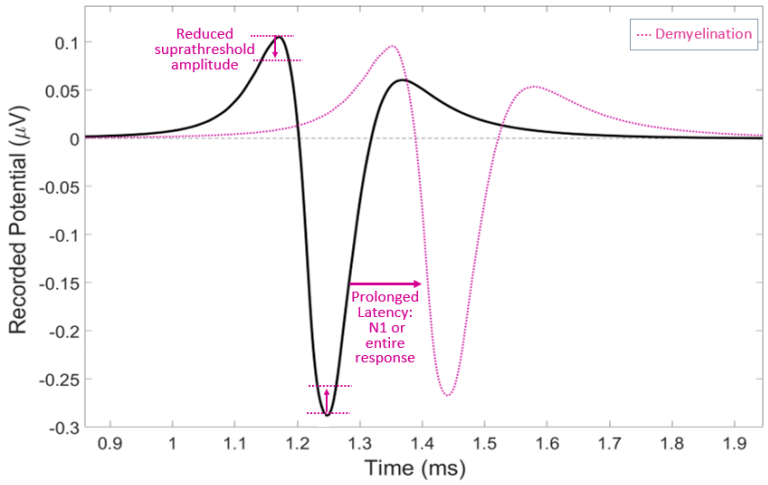


**(a)**

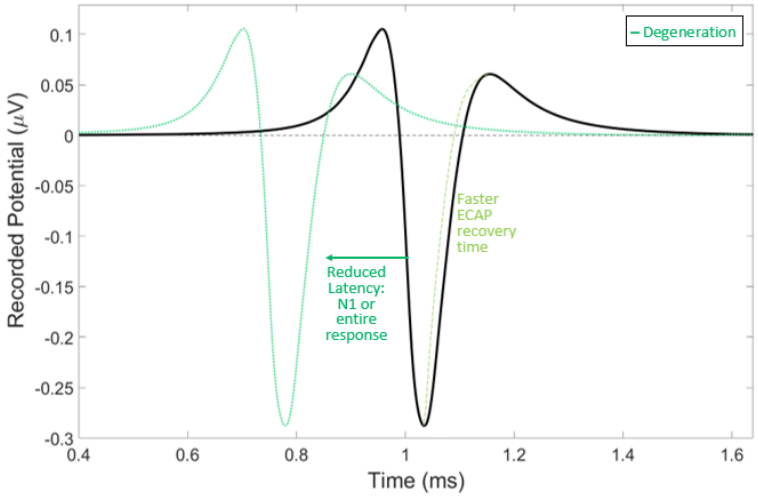


**(b)**

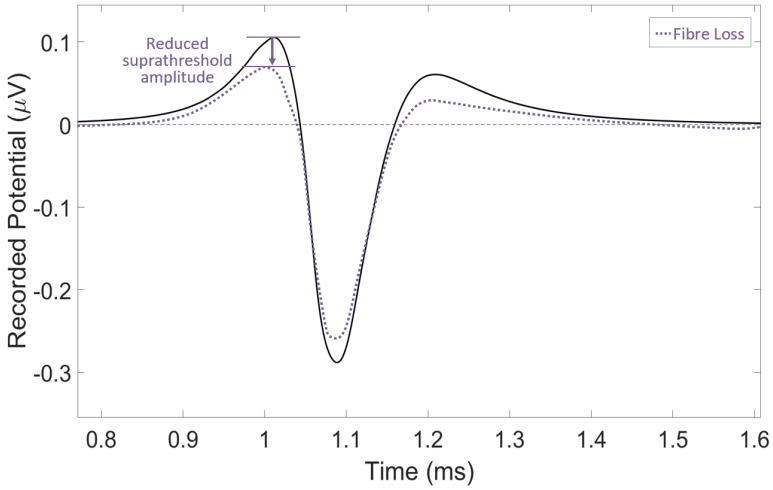


**(c)**

**Figure 3.5.** Template of SFAP and eCAP responses to (a) degeneration (b) demyelination and (c) fibre loss.

Table 3.2 shows the relation of eABR responses to neural damage. The effects of ANF demyelination, ANF degeneration and ANF loss on an eABR response are illustrated in figure 3.6 a to c.

**Table 3.2.** A summary of the qualitative eABR responses to neural damage in comparison to normal eABR waveform responses.

| **Observed response** | **References** | **Damage Mechanism** |
|---|---|---|
| Reduced suprathreshold amplitudes of waves I-V. | Starr, Picton and Kim 2001<br>Skoe and Tufts 2018<br>Wan and Corfas 2017 | Demyelination |
| Prolonged wave I latency. | Zhang et al. 2017<br>Ito et al. 2004<br>Skoe and Tufts 2018 | |
| Increased interpeak latency. | Rance and Starr 2015 | |
| Reduced wave I suprathreshold amplitude. | Liberman and Kujawa 2017 | Degeneration |
| Prolonged wave V latency. | Jerger and Johnson 1988<br>Skoe and Tufts 2018<br>Bhattacharyya 2021 | |
| Increase in relative wave V to I amplitude | Rance and Starr 2015<br>Hickox and Liberman 2014, Schaette and McAlpine 2011 and Gu et al. 2012 cited in Verhulst, Bharadwaj et al. 2015 | |
| No eABR can be elicited: cochlear nerve aplasia. | Han et al. 2019 | Fibre Loss |
| Higher thresholds in eABRs: cochlear hypoplasia | Yamazaki et al. 2015 | |
| Reduced eABR Wave I amplitudes | Furman, Kujawa and Liberman 2013, Stamper and Johnson 2015 and Schaette and McAlpine 2011 cited in Verhulst, Jagadeesh et al. 2016 | |
| Reduced eABR Wave V amplitudes | Di Stadio et al. 2019 | |

The template below illustrates the expected eABR responses to demyelination, degeneration and fibre loss. The three figures in the template illustrate the expected change of eABR characteristics such as latency, interpeak latency and amplitude when various ANF damage mechanisms are applied. The solid black waveforms represent the eABR response of a healthy nerve, while the coloured lines represent the expected eABR response of a damaged nerve.

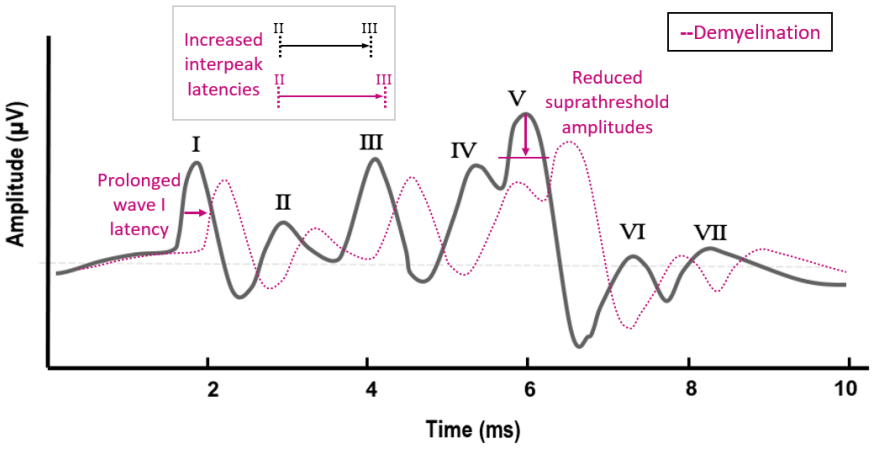


(a)

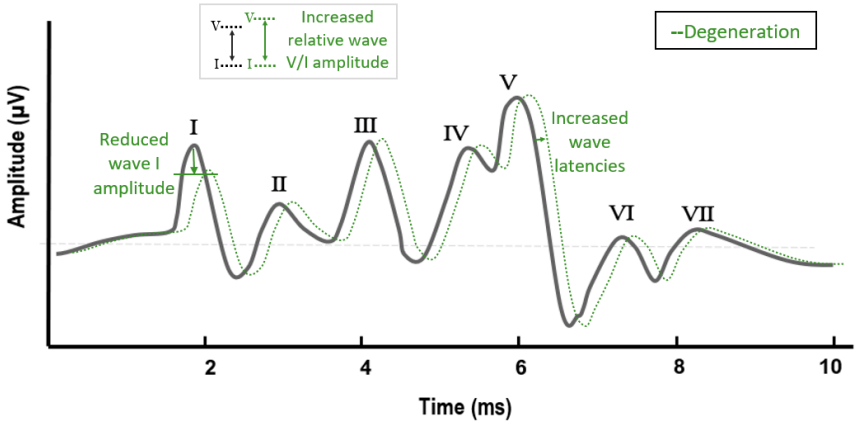


(b)

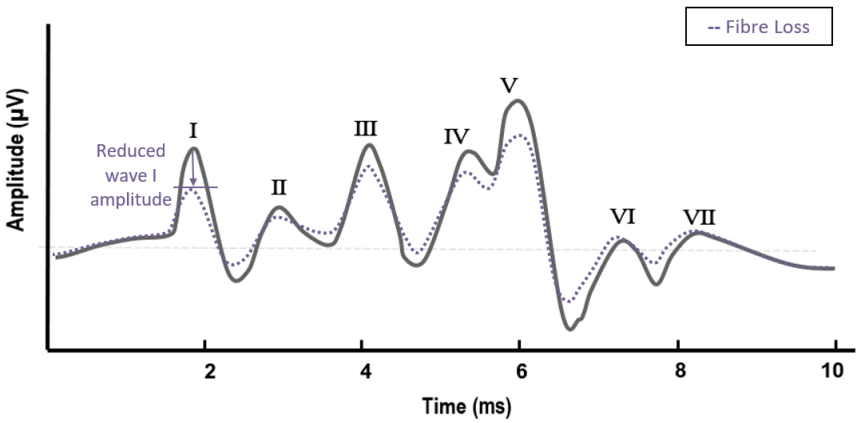


(c)

**Figure 3.6.** Template of eABR responses to (a) degeneration (b) demyelination and (c) fibre loss.

### 3.3.2 Applying ANF damage to models

Both the single fibre model and simplified ANF population model were evaluated as predictors of the neural response to ANF damage as observed in electrophysiological measurements established in the literature. Only the population model could be evaluated as a predictor of the effects of fibre loss.

#### 3.3.2.1 Demyelination simulation

Demyelination of the AN was simulated by reducing the ANF's dendrite and axon myelin layers to examine the effect on the eCAP. The ANF consisted of six unmyelinated dendritic nodes, six myelinated dendritic internodes with 40 layers of myelin, three pre- and one post-somatic unmyelinated compartments, an unmyelinated soma, 69 central axon nodes and 69 myelinated central axon internodes with 80 layers of myelin. All unmyelinated sections were simulated with a single layer of myelin, except for the soma, which had three layers (Rattay, Lutter and Felix 2001). In the demyelination simulations the dendrite myelin layers were reduced from 40 to 37 and then 34. When myelin was reduced to less than 34 layers, an action potential was triggered in the nerve fibre, but could not propagate along the nerve. The axon's demyelination was applied by removing 20 layers incrementally to reduce the myelination from 80 to 40 layers.

#### 3.3.2.2 Degeneration simulation

Neural degeneration was simulated by progressively removing compartments from the dendritic end of the nerve fibre. The location of the electrode relative to the fibre terminal affects the stimulation intensity required to elicit a response. Since the electrode location was fixed over node 2, systematic truncation of the nerve fibre resulted in progressively higher stimulation intensities required to generate responses in the nerve fibres. Both ANF degeneration and stimulus intensity affect eCAP amplitude and latency. To isolate and best display the effect of ANF degeneration on eCAPs, it was necessary to select a range of fibre truncations which allow neural excitation at the same stimulation intensity for the simulations in this section.

#### 3.3.2.3 Fibre loss simulation

Partial ANF loss can be the result of either a congenital condition or severe neural degeneration. In a modelling context, fibre loss can be implemented through the selective removal of ANFs.

## 3.4 EVALUATING THE SINGLE FIBRE NERVE MODEL AS A PREDICTOR OF NEURAL RESPONSE TO ANF DAMAGE.

The effects of the gradual demyelination and degeneration of the single nerve fibre modelled in MATLAB are presented below.

### 3.4.1 Demyelination: single fibre

The effects of demyelination of the dendrite, the axon and both the dendrite and axon were investigated. Figure 3.7 illustrates the effects of (a) demyelination of only the dendrite and (b) only the axon on the SFAP. Both the axon and dendrite demyelination follow the same trend as that of full fibre demyelination, as illustrated in figure 3.8.

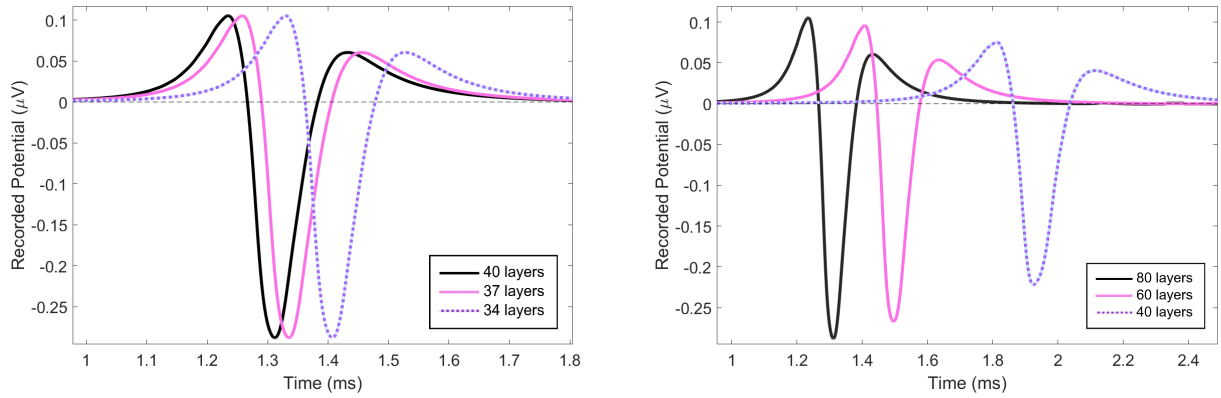


**(a)** **(b)**

**Figure 3.7.** Demyelination of the (a) dendrite and (b) axon of a single ANF, illustrating varying degrees of increased latencies and RRPs, and reduced amplitudes of the SFAP response.

All three of these modelled ANF SFAP responses to demyelination displayed the expected increased latencies, RRPs, and reduced amplitudes varying degrees.

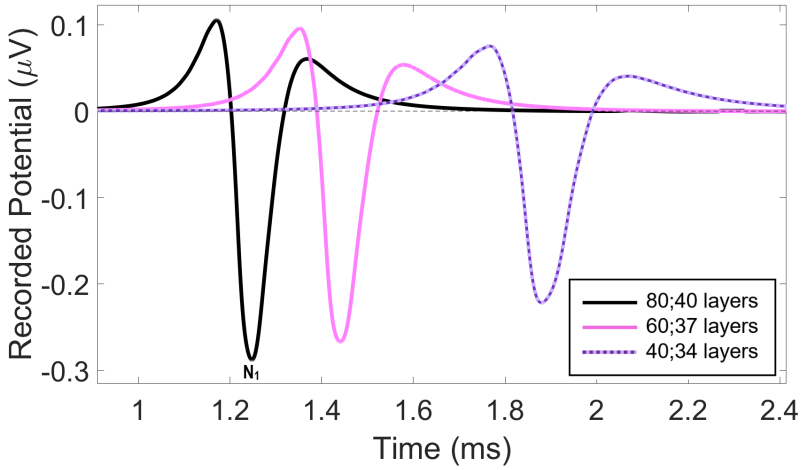


**Figure 3.8.** Demyelination of the full neural length of a single neural fibre, also illustrating increased latencies and RRPs and reduced amplitudes of the SFAP response.

### 3.4.2 Degeneration

Figure 3.9 shows the SFAP response to the neural degeneration up to the seventh, ninth and eleventh neural compartment at stimulation near saturation. These three truncations all generated neural responses at the same stimulus intensity, so that SFAP latency and amplitudes may be compared. The single fibre model predicts a negligible latency reduction in response to fibre degeneration. The c0 value referred to in the legend of figure 3.9 indicates the compartment at which the neural fibre starts. Thus, for c0 = 7 the first 6 compartments of the fibre are removed etc.

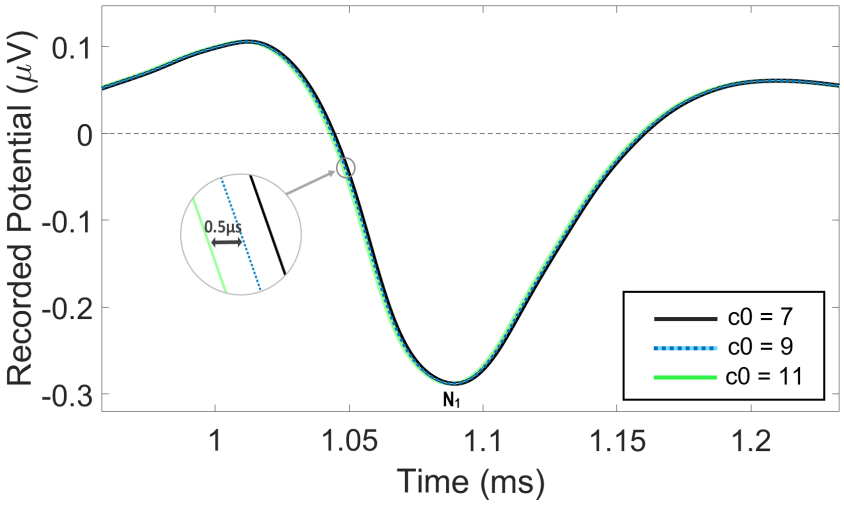


**Figure 3.9.** Figure illustrating the effect of degeneration in a single fibre's AP response.

#### 3.4.2.1 Compound damage

Compound damage to the ANFs was simulated by gradually removing myelin layers from the ANFs while progressively degenerating the fibre.

Figure 3.10 shows the SFAPs in response to neural degeneration and demyelination of the full nerve fibre. The results show the truncation of six compartments, with no myelin damage; the truncation of eight compartments with 37 layers of dendrite myelin and 60 layers of axon myelin; and finally the truncation of ten compartments with 34 layers of dendrite myelin and 40 layers of axon myelin.

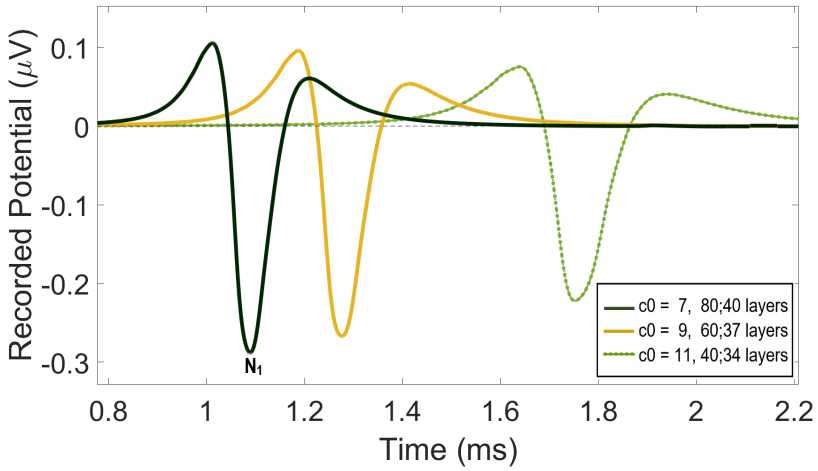


**Figure 3.10.** Total single fibre degeneration and demyelination.

From the compound damage response, it seems that one of the damage mechanisms will dominate the overall SFAP response. The negligible effect of degeneration in the single fibre model is maintained when compound damage is applied so that the SFAP response is dominated by demyelination which is characterised by increased N1 latency.

#### 3.4.2.2 Fibre loss

The effects of fibre loss could not be modelled for a single fibre model. The simplified population model was used to investigate the effects of fibre loss.

## 3.5 EVALUATING THE NEURAL POPULATION MODEL AS A PREDICTOR OF NEURAL RESPONSE TO ANF DAMAGE

The effects of the gradual demyelination, degeneration and fibre loss of the MATLAB neural fibre population model are presented below.

### 3.5.1 Modelling ANF population damage

A single fibre action potential is not a true eCAP, as it only reflects the activity of one neuron. To simulate a true compound action potential, an ANF population is required. The placement of the electrode relative to the nerve will also affect the generated eCAP. In a single fibre model there is no population for the electrodes to be placed relative to, and as a result the recording electrode is placed a few compartments down from the stimulating electrode on the single nerve fibre. Figures 3.11 and 3.12 illustrate the two possible electrode placements.

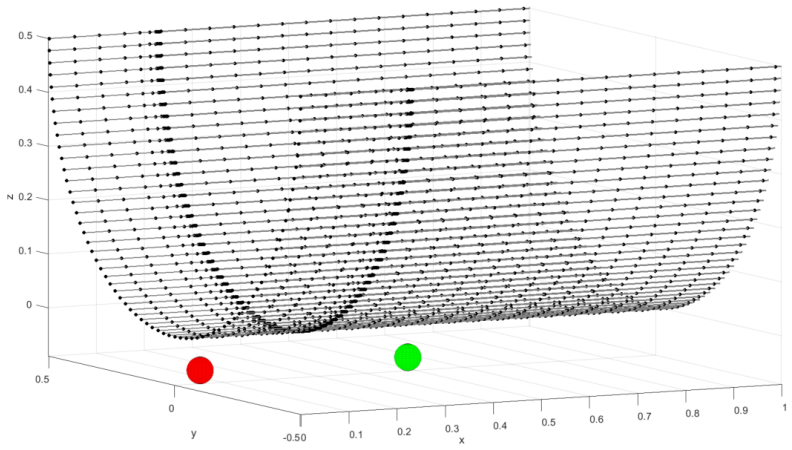


**Figure 3.11.** Electrode placement along nerve fibres.

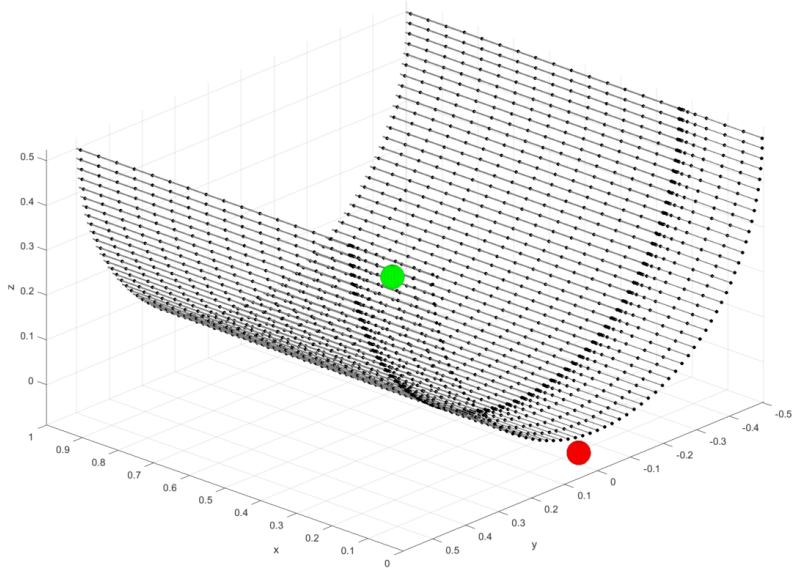


**Figure 3.12.** Electrode placement across nerve fibres.

The effect of these electrode placements on population eCAP responses to fibre degeneration can be seen in figure 3.13. The images demonstrate how important realistic electrode placement is to the eCAP modelling process.

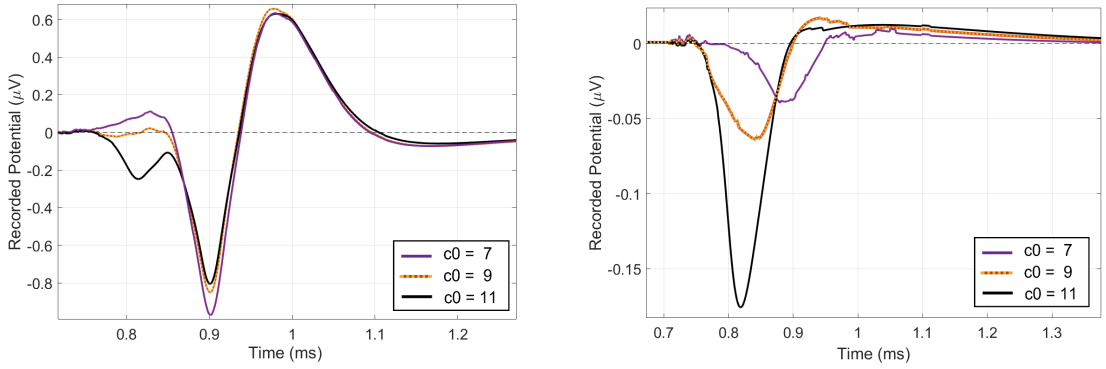


**(a)** **(b)**

**Figure 3.13.** The effect of electrode placement on neural population eCAP responses to degeneration. The figure shows the eCAPs as recorded by electrodes placed (a) along and (b) across the nerve fibre population, as illustrated in figures 3.12 and 3.11.

The improved accuracy of the AP generation as a result of the spacial separation of the fibres in the population model provided a closer approximation to measured compound action potentials than that of the single fibre model. The recording electrode was placed at the boundary of the population, over node 2 of fibre 100. The stimulus electrode was placed approximately in the middle of the population, over the second node of fibre 51 (Fig. 3.4). A biphasic, cathodic-first stimulus with a 25$\mu$s pulse width and IPG of 8$\mu$s was used in these simulations. The modelling temperature was again set at 37°C for all simulations. A two-pulse forward masking technique was used for artefact reduction in the eCAP simulation.

#### 3.5.1.1 Demyelination

The effects of demyelination of the dendrite, the axon and both the dendrite and axon of the entire ANF population were investigated. Figures 3.14(a) and 3.14(b) illustrate the demyelination of the dendrites and axons respectively. Figure 3.15 illustrates the effect of demyelination of both the dendrite and axon. All three scenarios follow the same trend. The eCAP latencies and amplitudes predicted by the single fibre model and population model cannot be directly compared, as the placement of the stimulation and recording electrodes differs between the models. However, both models show an

increase in latency and relative refractory times, as well as a minor reduction in eCAP amplitude with increasing demyelination, which is consistent with the literature (see table 3.1).

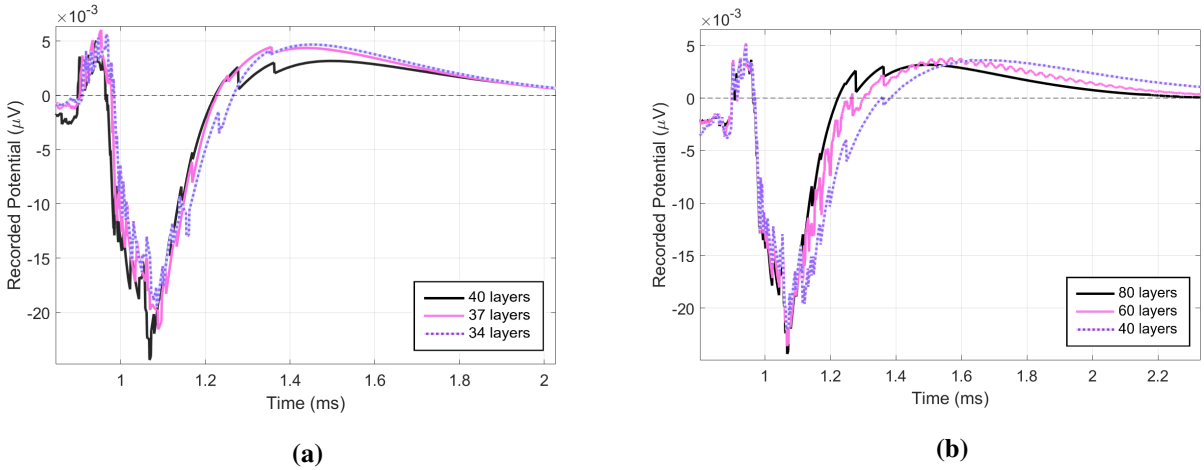


**Figure 3.14.** The eCAP response of a population of nerve fibres after various levels of demyelination were applied to the nerves' (a) dendrites and (b) axons, demonstrating increasing latencies and RRPs and decreasing amplitudes as demyelination increased.

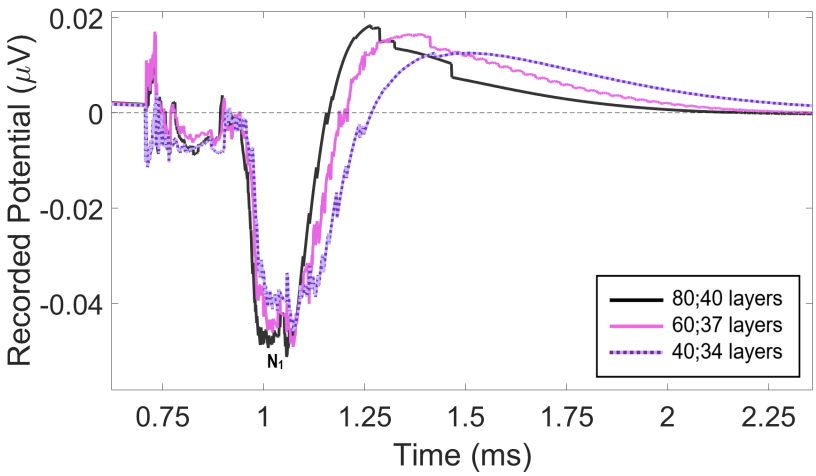


**Figure 3.15.** The eCAP response of a population of nerve fibres after various levels of demyelination were applied to the full neural length, demonstrating increasing latencies and RRPs and decreasing amplitudes as demyelination increased.

### 3.5.1.2 Degeneration

Figures 3.9 and 3.16 show the eCAP response to the neural degeneration of up to the seventh, ninth and eleventh neural compartments at stimulation near saturation. The population model predicts

the expected reduction in eCAP latency with increased degeneration of the fibre model, though the reduction predicted for the single fibre model is almost negligible.

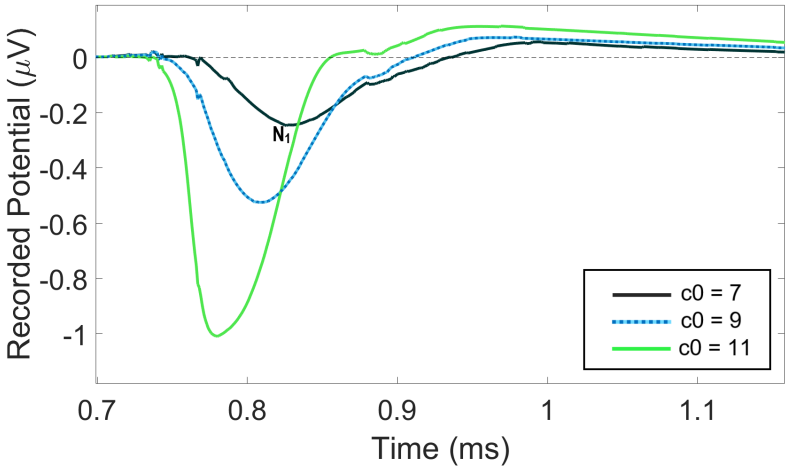


**Figure 3.16.** Figure illustrating the effect of degeneration in a ANF population's eCAP response.

#### 3.5.1.3 Fibre loss

Fibre loss can only be modelled in a population model. Although different configurations of fibre loss may be possible, in this simulation fibre density was uniformly reduced over the population. The model predicts the expected reduction in amplitude, as fewer fibres contribute to the eCAP. Fibre loss seems to affect the eCAP latency with shorter latencies predicted for fewer fibres for this particular simulation setup. However, the exact manner in which the latency is affected may depend on the specific configuration of fibre loss.

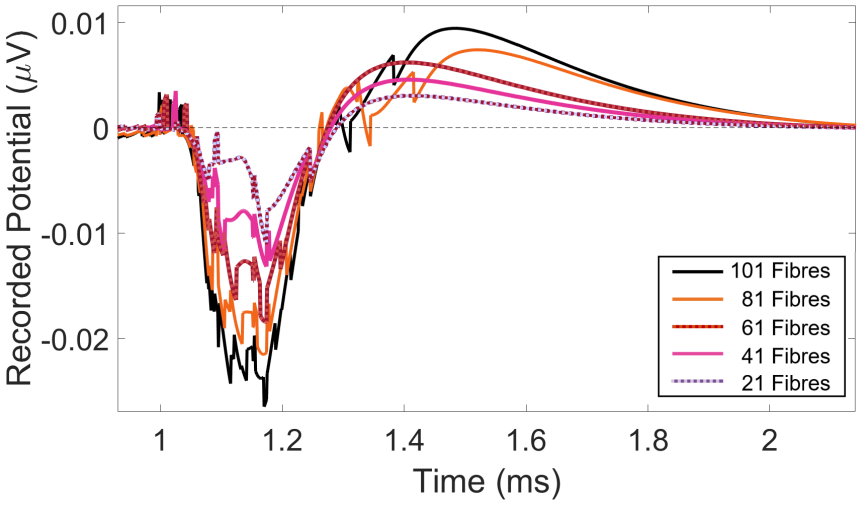


**(a)**

**Figure 3.17.** Fibre loss population.

#### 3.5.1.4 Compound damage

Compound damage to the ANFs was simulated by gradually reducing myelin layers from the ANFs and simultaneously degenerating the fibre incrementally. Figure 3.18 shows the eCAPs in response to neural degeneration and demyelination of the full nerve fibre.

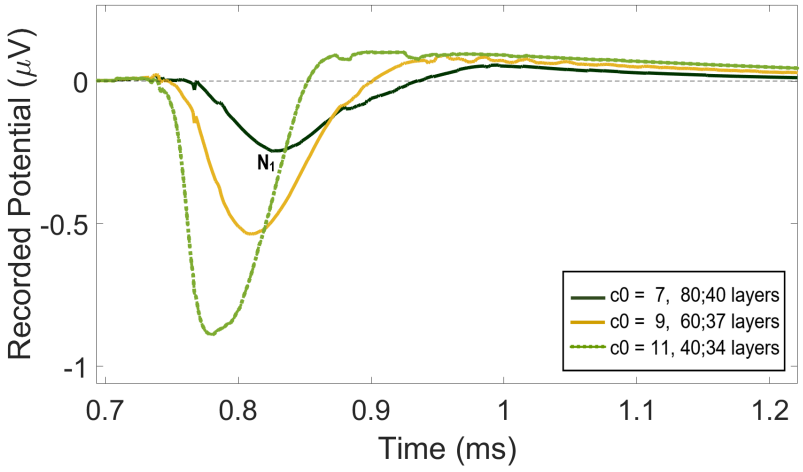


**Figure 3.18.** Total population degeneration and demyelination.

From the predictions from both the single fibre and population models' response to compound damage, it is evident that a single mechanism dominates the eCAP response. In the population model the

effect of compound damage on the eCAP response is dominated by degeneration, characterised by reduced N1 latency, faster recovery and an increase in the eCAP amplitude. The increase in amplitude may reflect increased excitability of the ANFs as a result of dendritic degeneration (Šišková et al. 2014). This response contrasts with the response of the single fibre model to compound damage, where demyelination appears to be dominant. This suggests that the electrode and nerve fibre configuration of the model used to predict eCAP responses is an important factor to consider, as the model configuration may emphasize a specific damage mechanism.

The predominance of a single damage mechanism in the compound damage response can be seen in the separate damage simulation setups as well. Table 3.3 illustrates the average latency difference between population demyelination and degeneration.

**Table 3.3.** Comparison of population model eCAP N1 Latency: Degeneration vs Demyelination.

| Nerve Fibre Condition | N1 Peak Latency ($\mu$s) | Latency Difference ($\mu$s) |
|---|---|---|
| **Degeneration of 6 compartments (c0 = 7)** | 829 | |
| **Degeneration of 8 compartments (c0 = 9)** | 808 | 21 |
| **Degeneration of 10 compartments (c0 = 11)** | 778 | 30 |
| **Demyelination (Dendrite 40 layers, Axon 80 layers)** | 1057 | |
| **Demyelination (Dendrite 37 layers, Axon 60 layers)** | 1073 | 16 |
| **Demyelination (Dendrite 34 layers, Axon 40 layers)** | 1075 | 2 |

The results shown in the table above demonstrate that the magnitude of the latency shifts or differences produced by degeneration in the eCAP is larger than those generated by demyelination.

## 3.6 DISCUSSION

This section of the study evaluates the prediction of various damage mechanisms and subsequent electrophysiological responses by computational models by comparing the model responses to what is reported in the literature . The models predict eCAP responses to three types of neural damage and a combination thereof to provide a basis for including appropriate neural damage when modelling the auditory periphery for diagnostic purposes.

### 3.6.1 Factors which influence model accuracy

Two models were implemented, a single fibre model and an elementary population model suitable to be adapted for integration in volume conduction models. The orientation of the stimulating and recording electrodes relative to the peripheral fibre terminal proved important. In the single fibre model the recording electrode was placed over the central process of the fibre. However, the simulations show that degeneration affects the initiation of the action potential at the periphery where the damage is inflicted rather than the subsequent propagation of the action potential. For this reason it is necessary to place the recording electrode in the proximity of the dendrite. The single fibre model proved more sensitive to demyelination than degeneration when subjected to combined damage, in contrast to the population model's response. The single fibre model was used to investigate the suitability of this neural model to predict neural responses to ANF damage. The single fibre predictions demonstrated the damage mechanisms from literature. Since the modelling setup for the single fibre model does not correspond to the anatomical placement of electrodes in a cochlea, the predictions by the model are not suitable to represent complex eCAP responses or combined damage scenarios. Therefore, a population model has to be used when investigating person-specific AN damage.

### 3.6.2 ECAP response to damage

Degeneration of the ANFs caused shorter latencies and faster eCAP recovery functions. In both models demyelination of the nerve fibres resulted in delayed N1 latencies and reduced amplitudes. Combined degeneration and demyelination of the nerves showed that the eCAPs generated by the population model proved more sensitive to the neural degeneration than the demyelination. The latency changes are more profound for ANF degeneration than demyelination (Table 3.3 on page 46).

These eCAP responses can be used to analyse measured eCAP responses and might allow conclusions as to the subject's cochlear neural health. Reduced suprathreshold amplitudes combined with prolonged N1 latency of the eCAP response would indicate demyelination of the measured ANFs. Demyelination would present a prolonged wave I latency, increased inter-peak latencies and reduced suprathreshold amplitudes in eABR measured waveforms. ANF degeneration is indicated by reduced N1 latency, faster relative refractory period in eCAPS as well as increased wave latencies, reduced wave I amplitudes and an increased relative wave V/I amplitude of eABR measured waveforms. ANF loss is characterised by reduced suprathreshold eCAP and eABR amplitudes in cases of hypoplasia. In cases of severe fibre loss, it may be impossible to evoke eCAP and eABR waveforms.

### 3.6.3 Application of the findings

Using these findings to establish a reliable and consistent protocol for determining the type and extent of AN damage would allow the development of better user-specific model-based diagnostics. From this study a method to include rudimentary user-specificity to the neural component of a computational model of the auditory periphery may be proposed.

(1) Measure the eCAP (and the eABR) response for all active electrodes.

(2) Identify whether degeneration, demyelination or fibre loss dominates the neurophysiological response for the ANF population targeted by the stimulating electrode.

(3) If demyelination was identified as the primary neural damage mechanism, select and apply initial demyelination parameters to the ANF population in the proximity of the stimulating electrode. Two parameters are associated with demyelination: the number of myelin layers lost on the dendritic section of the fibre and the number of myelin layers lost on the axonal section of the fibre. Conversely, if degeneration was identified as the dominant damage mechanism, select and apply an initial degeneration parameter to the ANF population in the proximity of the stimulating electrode. The parameter associated with degeneration is the number of internodal dendritic sections that are truncated from the fibre model. If fibre loss was indicated, remove nerve fibres from the modelled population.

(4) Adjust the damage parameters to reflect trends in latency across electrodes. Note that the level of correspondence between measured and predicted eCAPs may intrinsically depend on the modelling setup, e.g. the level to which the geometry of the model reflects the anatomy of the cochlea in which the measurements were taken, the number and distribution of neurons in the model, and the location and orientation of the electrodes relative to the neurons.

## 3.7 CHAPTER OVERVIEW

This chapter provides a consolidated overview of the present state of knowledge about the interpretation of eCAP and eABR measurements to qualify the health (demyelination and degeneration) and survival (fibre loss) of ANFs. This qualification is necessary to formulate an approach to include the status of the ANFs in computational models of the auditory periphery. It was shown that the sensitivity of eCAP predictions to specific mechanisms of neural damage is affected by the relative orientation of the stimulating and measurement electrodes in the model. A model where the stimulating and

measurement electrodes are aligned in the same dimension along the length of a single fibre is not sensitive to degeneration and is thus not an appropriate model to support adjustment of model parameters to reflect neural health. This implies that at least two dimensions are required to allow placement of the stimulating and measurement electrodes perpendicular to the peripheral processes of the fibres thereby preserving the relationship between measured and modelled eCAPs. A method is proposed for the systematic implementation of user-specific neural damage in CI models. This method needs to be validated in *in vivo* studies with CI users.

# CHAPTER 4 METHODS: ELECTROPHYSIOLOGICAL TESTING AND PERSON-SPECIFIC MODELLING

## 4.1 CHAPTER OVERVIEW

This chapter provides an overview of the methodology used for the clinical experimental procedure as well as the subsequent modelling process. Section 4.2 describes the setup of all necessary hardware and software used to obtain the clinical eCAP and eABR measurements. Section 4.3 describes the process used to generate and incorporate the ANF model geometry into a 3D VC cochlear model. This section also describes how the voltage outputs generated by the 3D model are adapted to be used as input to the time-dependant ANF model in Matlab. Section 4.4 provides an overview of the technique for generating eCAP waveforms using user-specific voltage inputs obtained from the 3D model. Section 4.5 outlines the procedure used to determine electrode-to-modiolus distances using the user's CT scans. A summary is presented in section 4.6 which concludes this chapter.

The electrophysiological results measured during the clinical session were analysed for the damage characteristics of the different damage mechanisms identified from the literature. These results were then compiled into a damage profile for the CI user, indicating which sections of the auditory nerve might have ANF degeneration, ANF demyelination, or ANF loss.

Using the CI user's CT scans a person-specific cochlea and auditory nerve model with the implanted electrode array was then generated using the University of Pretoria Bioengineering Group's existing

model generation software. The VC cochlear model provided the potential distribution at the neural tissue which was used as input for the user's computational auditory neural model.

The computational model was used to predict eCAP responses to stimuli. The damage profile determined from clinical measurements was then applied to the corresponding locations within the computational auditory nerve model. The model was subsequently used to examine the effect of the damage applied to the nerve on the predicted eCAP responses. The relation of both the damaged and healthy eCAPs predicted by the model to the clinical eCAP measurements could then be examined.

## 4.2 EXPERIMENTAL DESIGN: ECAPS AND EABRS

The aim of this section of the study was to evaluate the health and survival of the auditory nerve of a specific CI user by conducting electrophysiological measurements. This study consists of two risk-free, standard electrophysiological tests. These tests measure eCAPs and eABRs, which reflect person-specific information about the auditory nerve's reaction to electrical stimulation from the CI, which in turn is used to determine the auditory nerve's health and survival.

The CI user who participated in these clinical measurements has a Cochlear Nucleus CI512 cochlear implant in the right cochlea. The implant includes a receiver, which obtains and decodes the electrical signal from the sound processor, a stimulator and a perimodiolar electrode array that transmits the signal to the cochlea. This cochlear implant is used to measure eCAP responses from the auditory nerve. The CI system delivers an electrical pulse to a specific intracochlear electrode and records the evoked auditory neural response at a nearby electrode. After the potentials have been measured, they are analysed by the system's programming interface.

### 4.2.1 ECAP measurements

The eCAP measurements for this study were conducted using the AutoNRT algorithm, which was originally designed to determine the eCAP threshold current level (T-NRT). The acronym NRT used by CustomSound refers to Neural Response Telemetry which describes the measurement of the compound action potential of the distal portion of the auditory nerve (eCAP) in CI users. The algorithm is divided into two logical phases: an 'ascending series' and a 'descending series'. The ascending series measures NRT at rising current levels until the programmed expert system detects an eCAP. The descending series then performs NRT measurements at decreasing current levels with smaller step

sizes to determine the threshold more precisely. The algorithm then provides all eCAP measurements, as shown in figure 4.1, which may be analysed to assess the potential types and severity of damage to the user's ANF population. The stimulus levels used to evoke the eCAP responses are selected by the algorithm and may vary among electrodes.

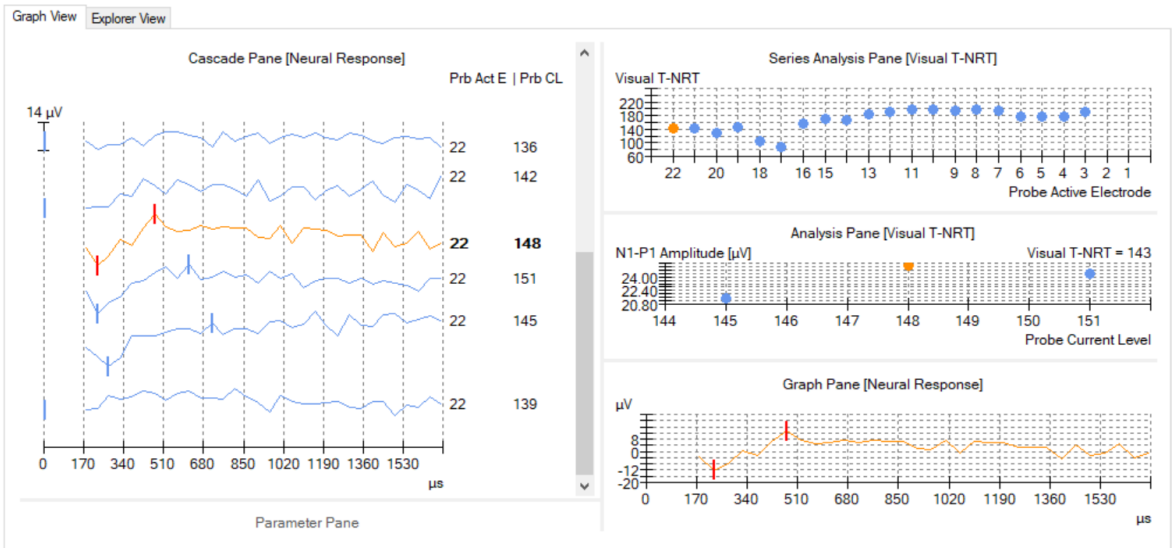


**Figure 4.1.** CustomSound EP AutoNRT eCAP outputs for electrode 22.

Table 4.1 shows the AutoNRT stimulus and recording parameters for the AutoNRT measurements on all electrodes.

#### 4.2.1.1 Protocol for eCAP measurements:

This section describes the protocol used to measure eCAPs during the experimental session for this study.

1. Connect the sound processor to the Programming Pod via the USB cable.
2. Connect the Programming Pod to the computer that is running the Custom Sound EP programme.
3. Select the recipient and implant in CS-EP.
4. Run an AutoNRT series for all electrodes.

The external processor of the cochlear implant stimulates each electrode in the implanted electrode array in turn. For each electrode an AutoNRT threshold and eCAP measurement is taken by compounding

**Table 4.1.** Table Of AutoNRT Parameters.

| AutoNRT Parameters | Value |
|---|---|
| Probe indifferent electrode: | MP1 |
| Masker indifferent electrode: | MP1 |
| Recording indifferent electrode: | MP2 |
| Masker active electrode: | Probe active electrode |
| Recording active electrode: | Probe active electrode +2 Offset |
| Masker current level: | Probe current level + 10 Offset |
| Probe stimulation rate (Hz): | 80 |
| Probe pulse width ($\mu$s): | 25 |
| Masker pulse width ($\mu$s): | 25 |
| Gain (dB): | 50 |
| Delay ($\mu$s): | 122 |
| Artefact cancellation technique: | Forward masking |

the measured response from all the other electrodes in the array. No feedback needs to be provided by the user, as measurements are taken automatically.

### 4.2.2 EABR measurements

EABRs are used to assess hearing thresholds by measuring the synchronous neural fibre activity along the auditory pathway. The eABR measurements require three surface electrodes to be attached to the skin. A ground electrode is attached on the mastoid or low on the forehead on the ipsilateral side to the CI, a positive electrode is attached to the forehead and a negative electrode to the contralateral mastoid as shown in figure 4.2. The implanted electrode array applies the stimulus to the user's cochlear nerve, and the three surface electrodes are then used to measure the eABR evoked by the stimulus. This procedure also requires no feedback from the participant, as the eABRs are an objective measurement of an elicited response. The eABR machine used in this study was the Interacoustics Eclipse AEP. The hardware setup for the eABR measurements is illustrated in figure 4.3.

#### 4.2.2.1 Protocol for eABR measurements:

This section describes the protocol used to measure eABRs during the experimental session for this study.

1. Apply electrode gel to the skin and scrub the area to prepare the skin for electrode attachment.
2. Attach electrodes to the forehead, lower ipsilateral forehead and contralateral mastoid.
3. Connect the Pod to the computer and CI processor.
4. Connect the trigger cable to the Pod and the EP system.
5. Switch the pod to 'trigger'.
6. Run EP acquisition software on the EP machine.
7. Select an external, positive-edge trigger.
8. Set up the recording screen to show the running average.
9. Set up Custom Sound EP (CS-EP) software on the computer and connect to the processor.
10. Configure the eABR stimulation screen in Custom Sound.
11. Start recording on the EP machine.
12. In CS-EP software, check triggering and then start eABR.
13. Take note of the stimulus level and electrode number selected in the CS-EP software for each measurement.
14. A qualified audiologist identifies and indicates the eABR peaks on the measured waveforms.

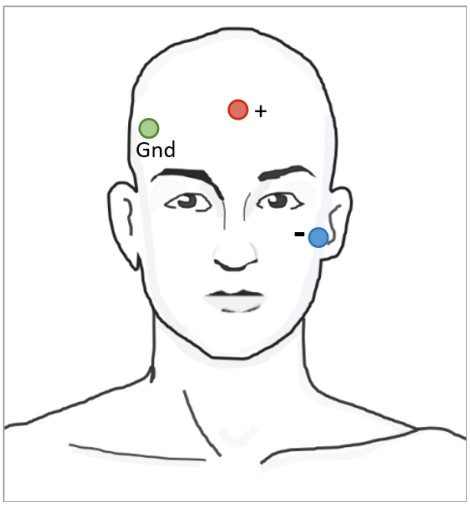


**Figure 4.2.** Electrode placement for eABR measurements of neural response to stimulation by a CI implanted in the user's right ear.

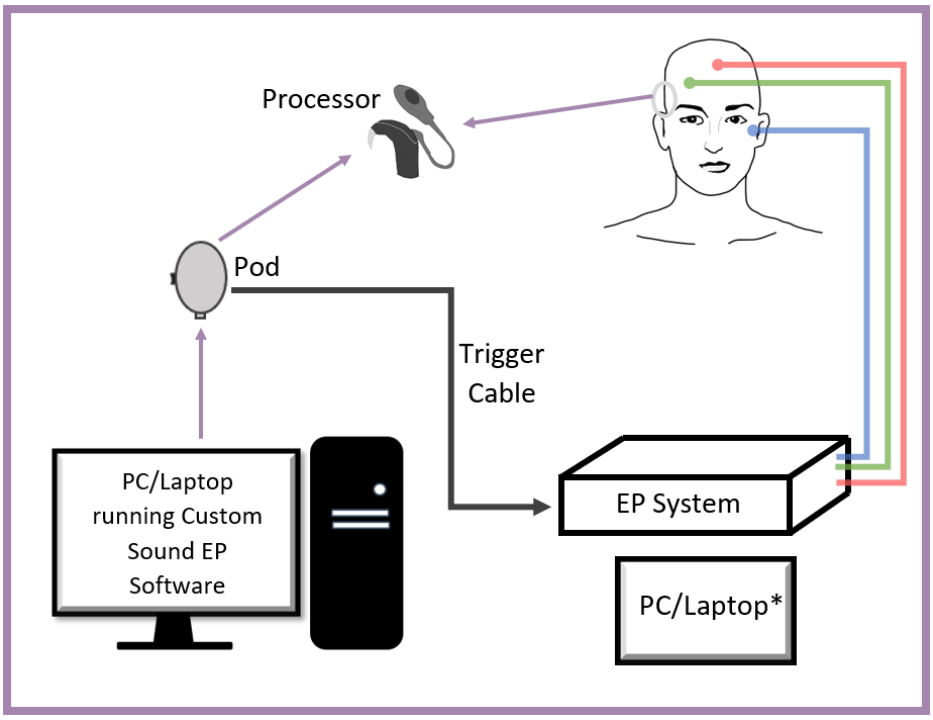


**Figure 4.3.** Hardware setup for eABR measurements.

## 4.3 DEVELOPMENT OF A PERSON-SPECIFIC AUDITORY NERVE MODEL

To aid the analysis of the clinical eCAP results, a user-specific three-dimensional (3D) VC model of the cochlea, electrode array, and auditory nerves of the CI user was used. The model provides a means of testing the effect of the theorised auditory neural damage on eCAP responses in simulation.

The University of Pretoria Bioengineering Research Group focusses on user-specific modelling of the human cochlea (Hanekom 2001; Malherbe, Hanekom and Hanekom 2015). The group's models are three-dimensional (3D), finite element VC models that are integrated with neural models to predict the current distribution within the cochlea and subsequent neural excitation as a result of stimulation (Hanekom and Hanekom 2016). The model construction entails the generation of 3D geometric entities based on anatomical measurement data from CT scans. After the model's geometry is created, electrical tissue properties are applied. Additionally, electrodes are added to the model, with their location determined by the user's cochlear CT scan measurements. The model may then be utilised to examine the response of the cochlea and AN to applications of stimuli by the electrodes.

### 4.3.1 Person-specific model generation

A CT scan for the CI user taken in April 2022 was obtained. The scan was then orientated and re-sliced to present a view of the cross-section of the cochlea from the side at every angle. Set points on the CT scans, as shown in figure 4.4, were then measured at every five degrees and compiled to a file which was used to generate the 3D model of the cochlea in COMSOL (*COMSOL Multiphysics*® 2020) using Bioengineering's existing model generation software. The nerve and cochlear trajectories used in the generation of the 3D model can be seen in figure 4.5. A surface which represents the geometric space that the auditory neurons occupy was then added to the cochlear model and assigned neural tissue properties.

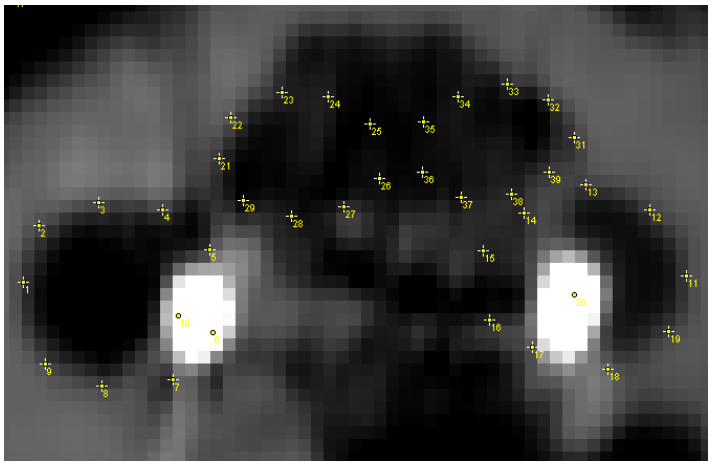

**Figure 4.4.** Landmark point measurements taken at every 5° of the CT scans.

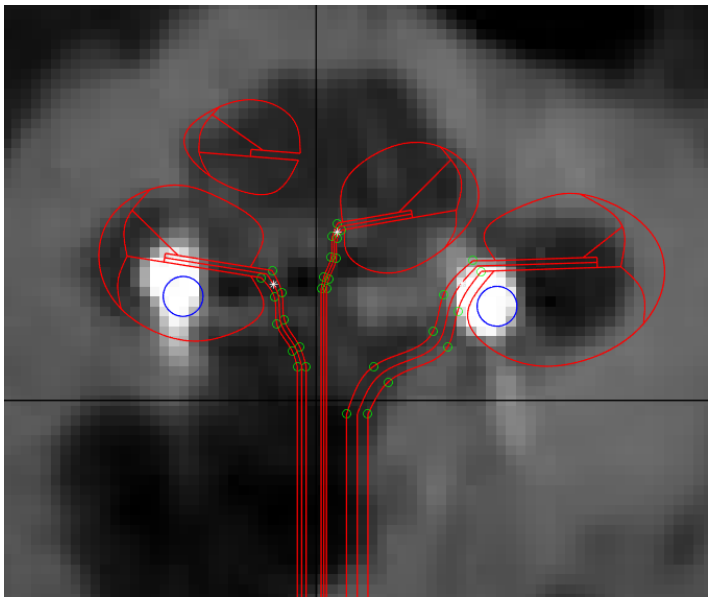

**Figure 4.5.** Overlay of the trajectories of the auditory nerve and cochlear channels on the CT scan.

In COMSOL, the 3D VC-model of the person-specific cochlea was then placed in a generic head model. The VC model's function was to calculate the potential distribution within the cochlea as a result of a current injected by a stimulating electrode. The electrode array was included in the VC model, with electrode 1 located at the most basal end of the cochlea and electrode numbers ascending to the cochlear apex. The potential distribution that served as input to the neural model was calculated on a plane in the neural volume. The position of the neural plane relative to the cochlea can be seen in figure 4.6 and neural plane with superimposed fibre trajectories can be seen in figure 4.7. The colour map used in the figures below depicts the relationship between the colours and the electric potential values in the VC model, with red representing the highest potential values and blue representing the lowest. The dark red area on the neural surface indicates the position of the stimulating electrode.

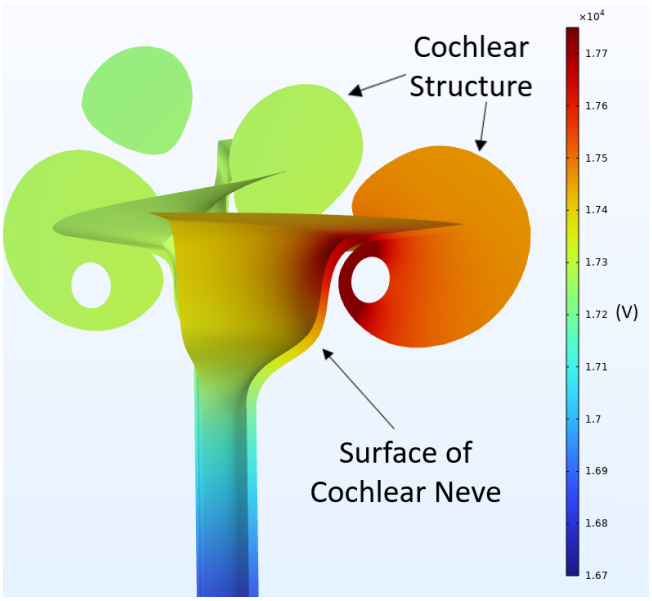


**Figure 4.6.** Placement of the neural plane in relation to the cochlear structure with open spaces indicating the trajectory of the electrode array. The image illustrates the electric potential across the cochlear structure and neural surface when a stimulation current is applied through electrode 6.

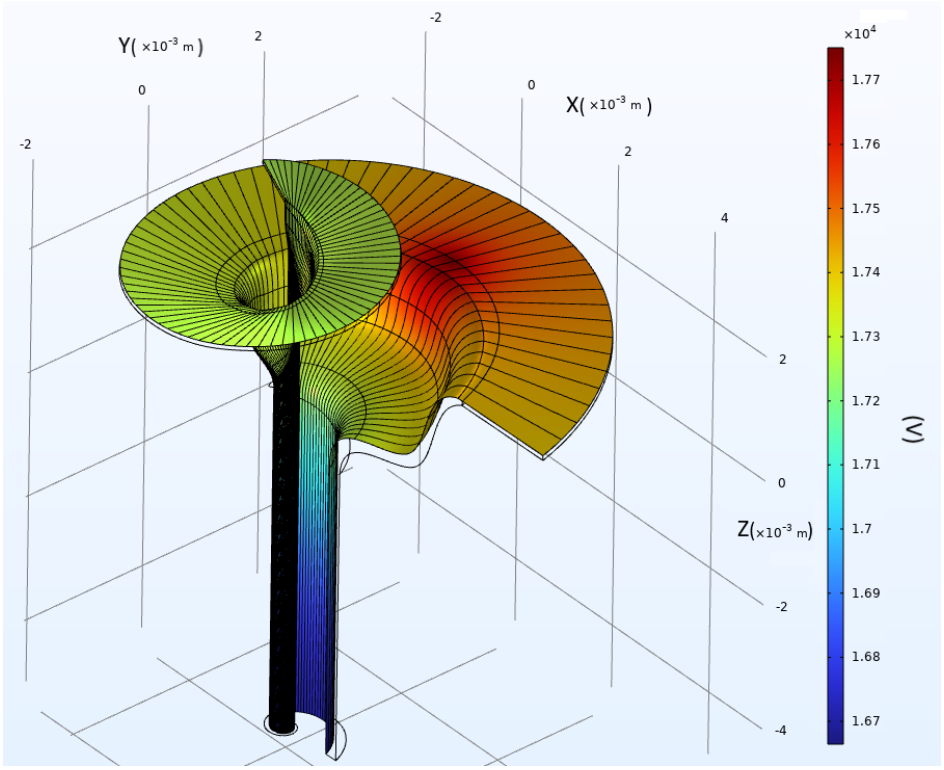


**Figure 4.7.** The auditory neural surface generated in the COMSOL model illustrating calculated potentials used as input to the neural model. This image illustrates the electric potential across the neural plane when a stimulation current is applied through electrode 6 as well as the fibre trajectories.

### 4.3.2 Application of person-specific model: ANF model input

A current of 1 A is injected sequentially via each electrode in the cochlear model. The voltage at discrete coordinates in the VC model is then calculated and output as text files. The use of the 1 A current means that the voltage at the coordinates also represents the resistance at the coordinates relative to the stimulating electrode, which in a purely restive model implies that a scaling factor can be used to calculate potential distributions at other other stimulus intensities.

The COMSOL model was used to generate a set of discrete coordinates with voltage values, like the set illustrated in figure 4.8, for each of the 22 electrodes in the electrode array. The colour map used in the figures below again depicts the relationship between the colours and the electric potential values, in this scale yellow represents the highest potential values and blue represents the lowest.

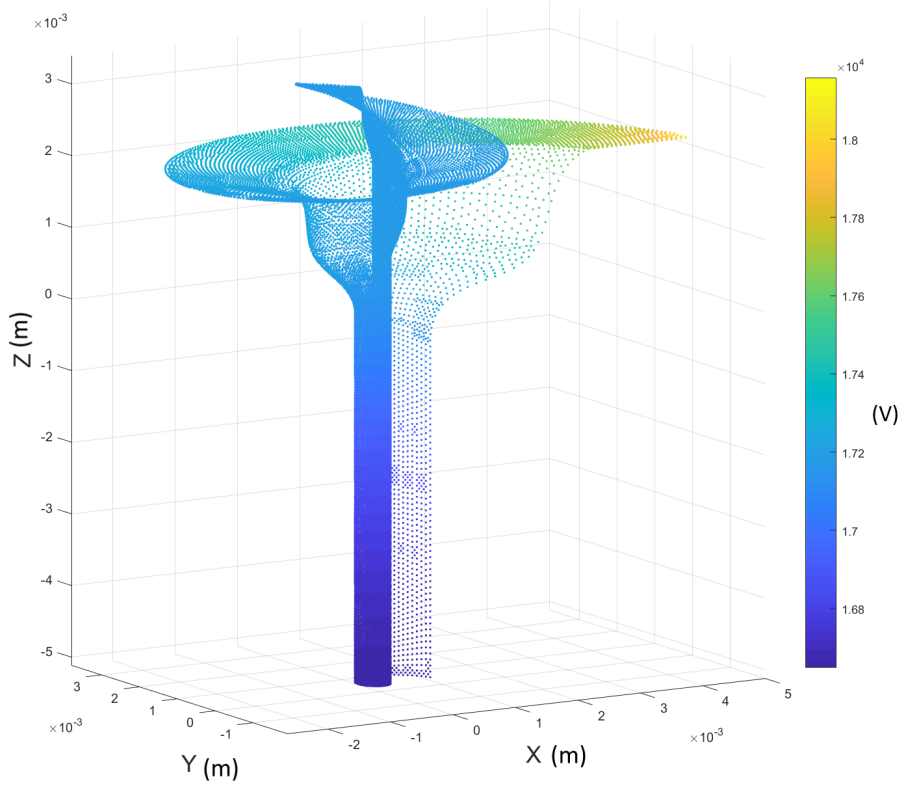


**Figure 4.8.** Figure illustrating voltages for 1 A stimulation with electrode 1 at discrete coordinates from COMSOL output. The colour bar is used to indicate the relation between colour and voltage.

Because a static solution is provided by the VC model for the potential distribution in the nerve plane and because the location of the finite element nodes did not necessarily correspond to the location of the nodes of Ranvier in the neural model, the output of the VC model had to be manipulated to

construct the time-dependent input for the ANF population model. This was necessary for eCAP generation. The procedure is outlined below.

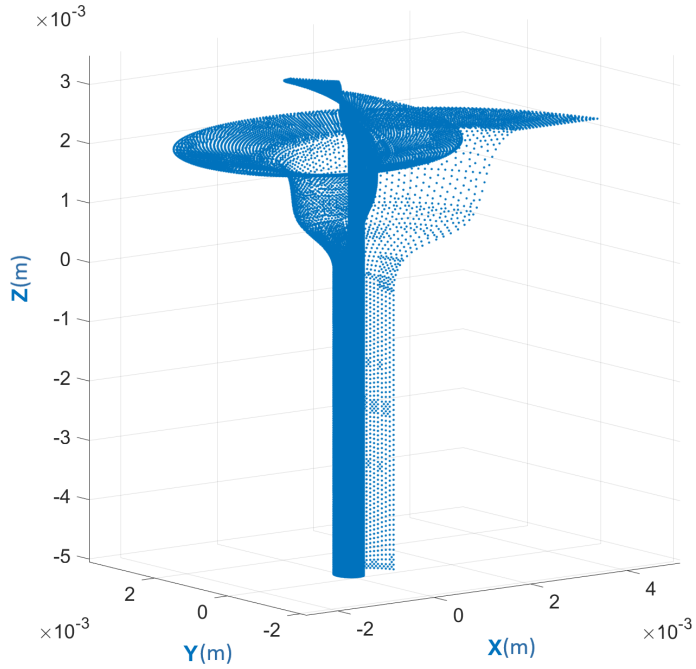


**(a)**

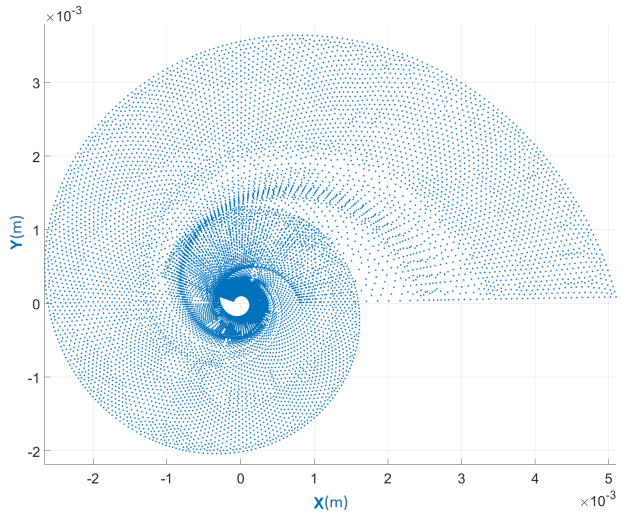


**(b)**

**Figure 4.9.** Original points at coordinates exported by COMSOL with (a) showing the side view of the coordinates and (b) showing the top view.

The following section explains in detail how the VC model output provides input to the ANF model. The discrete points output by COMSOL, as shown in figure 4.9 had to be differentiated into individual fibre trajectories every 5°. This was done by converting the Cartesian coordinates to cylindrical

coordinates and identifying all the points with theta values at multiples of 5°. The separated fibre trajectories had varying numbers of points per fibre and were then interpolated to have 459 points per fibre. The resulting population of 105 separated fibres are shown in figure 4.10

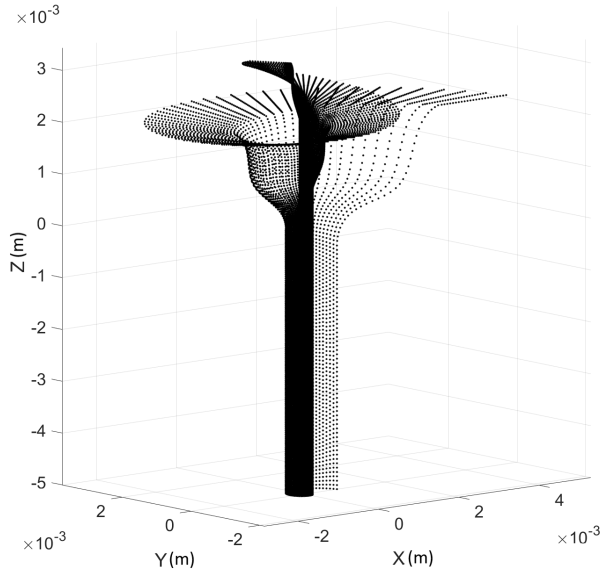


**(a)**

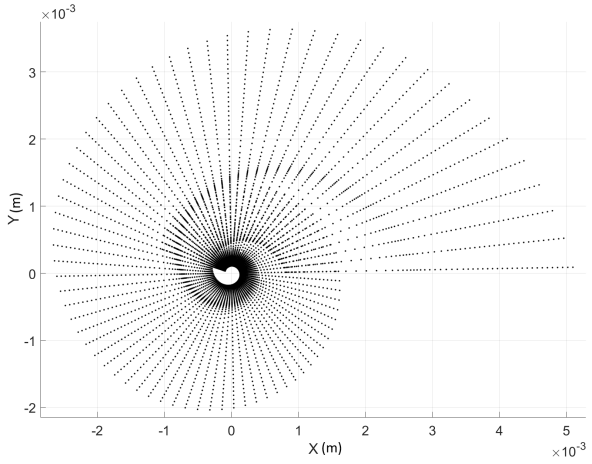


**(b)**

**Figure 4.10.** Original coordinate points differentiated into individual fibre trajectories at every 5°, with (a) showing the side view of the trajectories and (b) showing the top view.

The placement of the somas, dendritic compartments and nodes of Ranvier on the ANF trajectories could then be determined.

The first step was to determine the soma position on each fibre. This was done by developing an equation, shown below as (4.1) to identify the fibre trajectory point closest to the expected soma position on each fibre.

$$\text{soma position} = \text{fibre nr} \times (-0.57) + 110 \tag{4.1}$$

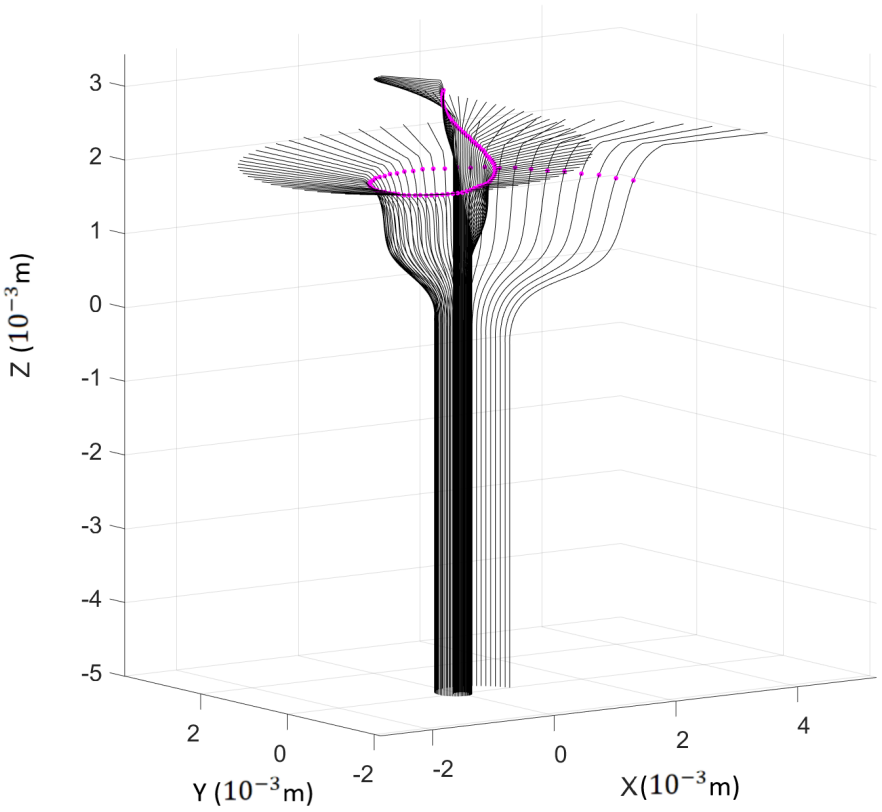


**Figure 4.11.** Placement of somas on the fibre trajectories.

The assigned soma positions can be seen in figure 4.11. On each fibre, the distance between the dendritic terminal and the soma position could then be calculated. This distance is used to calculate the value of $x$, which is a factor used to scale the dendrite internodal distances. The internodal distances were then used to derive the dendritic compartment coordinates, as presented in Kalkman, Briaire, Dekker et al. (2014).

The length of the axons of fibres was determined by calculating the distance between the somas and the axon terminals in the model. The maximum number of Ranvier nodes that could be placed on the axons was then determined. The coordinates of the axon compartments could then be calculated using

the ANF trajectories and the maximum number of Ranvier nodes. All nerve fibres were assigned the same number of axonal nodes, based on the minimum number of nodes assigned to any fibre in the population.

In this study, nodes refer to the nodes of Ranvier along the fibre. A compartment is a modelling unit that represents a section of the nerve fibre which may be a node or an internodal myelinated section of the fibre, as illustrated in figure 3.1. The coordinates of the centres of the compartments on all fibres in the population are indicated on the fibre trajectories shown in figure 4.12.

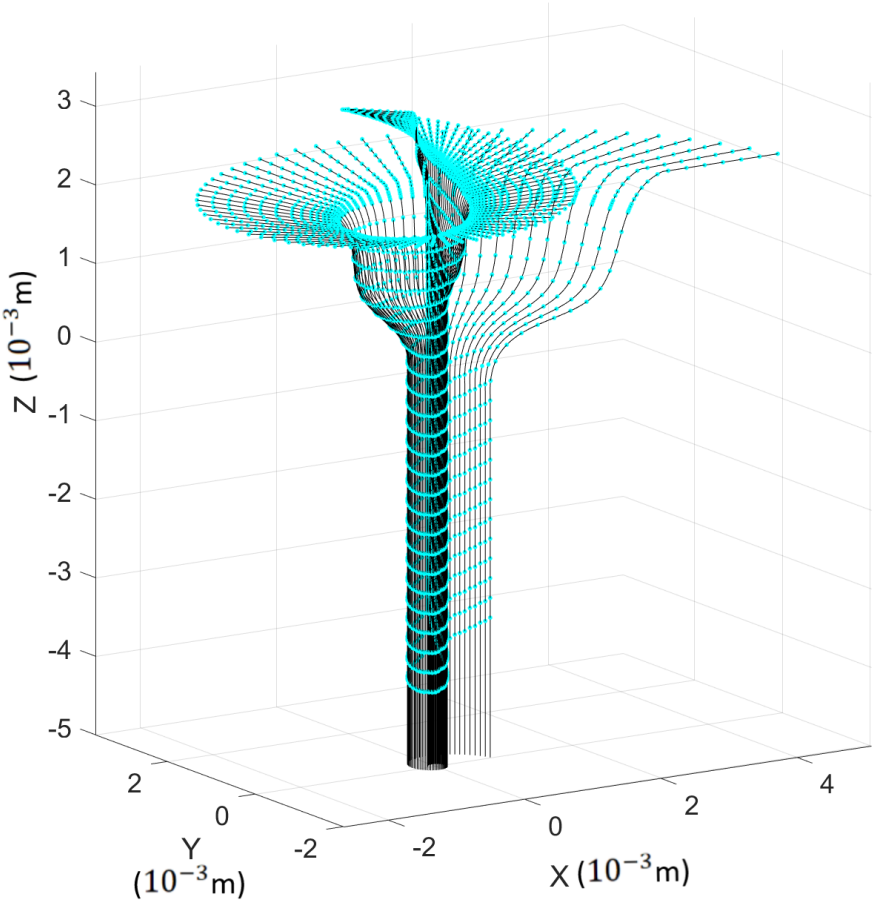


**Figure 4.12.** Coordinates of the centres of compartments on all 105 fibres.

The voltages along the fibre-trajectories in combination with the calculated coordinates of each compartment were then used to interpolate the voltage values at all compartments. This was done for all fibres, for each of the 22 electrodes. The voltage values for electrode 1 are illustrated in figure 4.13.

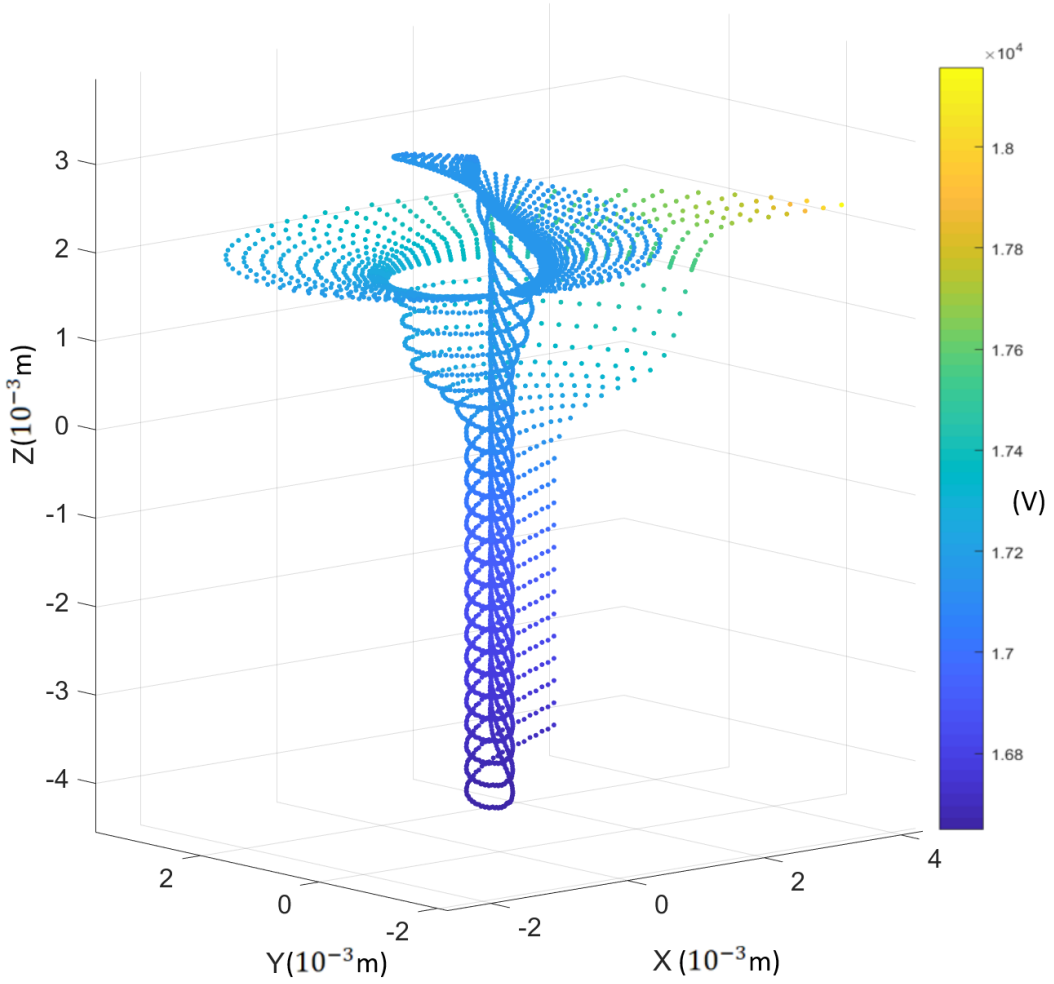


**Figure 4.13.** A visual representation of the voltage values at the centre of each compartment in response to stimulus by electrode 1, which is located at the most basal end of the cochlea.

Figure 4.14 shows a contour plot of the voltage distribution over the ANFs for stimulation from electrode 16.

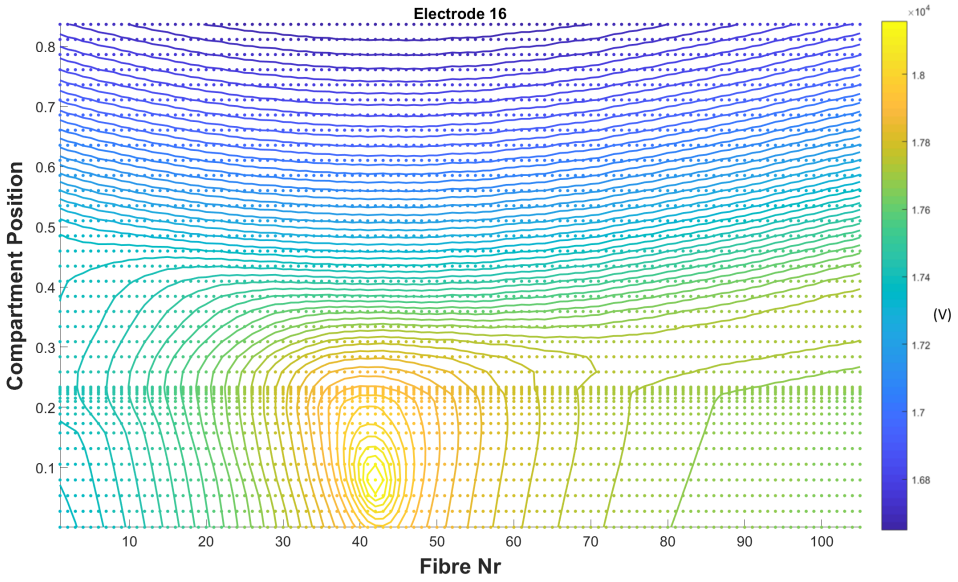


**Figure 4.14.** A contour plot of the voltage distribution, indicating compartment positions to stimulus by electrode 16

Due to the fact that these values were generated by a 1A stimulus, Ohm's law states that the voltage is equal to the resistance values of each fibre compartment in relation to each electrode. As a result, an R-matrix was created, which is a 4-dimensional matrix that contains the resistance between each electrode and each fibre compartment. It was then possible to use the generated R-matrix independently from the VC model. The R-matrix could be used to calculate the potential at each compartment for each fibre in response to various time-dependent stimulus types and intensities. The compartment potentials could be calculated by multiplying the time-dependent current by the R-matrix resistance values for each compartment, as shown in (4.2), where $e$ is the electrode number, $f$ the fibre number, and $c$ the compartment number. The potential at each compartment in response to time-dependent stimulus was used as input for the computational ANF population model.

$$V_{f,c}(t) = \sum_{e} R^{e}_{f,c} \times I^{e}(t) \tag{4.2}$$

## 4.4 ECAP SIMULATION

The time-dependant potential distribution, as derived in the previous section was used as input to the ANF population model. The ANF model could predict whether or not any specific time-dependent stimulus would excite a fibre or a portion of a population of fibres and produce propagating action potentials (APs), hence enabling the simulation of eCAPs.

Both the measured and predicted eCAPs used the forward-masking artefact rejection paradigm as well as having the recording electrode be the stimulating electrode +2.

The eCAP calculation used by the computational model is based on the so-called backward problem, which is based on the premise that sum of the currents from each compartment constitutes a small source current which is used in conjunction with the R-matrix values to determine the resultant potential at the recording electrode.

The first step in calculating the eCAP responses was to determine the compartmental current at each compartment of a fibre. The R-matrix values are then used to calculate the potential at the recording electrode for the compartmental current. The SFAP is then determined as the sum of all compartmental potentials. The simulated population action potential of the auditory nerve at the recording electrode is then calculated by adding the SFAPs of all fibres in the nerve model.

The damage profile was applied to the computational model by removing myelin layers, neural compartments or entire nerve fibres form the nerve. The model could then predict the eCAP responses of the damaged auditory nerve to stimulation from each electrode.

## 4.5 ELECTRODE-TO-MODIOLUS DISTANCE CALCULATION

The distance between the electrodes and the modiolus of the cochlea is one of the factors that influence the generated eCAP response and must therefore be considered when analysing the clinical and model-predicted eCAPs. According to reports in the literature, as the distance between the modiolus and electrodes increases, so does the ECAP threshold (Lee et al. 2020; Wermeskerken, Olphen and Graamans 2009). The electrode-to-modiolus distances for this study were measured on the CT scans of the user's cochlea. The distances were measured manually from the centre of each electrode to the centre of the modiolus, as illustrated by the yellow arrow in figure 4.15.

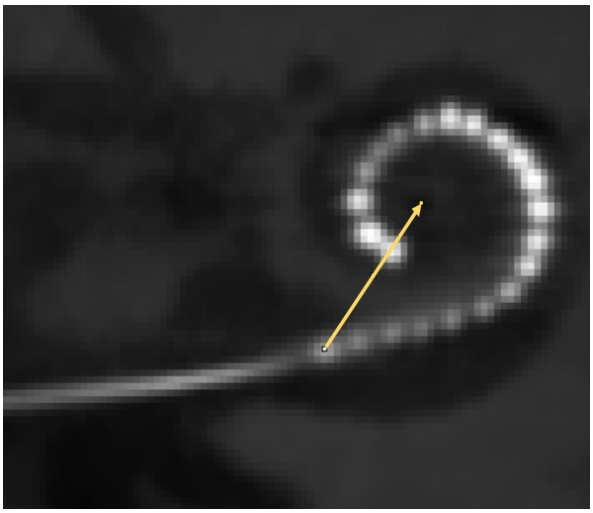

**Figure 4.15.** Measurement of electrode to modiolus distance for electrode 1.

## 4.6 CHAPTER SUMMARY

This chapter provided an overview of the methods used to conduct the clinical measurement and person-specific modelling components of this study. Two separate methods were described: the clinical experimental procedure and the method used to construct the user-specific model. The hardware setup for the clinical measurements are described along with the software used and the types of results measured. A description of the method used to generate an ANF trajectory in COMSOL which is integrated with the cochlear model is given. The procedure of converting the COMSOL model's predicted output values to the potential at each compartment in response to time-dependent stimulus that can be utilised as input for the Matlab neural population model, and subsequent eCAP modelling process is detailed in this chapter. A method for measuring the distance between electrodes and modiolus is also provided.

# CHAPTER 5 RESULTS

## 5.1 CHAPTER OVERVIEW

This chapter presents and interprets the results obtained throughout this study. In section 5.2 the eCAP measurements obtained during the clinical measuring session are presented and discussed. In section 5.3 important data points from the raw eCAP measurements are interpolated or extrapolated to the same levels to allow comparison of eCAP values across all electrodes. In section 5.4 the eABR measurements obtained during the clinical session are presented and interpreted. Section 5.5 discusses the predicted firing pattern of the fibres contributing to each electrode in the model. The eCAPs predicted by the user-specific model are presented in section 5.6 to illustrate the effect of neural damage. In section 5.7 a summary of these results is presented, which concludes the chapter.

## 5.2 CLINICAL ECAP MEASUREMENTS

During the clinical measurement session, AutoNRT measurements were taken for the CI user. To compare the eCAP generated at the same stimulation levels, the graphs were compiled to single figures to compare latency and amplitude values and subsequently determine possible neural damage. Stimulation levels for the AutoNRT measurements were set in current levels (CLs). Each figure illustrates the eCAP graphs at a specific stimulation level and the accompanying table contains the N1 and P1 peak values for the graphs, as identified by the CustomSound software. It is important to note that the AutoNRT protocol could not record any eCAP responses from electrodes 1 and 2 which are located at the most basal point of the CI user's implanted electrode array. This means that no conclusions regarding the health and survival of the nerve fibres contributing to electrodes 1 and 2 could be drawn, as no eCAP waveforms were available for examination on those electrodes. The CI user has had explantation and reimplantation surgery in the studied cochlea, which might have caused damage to the most basal part of the cochlea and round window, possibly resulting in the absence of eCAP responses.

### 5.2.1 AutoNRT measurements at various stimulation CLs.

The eCAP measurements in this study were taken at different levels for all electrodes in the implanted array. When the stimulus level at which an eCAP is evoked is increased, the eCAP amplitudes increase and the latencies decrease, and as a result, eCAP responses had to be compared at the same stimulation level to compare amplitude and latency values directly. Electrode responses which were measured at the same stimulation levels were grouped into figures to allow direct comparison. The AutoNRT algorithm measures the stimulation applied by the electrodes in clinical current level (CL) units. One CL is equivalent to 0.176 dB (relative to 1 $\mu$A).

The waveforms were overlaid in the same figure to allow comparison of amplitude and latency values. Ideally, eCAPs measured for all electrodes should be compared, but due to the stimulus levels selected by the AutoNRT algorithm, this was not possible. Stimulus levels where the greatest number of electrodes elicit a response allow for the broadest range of comparison. The figures are listed in descending order according to the number of electrodes that elicited a response at a stimulus level. The eCAP measurements could be measured at 199 and 202 CL for six electrodes.

The AutoNRT algorithm identified the latency and amplitude values of both the N1 and P1 peaks. These values are given in the tables accompanying the figures where each column contains the latency ($\mu$s) and amplitude ($\mu$V) values for the specified peak, separated by a comma. These values were evaluated for indicators of the various damage mechanisms. The findings contributed to the damage profile prediction.

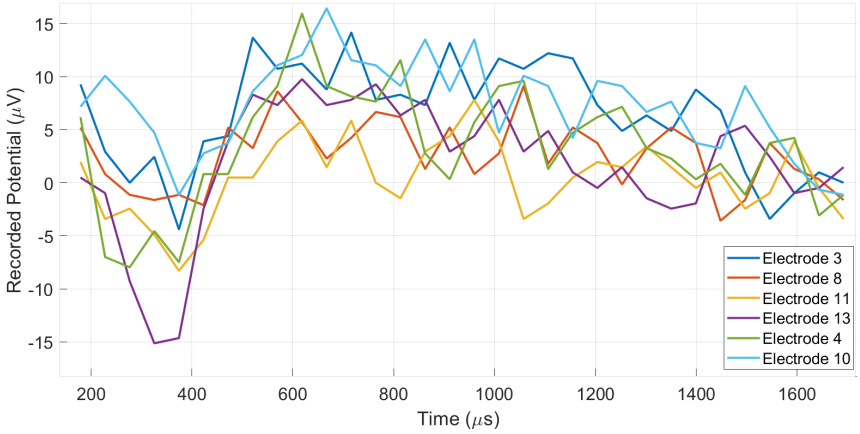


**(a)**

| Electrode | N1 peak values | P1 peak values |
|---|---|---|
| 3 | 374.20, -4.39 | 715.80, 14.15 |
| 8 | 423, -2.11 | 569.40, 8.62 |
| 11 | 374.20, -8.29 | 618.20, 5.85 |
| 13 | 325.40, -15.12 | 618.20, 9.76 |
| 4 | 276.60, -7.97 | 618.20, 15.94 |
| 10 | 347.20, -1.14 | 667, 16.43 |

**(b)**

**Figure 5.1.** Measured eCAP (a) graphs and (b) latency and amplitude values for all electrodes at 199 CL stimulation.

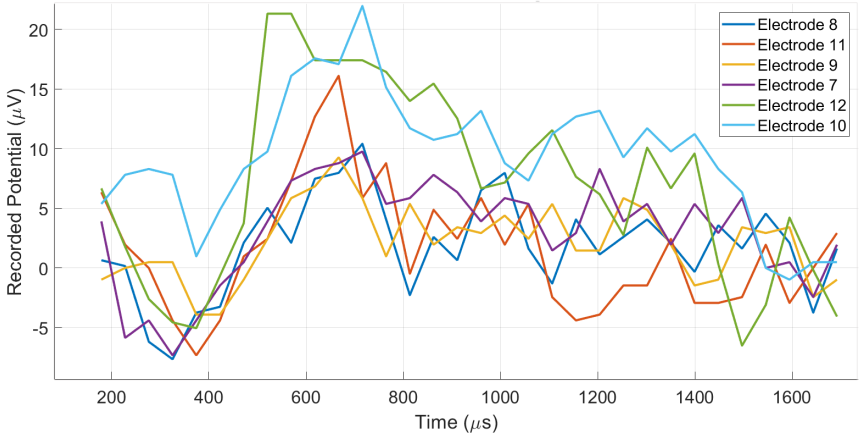


**(a)**

| Electrode | N1 peak values | P1 peak values |
|---|---|---|
| 8 | 325.40, -7.64 | 715.80, 10.41 |
| 11 | 374.20, -7.32 | 667, 16.10 |
| 9 | 423, -3.90 | 667, 9.27 |
| 7 | 325.40, -7.32 | 715.80, 9.76 |
| 12 | 374.20, -5.04 | 520.60, 21.30 |
| 10 | 347.20, 0.98 | 715.80, 21.96 |

**(b)**

**Figure 5.2.** Measured eCAP (a) graphs and (b) latency and amplitude values for all electrodes at 202 CL stimulation.

The eCAP measurements for 208 and 211 CL were compiled in figures with five electrodes that elicited a response.

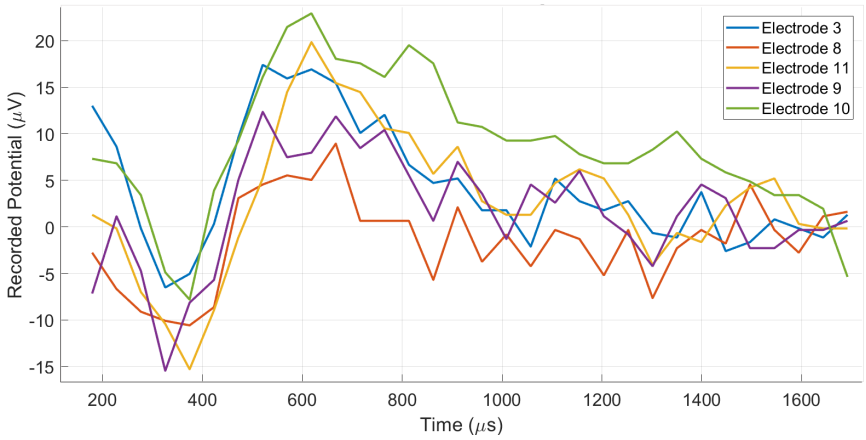


**(a)**

| Electrode | N1 peak values | P1 peak values |
|---|---|---|
| 3 | 325.40, -6.50 | 520.60, 17.40 |
| 8 | 374.20, -10.57 | 667, 8.94 |
| 11 | 374.20, -15.29 | 618.20, 19.84 |
| 9 | 325.40, -15.45 | 520.60, 12.36 |
| 10 | 374.20, -7.81 | 618.20, 22.93 |

**(b)**

**Figure 5.3.** Measured eCAP (a) graphs and (b) latency and amplitude values for all electrodes at 208 CL stimulation.

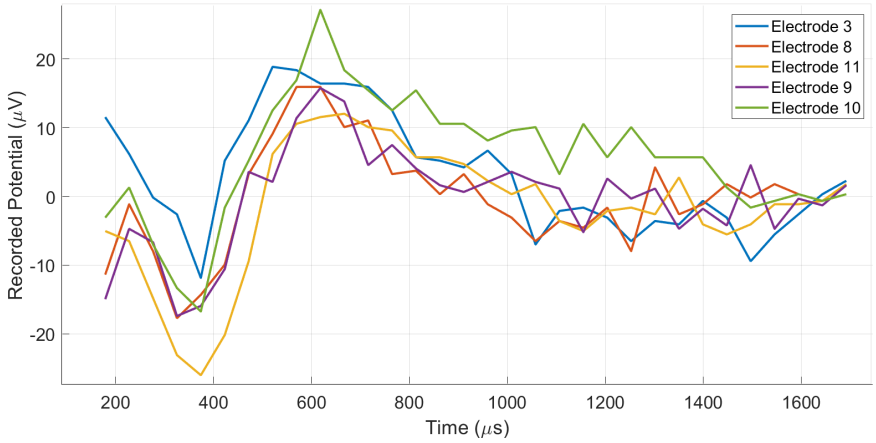


**(a)**

| Electrode | N1 peak values | P1 peak values |
|---|---|---|
| 3 | 374.20, -11.87 | 520.60, 18.86 |
| 8 | 326.40, -17.73 | 569.40 15.94 |
| 11 | 374.20, -26.02 | 667, 12.03 |
| 9 | 325.40, -17.40 | 618.20, 15.77 |
| 10 | 374.20, -16.75 | 618.20, 27.16 |

**(b)**

**Figure 5.4.** Measured eCAP (a) graphs and (b) latency and amplitude values for all electrodes at 211 CL stimulation.

The eCAP measurements for 178, 190 and 193 CL were compiled in figures with four electrodes that elicited a response.

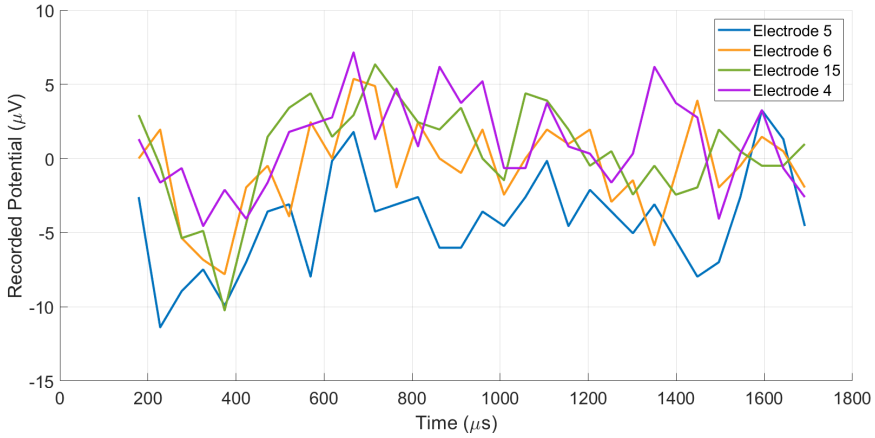


**(a)**

| Electrode | N1 peak values | P1 peak values |
|---|---|---|
| 5 | 227.80, -11.38 | 667, 1.79 |
| 6 | 374.20, -7.81 | 667, 5.31 |
| 15 | 374.20, -10.25 | 715.80, 6.34 |
| 4 | 325.40, -4.55 | 667, 7.16 |

**(b)**

**Figure 5.5.** Measured eCAP (a) graphs and (b) latency and amplitude values for all electrodes at 178 CL stimulation.

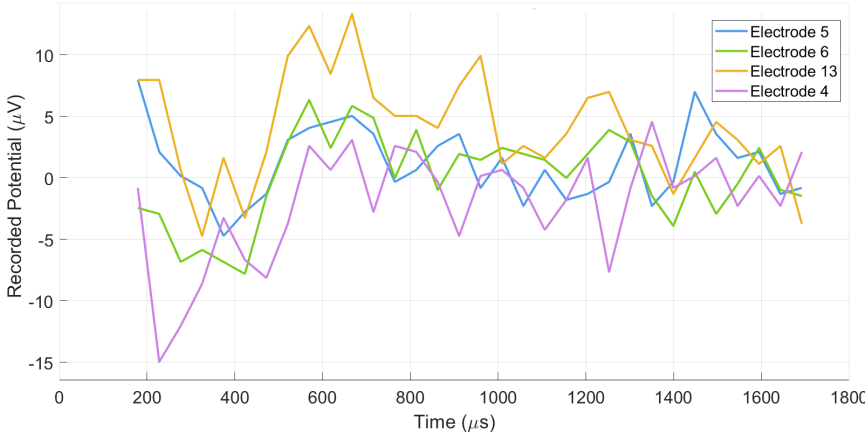


**(a)**

| Electrode | N1 peak values | P1 peak values |
|---|---|---|
| 5 | 325.40, -12.36 | 813.40, 7.16 |
| 6 | 276.60, -0.98 | 471.80, 9.76 |
| 13 | 423, -16.91 | 569.40, 5.04 |
| 4 | 325.40, -5.85 | 813.40, 9.27 |

**(b)**

**Figure 5.6.** Measured eCAP (a) graphs and (b) latency and amplitude values for all electrodes at 190 CL stimulation.

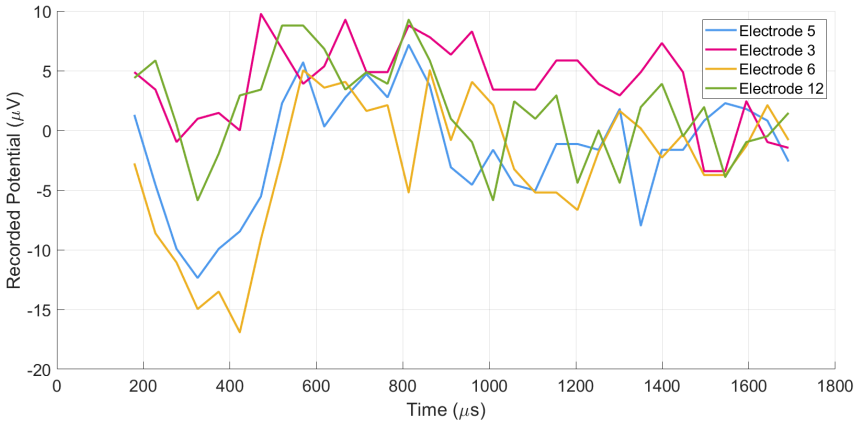


**(a)**

| Electrode | N1 peak values | P1 peak values |
|---|---|---|
| 5 | 325.40, -12.36 | 813.40, 7.16 |
| 3 | 276.60, -0.98 | 471.80, 9.76 |
| 6 | 423, -16.91 | 569.40, 5.04 |
| 12 | 327.40, -5.85 | 813.40, 9.27 |

**(b)**

**Figure 5.7.** Measured eCAP (a) graphs and (b) latency and amplitude values for all electrodes at 193 CL stimulation.

The eCAP measurements for 145, 181, 184, 187 and 205 CL were compiled in figures with three electrodes that elicited a response.

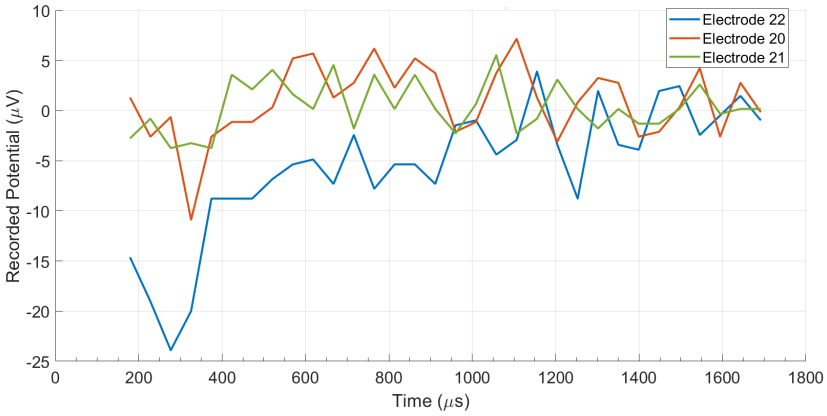


**(a)**

| Electrode | N1 peak values | P1 peak values |
|---|---|---|
| 22 | 276.60, -23.91 | 715.80, -2.44 |
| 20 | 325.40, -10.90 | 764.60, 6.18 |
| 21 | 276.60, -3.74 | 667, 4.55 |

**(b)**

**Figure 5.8.** Measured eCAP (a) graphs and (b) peak values for all electrodes at 145 CL stimulation.

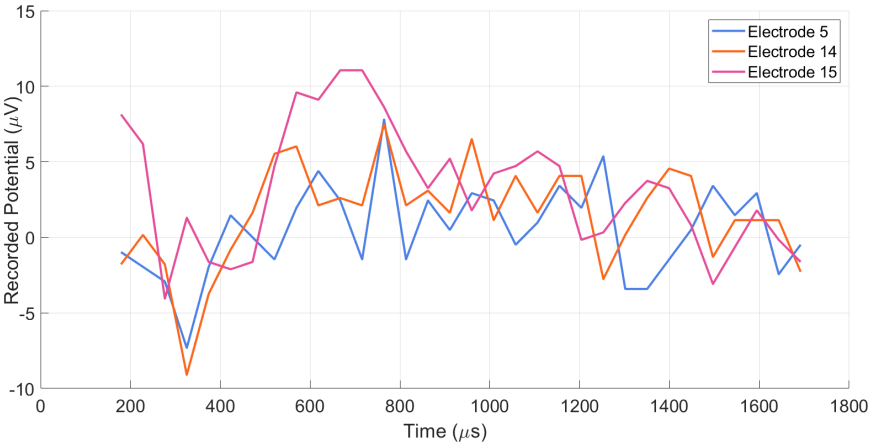


**(a)**

| Electrode | N1 peak values | P1 peak values |
|---|---|---|
| 5 | 325.40, -7.32 | 764.60, 7.81 |
| 14 | 325.40, -9.11 | 764.60, 7.48 |
| 15 | 276.60, -4.07 | 667, 11.06 |

**(b)**

**Figure 5.9.** Measured eCAP (a) graphs and (b) latency and amplitude values for all electrodes at 181 CL stimulation.

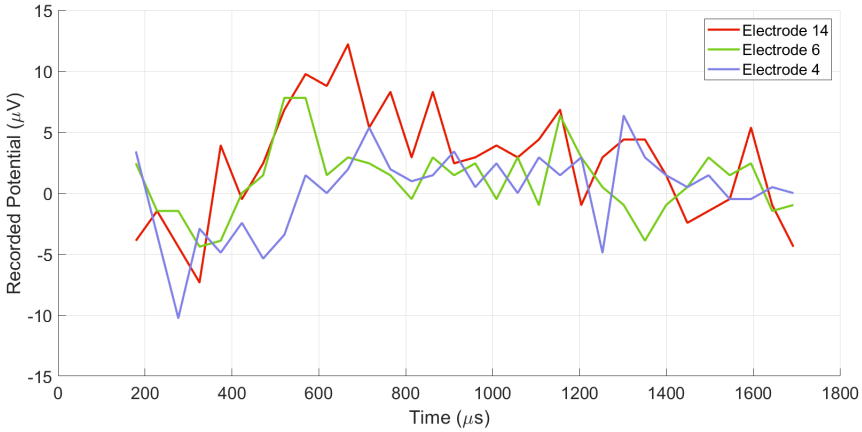


**(a)**

| Electrode | N1 peak values | P1 peak values |
|---|---|---|
| 14 | 325.40, -7.32 | 667, 12.20 |
| 6 | 325.40, -4.39 | 520.60, 7.81 |
| 4 | 276.60, 10.25 | 715.80, 5.37 |

**(b)**

**Figure 5.10.** Measured eCAP (a) graphs and (b) latency and amplitude values for all electrodes at 184 CL stimulation.

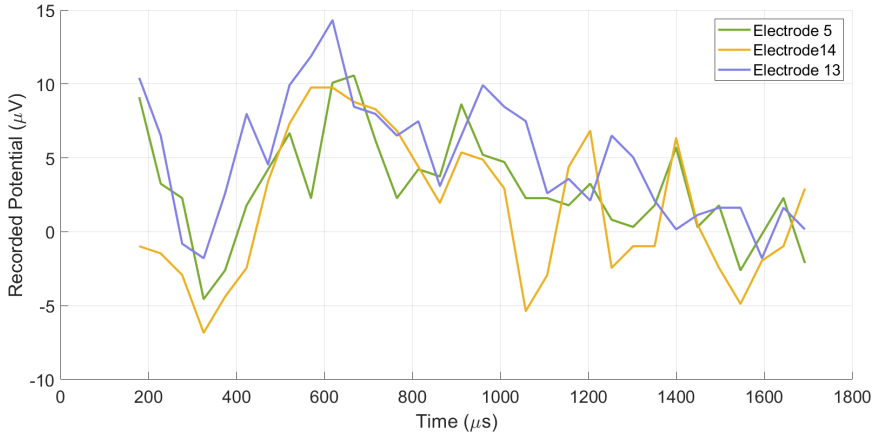


**(a)**

| Electrode | N1 peak values | P1 peak values |
|---|---|---|
| 5 | 325.40, -4.55 | 667, 10.57 |
| 14 | 325.40, -6.83 | 569.40, 9.76 |
| 13 | 325.40, -1.79 | 618.20, 14.31 |

**(b)**

**Figure 5.11.** Measured eCAP (a) graphs and (b) latency and amplitude values for all electrodes at 187 CL stimulation.

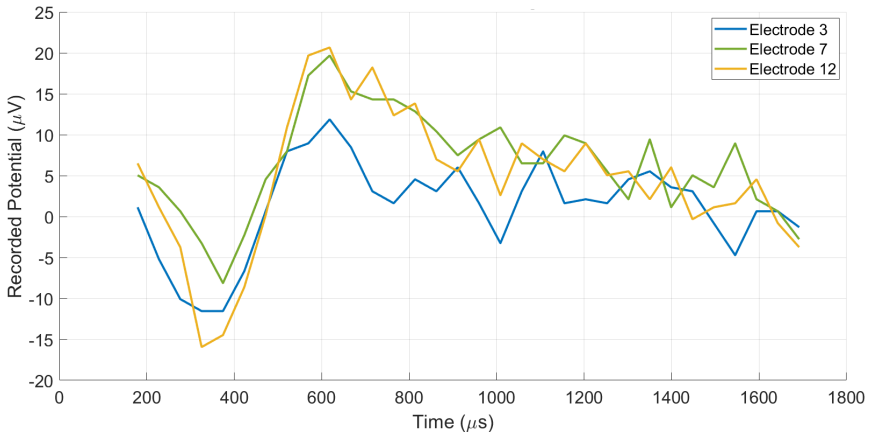


**(a)**

| Electrode | N1 peak values | P1 peak values |
|---|---|---|
| 3 | 325.40, -11.55 | 618.20, 11.87 |
| 7 | 374.20, -8.13 | 618.20, 19.68 |
| 12 | 325.40, -15.94 | 618.20, 20.65 |

**(b)**

**Figure 5.12.** Measured eCAP (a) graphs and (b) latency and amplitude values for all electrodes at 205 CL stimulation.

To identify potential neural damage from eCAP measurements, it is important to have an overview of all electrodes' eCAP amplitudes and latencies. All of the indicators of neural damage identified in the literature are relative values. The reduction or increase of the latency or amplitude values refers to a relative deviation from the normal latency or amplitude values for a particular individual. To identify values that deviate from a user's normal eCAP waveforms, all electrodes must be examined. However, as shown in figures 5.1 to 5.12, responses at the same stimulus intensity were limited to a subset of electrodes. To be able to analyse the eCAP response to all electrodes at the same stimulus level, the relevant values (N1 latencies, P1 latencies, N1 amplitudes and P1 amplitudes) from the raw eCAP measurements were interpolated or extrapolated to the same levels. A level at 5.5 dB above the threshold (T) and comfortable (C) stimulation levels determined in the user's most recent mapping session was chosen as the interpolation or extrapolation target. The 5.5dB level was chosen as it allowed a small range for interpolation or extrapolation between or just outside the available data points. The amplitude and latency data for the original eCAP measurements at 5.5dB above the T and C levels were interpolated and extrapolated using linear regression.

## 5.3 DATA ANALYSIS

To identify outlying data points, prediction bands were added to the data graphs of the interpolated and extrapolated values. The prediction bands were drawn around the linear regression line for the data. In statistical analysis, prediction bands are frequently employed to indicate the likelihood that a data point will fall within the predicted band. It is often used when predictions are based on limited or noisy data.

In this study, only the N1 amplitude and latency values are examined to determine possible neural damage. For this reason, only the graphs of the N1 peak values are shown below.

The T and C levels determined by the user's MAPS were used to establish a reference level to use the interpolation of the peak data points. The T level is the lowest stimulation current level that evokes a hearing sensation. The C level is the greatest current level at which a patient can comfortably listen to the stimulation. "Mapping" refers to the process of programming the CI's speech processor. The establishment of the electrical stimulation limits, i.e. T and C levels, for each electrode in the CI array, are stored in the user's MAP. The data interpolation and extrapolation was done for all electrodes to 5.5 dBs above the T and C levels. This interpolation and extrapolation was done using the measured peak-values from the AutoNRT graphs. Both 75% and 90% prediction bands were applied to the interpolated and extrapolated data points. This allowed the identification of the most probable damage locations as well as slightly less probable damage locations.

### 5.3.1 ECAP measurements at 5.5dB above T level

The 90% and 75% prediction bands allow the identification of the 2 and 5 outlier data points, respectively.

The data points that lie outside the coloured prediction bands depict potential outlier values that could indicate ANF damage. The data points above the prediction band denote an increase in the relevant eCAP characteristic, such as amplitude, while the data points below the prediction band denote a decrease in the characteristic. These data points indicate that the nerve fibres which contribute to the electrodes at which outlier values are identified could possible have been affected by a correlating damage mechanism. These possible damage types and locations are used in the compilation of the ANF damage profile for the user.

#### 5.3.1.1 90% Prediction bands

The figures below illustrate the 90% prediction bands for the interpolated and extrapolated data above T level.

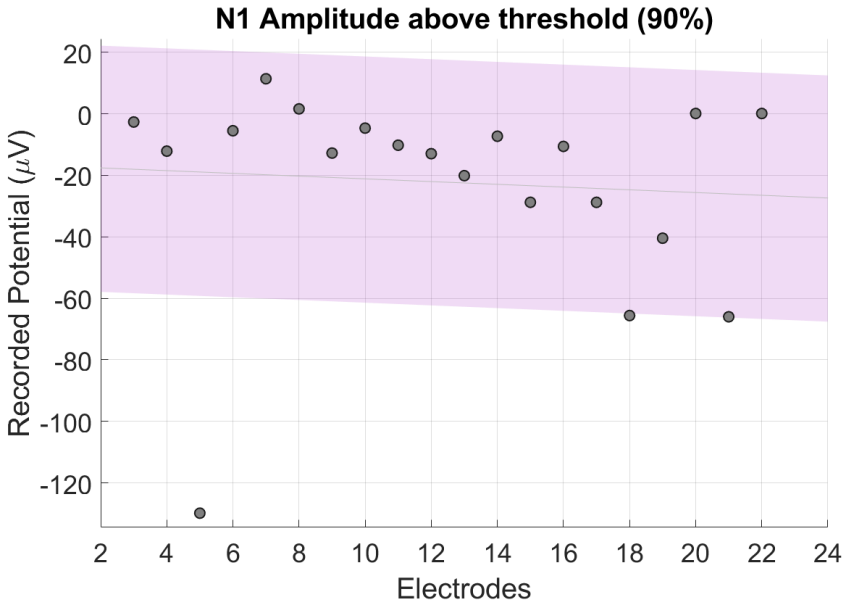


**(a)**

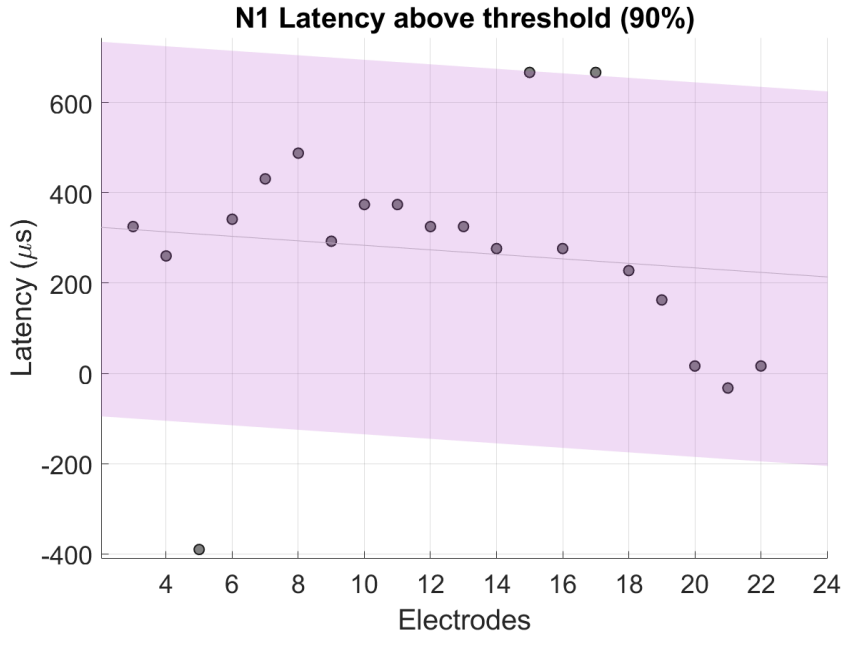


**(b)**

**Figure 5.13.** N1 (a) amplitude and (b) latency above T level with 90% confidence band.

#### 5.3.1.2 75% Prediction bands

The figures below illustrate the 75% prediction bands for the interpolated and extrapolated data above T level.

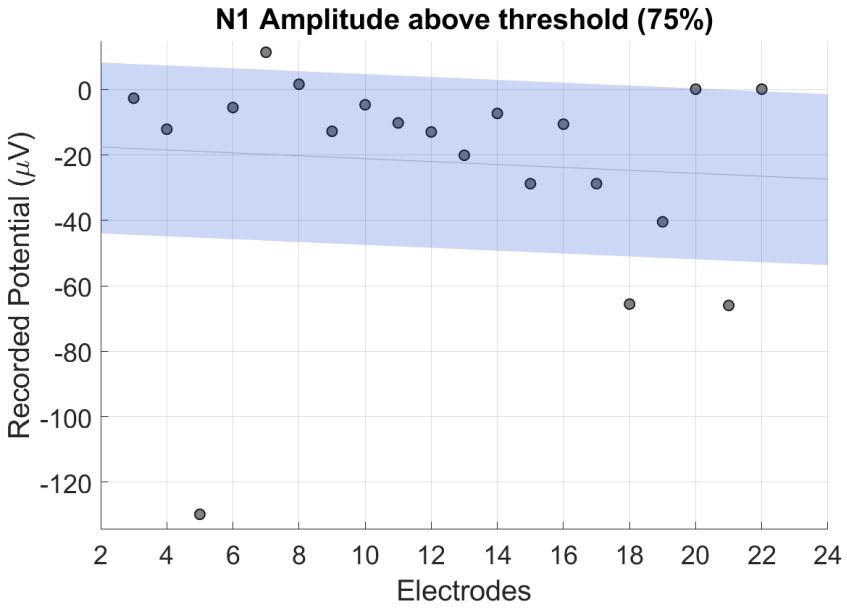


**(a)**

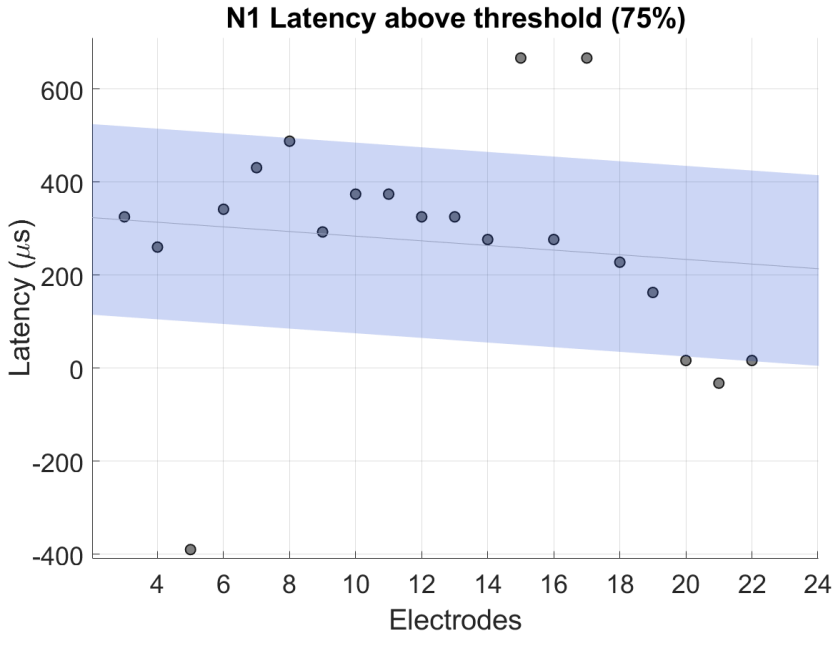


**(b)**

**Figure 5.14.** N1 (a) amplitude and (b) latency above T level with 75% confidence band.

### 5.3.2 ECAP measurements at 5.5dB above C level

Interpolating and extrapolating data to levels above both the T and C level provides two measures for diagnosing potential neural damage.

#### 5.3.2.1 90% Prediction bands

The figures below illustrate the 90% prediction bands for the interpolated and extrapolated data above C level.

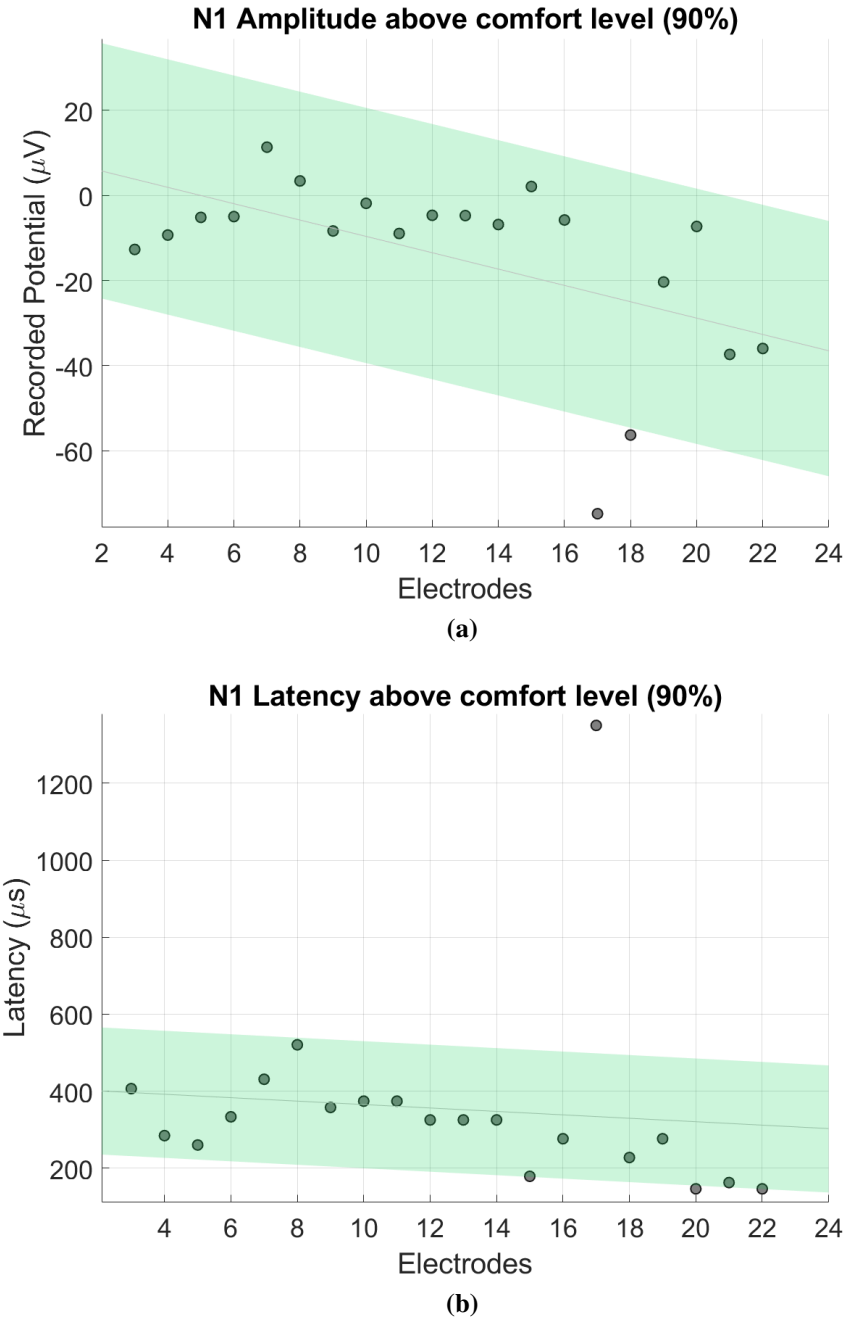


**Figure 5.15.** N1 (a) amplitude and (b) latency above C level with 90% confidence band.

#### 5.3.2.2 75% Prediction bands

The figures below illustrate the 75% prediction bands for the interpolated and extrapolated data above C level.

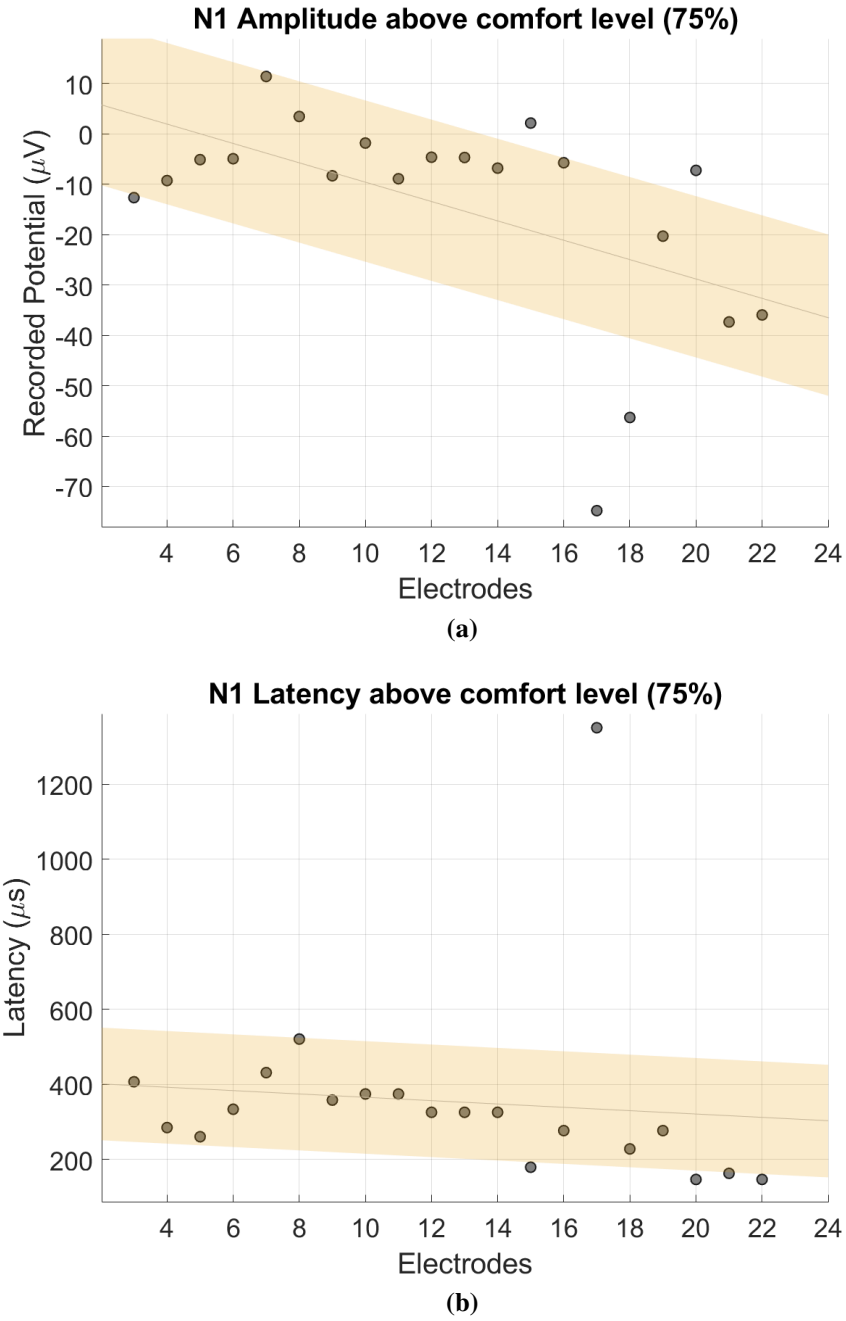


**Figure 5.16.** N1 (a) amplitude and (b) latency above C level with 75% confidence band.

## 5.4 EABR MEASUREMENTS

The user's eABR measurements were taken during the same clinical session. The eABR measurements can be used to support the conclusions drawn from the eCAP data about possible neural damage. Multiple measurements were conducted to ensure conclusive wave peak values. The eABR waveforms consist of approximately seven vertex positive waves. Many of the early latency eABR wave peaks are obscured by a stimulus artefact. In the clinical eABR measurements for this study only wave V was identifiable, which limited the conclusions that could be made regarding possible ANF damage.

The clinical eABR measurement technique was time intensive and required the user to remain motionless for extended periods of time. As a result, only nine electrodes were measured for eABR responses. These electrodes were randomly distributed along the length of the array. The results were output by the eABR software as pdf files containing the graphs and peak values for each electrode. This meant that the eABR graphs could not be extracted to Matlab for further analysis or compilation. During the measurement session, a trained audiologist identified the eABR peaks. The latency and amplitude values of the peaks are displayed in the tables accompanying the waveform figures. The trace names contained in the tables, such as 1L1 and 1L2, are the names generated by the eABR measuring software for the individual traces. A few eABR measurements of note are given in this section. All additional eABR measurements are included in the addendum.

| Trace | ms | µV |
|---|---|---|
| 1L | 4.60 | 0.771 |
| 1L2 | 3.87 | 0.938 |

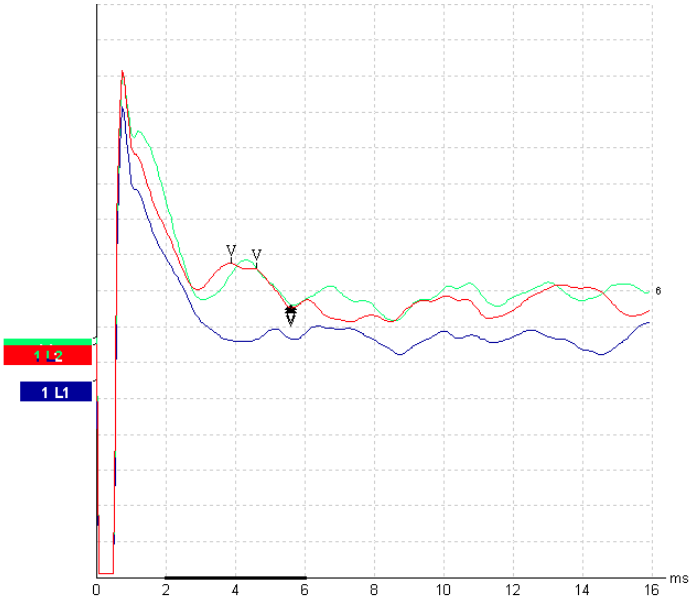


**Figure 5.17.** eABR response to stimulation on electrode 6 with the peak values recorded in the table on the left.

A few of the electrodes displayed a large atypical response, like the response depicted by the grey waveform in figure 5.18, which obscured the expected eABR response waves. The possible cause for this response is discussed in chapter 6.

| Trace | ms | µV |
|---|---|---|
| 1L | 4.07 | 0.878 |
| 1L5 | 4.13 | 1.197 |
| CR | 2.40 | 12.56 |

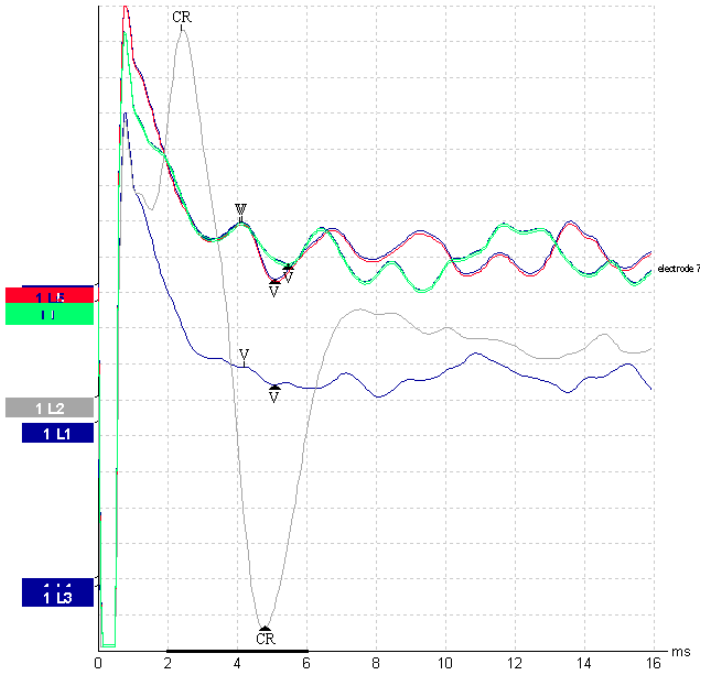


**Figure 5.18.** eABR response to stimulation on electrode 7 with the peak values recorded in the table on the left. The CR trace values are the values of cursor-selected points on the grey trace.

| Trace | ms | µV |
|---|---|---|
| 1L | 4.07 | 0.567 |
| 1L2 | 4.07 | 0.413 |

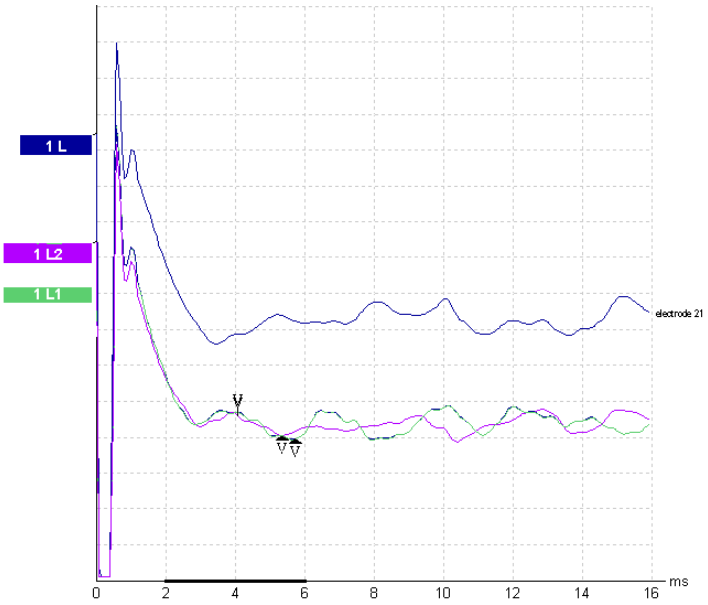


**Figure 5.19.** eABR response to stimulation on electrode 21 with the peak values recorded in the table on the left.

Some of the eABR measurements presented in this section showed a large uncharacteristic response, which obscured the useful eABR waves, as was shown in figure 5.18. The origin of this wave is possibly a myogenic response triggered by the stimulus (Fifer and Novak 1990). The constraints of these clinical measurements, in that only wave V can be identified, limit the conclusions that can be drawn from the data regarding the user's neural damage, as many of the indications of the different damage mechanisms refer to the peaks, latencies and relative differences of the obscured waves. In only two instances the data was sufficient to make useful observations: a slightly prolonged latency of the eABR wave V on electrode 6 might indicate degeneration, and a small reduction in the wave V amplitude of electrode 21 could indicate demyelination of the contributing fibres. The possible degeneration of the nerve fibres in the proximity of electrode 6 supports the interpretation of the eCAP measurements.

## 5.5 MODELLING NEURON FIRING RESPONSE FOR EACH ELECTRODE AT T LEVEL.

After obtaining and analysing the clinical measurements for this study, the Bioengineering Group's existing model generation software was used to generate a person-specific VC model of this user's cochlea. The voltages along the fibre trajectories in response to stimulation from each electrode in the implanted electrode array were determined using this model. This information was then used as input for the computational ANF population model. Using this model, an indication of the neurons that are activated by each electrode was determined at a level near threshold, i.e. where several fibres would fire. A representation of the fibres which contribute to the eCAP response of each electrode was then compiled, as shown in figure 5.20.

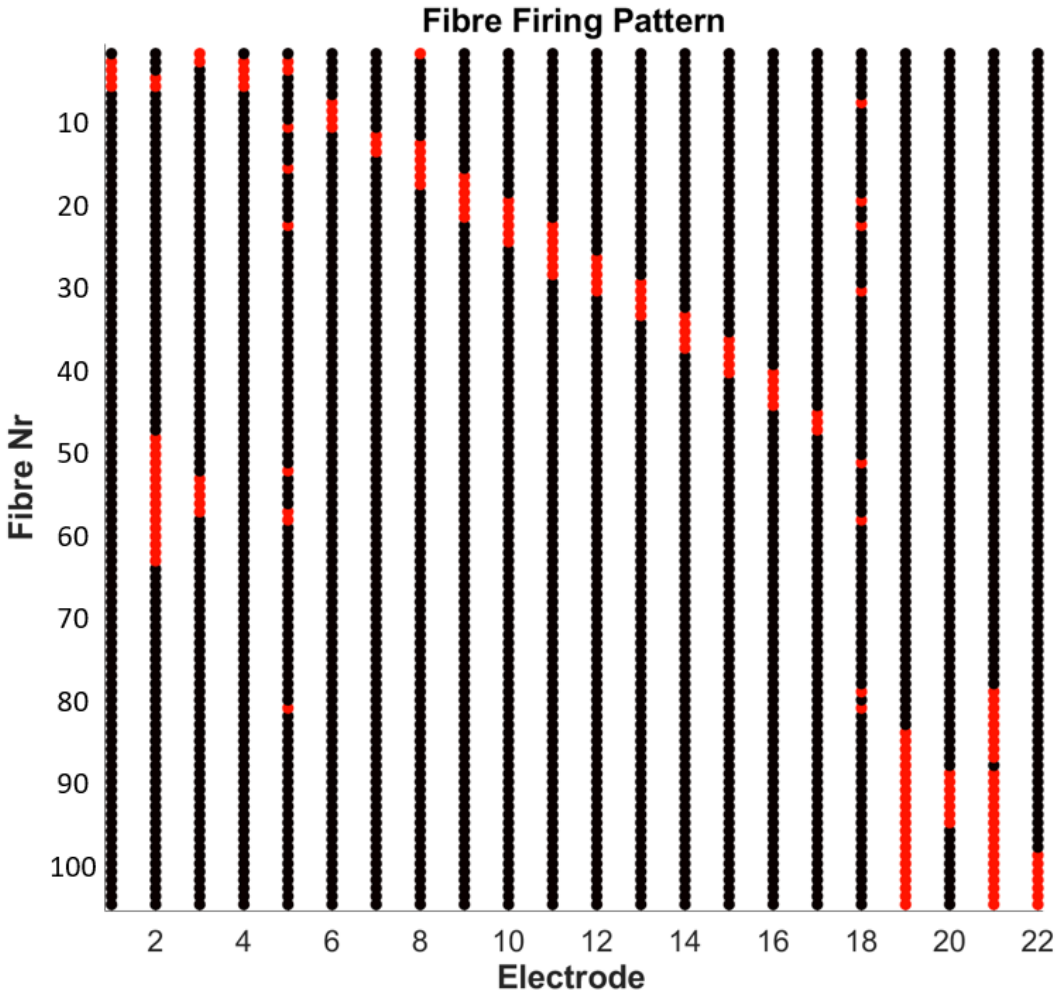


**Figure 5.20.** Figure depicting the firing pattern of ANFs in the person-specific model, with red dots indicating the ANFs that fire and black dots indicating those that do not.

In general, this firing pattern of the fibres reflects the geometric placement of the electrodes in the cochlea. However, the pattern also shows multiple regions of excitation for electrodes 5 and 18. When considering the location of the firing fibres relative to the locations of these two electrodes, the regions of excitation appear to consist of the fibres neighbouring the electrode in the cochlea as well as ectopic locations in the vicinity of the electrode. For electrode 5, fibres in the base are excited (lower fibre numbers) as well as fibres approximately 180 degrees further on in the cochlea (excitation of the axons in the modiolus; fibre numbers 50 to 60) and again at approximately one turn from the electrode (fibre 80). For electrode 18, neighbouring fibres (fibres 50 to 60) are excited while fibres approximately 180 degrees from the electrode are ectopicly excited in the modiolus (fibre numbers below 30 in the base and fibre numbers above 75 in the apex). The firing fibres near the middle of the fibre population for electrodes 2 and 3 suggest that the excitation spread may occur not only in neural populations

adjacent to the electrode, but also in more distant neural populations as a result of electrode current spreading across cochlear turns (i.e. cross-turn or ectopic stimulation). The overlap of the cochlear spiral's dendrites can be seen in figure 5.21.

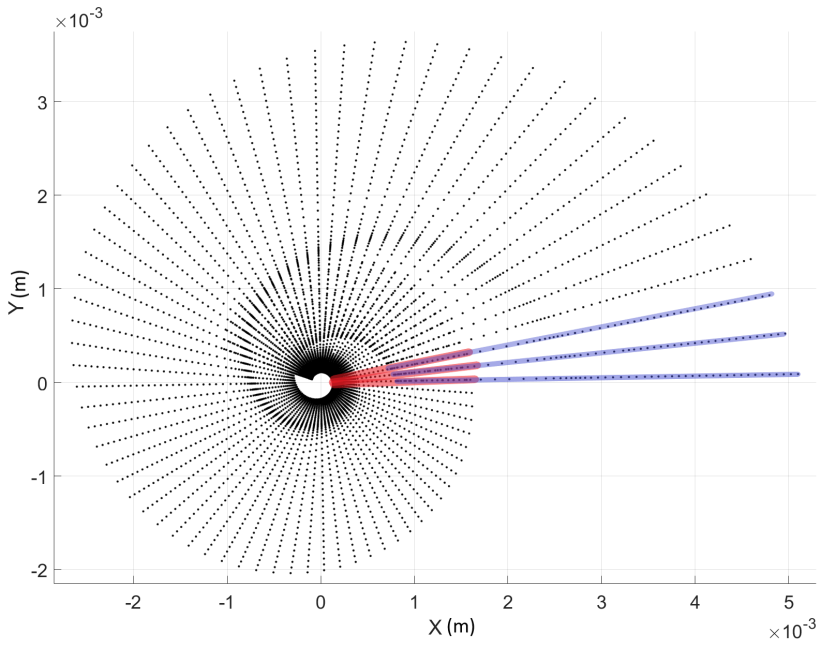


**Figure 5.21.** Figure illustrating overlap of the inner (red) and outer (blue) layer of nerve fibre dendrites.

## 5.6 MODEL PREDICTED ECAPS

The anatomy of the person-specific cochlear model was based on the user's CT scans. This cochlear model was used to determine the voltage distribution in the cochlea and along the nerve fibres due to electrical stimulation by the implanted electrode array. The model also incorporated the electrode positions, as determined from the CT scans, to determine the effect of the placement of the electrodes relative to the nerve fibres. For this study, the auditory nerve was represented using an even distribution of nerve fibres along the length of the cochlear model. The recording electrode used in the simulations was located two electrode positions apical to the stimulating electrode. For electrodes 21 and 22, the recording electrode was located two positions basal from the stimulating electrode. This is the same stimulation pattern that was used in the clinical measurements.

### 5.6.1 Damage profile

The damage profile that was determined using the clinical electrophysiological results presented in this chapter was used to apply the different types of damage mechanisms to neurons in the proximity of individual electrodes. The possible damage on the nerve fibres adjacent to specific electrodes was determined by examining the compiled single stimulation level figures and the interpolated or extrapolated data with prediction bands for the electrophysiological indicators of neural damage indicated in the literature. These indicators include increased or decreased N1 latency and amplitude reduction. Both the compiled figures and interpolated or extrapolated data were combined to allow a better estimation of the neural damage profile for the user. The 75% prediction bands were used in the analysis to include more data points in the damage range to ensure that the prediction bands don't only identify outliers.

One example of how the damage profile was determined is that electrode 21 displayed a reduced N1 latency compared to the other electrodes in the compiled clinical eCAP results shown in figure 5.8 and the 75% prediction band for the data points above both T and C levels, which is an indicator of ANF degeneration.

The possible types and locations of ANF damage, as identified in this process, are given in table 5.1.

| Electrode | Same Stimulation Level Figures | Prediction Bands for Data above Comfort Level | Prediction Bands for Data above Threshold Level |
|---|---|---|---|
| 1 | | | |
| 2 | | | |
| 3 | | | |
| 4 | Degeneration | | |
| 5 | Degeneration | | Degeneration (Possible Fibre Loss) |
| 6 | Degeneration | | |
| 7 | | | |
| 8 | Demyelination | Demyelination | Demyelination |
| 9 | | | |
| 10 | | | |
| 11 | | | |
| 12 | | | |
| 13 | | | |
| 14 | | | |
| 15 | Degeneration | Degeneration | |
| 16 | | | |
| 17 | | Demyelination | Demyelination |
| 18 | | | |
| 19 | | | |
| 20 | | | |
| 21 | Degeneration | Degeneration | Degeneration |
| 22 | Degeneration | Degeneration | Degeneration |

**Table 5.1.** Damage profile used in this study.

### 5.6.2 Damage on nerve fibres contributing to individual electrodes

#### 5.6.2.1 Degeneration

Degeneration was applied to the fibres that contribute to the response on electrodes 4, 5, 6, 15, 21 and 22. The first eight compartments of the fibres were removed to simulate degeneration of the dendrite. The output of the model for healthy and degenerated populations are given in figures 5.22 to 5.27. The eCAP responses generated by the degenerated ANF populations display the expected reduction in the latency of peak N1.

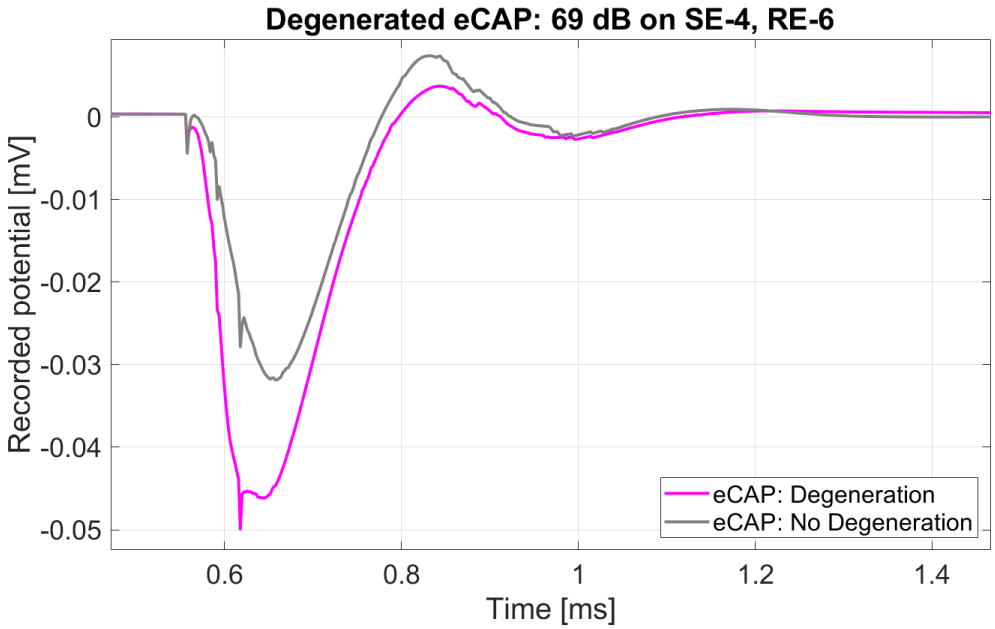


**Figure 5.22.** Degenerated and healthy population population eCAP responses measured on electrode 4. Electrode 4 was the stimulation electrode (SE) and electrode 6 was the recording electrode (RE) for this simulation.

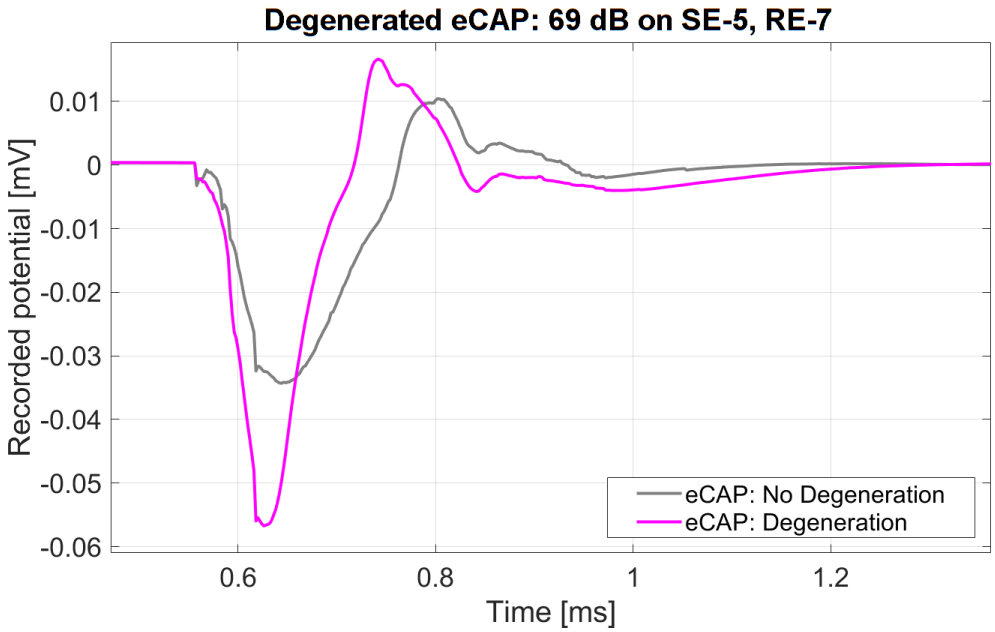


**Figure 5.23.** Degenerated and healthy population eCAP responses measured on electrode 5. Electrode 5 was the SE and electrode 7 was the RE for this simulation.

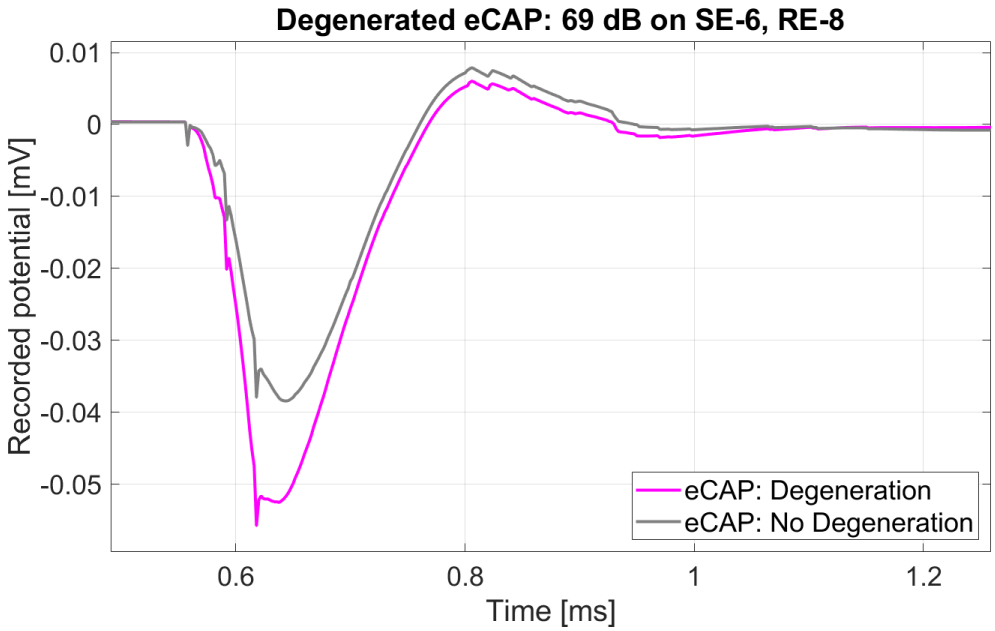


**Figure 5.24.** Degenerated and healthy population population eCAP responses measured on electrode 6. Electrode 6 was the SE and electrode 8 was the RE for this simulation.

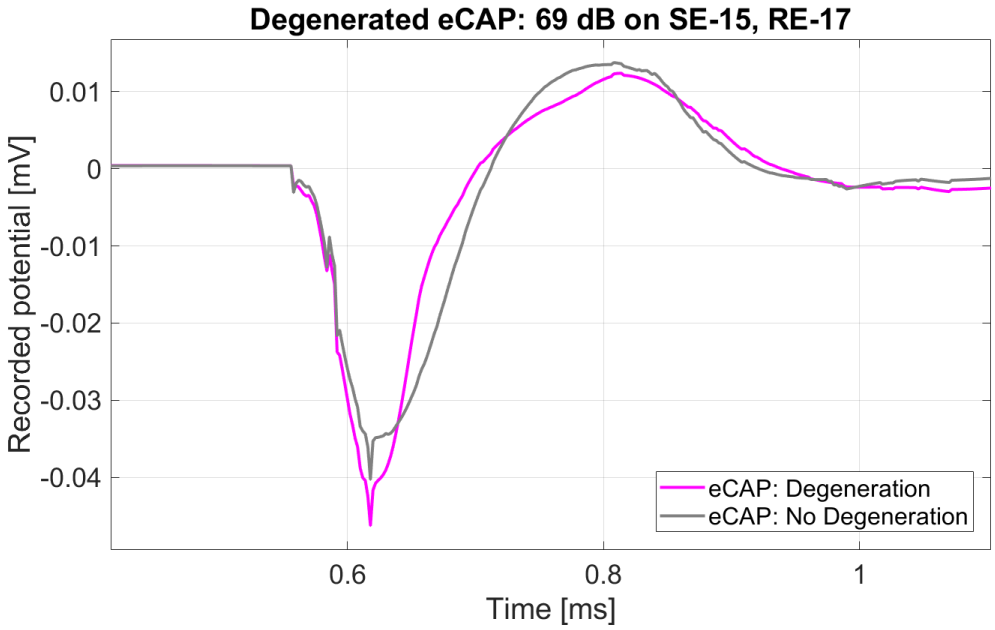


**Figure 5.25.** Degenerated and healthy population eCAP responses measured on electrode 15. Electrode 15 was the SE and electrode 17 was the RE for this simulation.

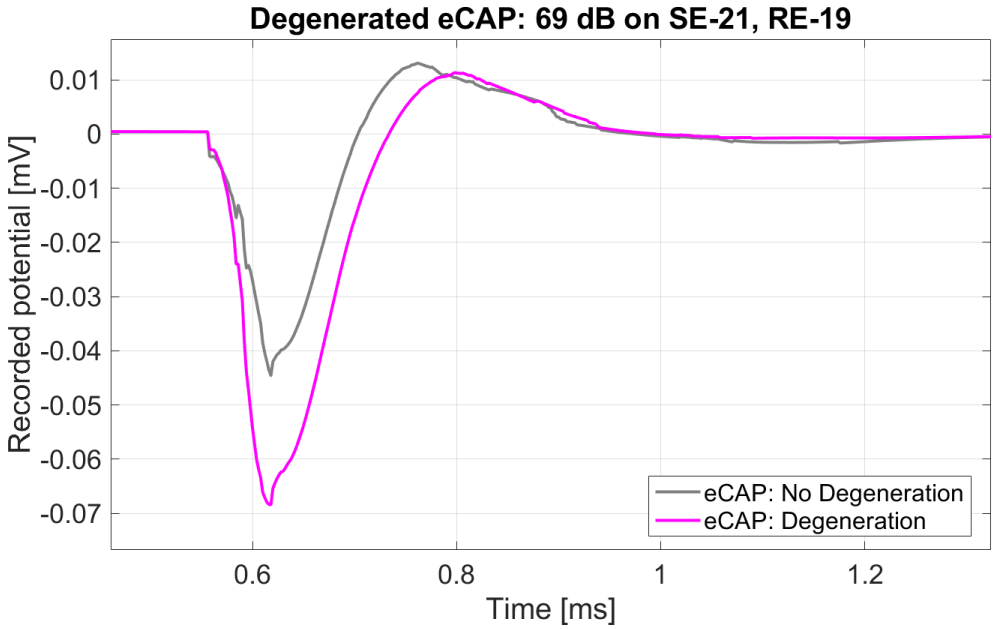


**Figure 5.26.** Degenerated and healthy population eCAP responses measured on electrode 21. Electrode 21 was the was the SE and electrode 19 was the RE for this simulation.

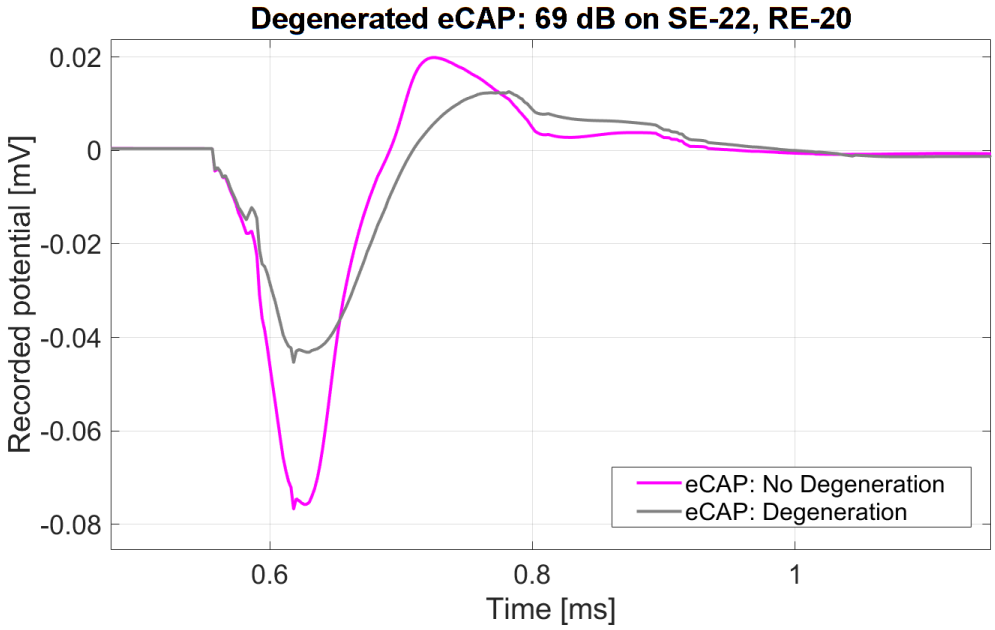


**Figure 5.27.** Degenerated and healthy population population eCAP responses measured on electrode 22. Electrode 22 was the SE and electrode 20 was the RE for this simulation.

#### 5.6.2.2 Demyelination

Demyelination was applied to both the dendrites and axons of the fibres which contributed to electrode 8 and 17. The eCAP responses generated by the demyelinated ANF populations display the expected reduction in amplitude, as well as a slight delay in the latency of peak N1.

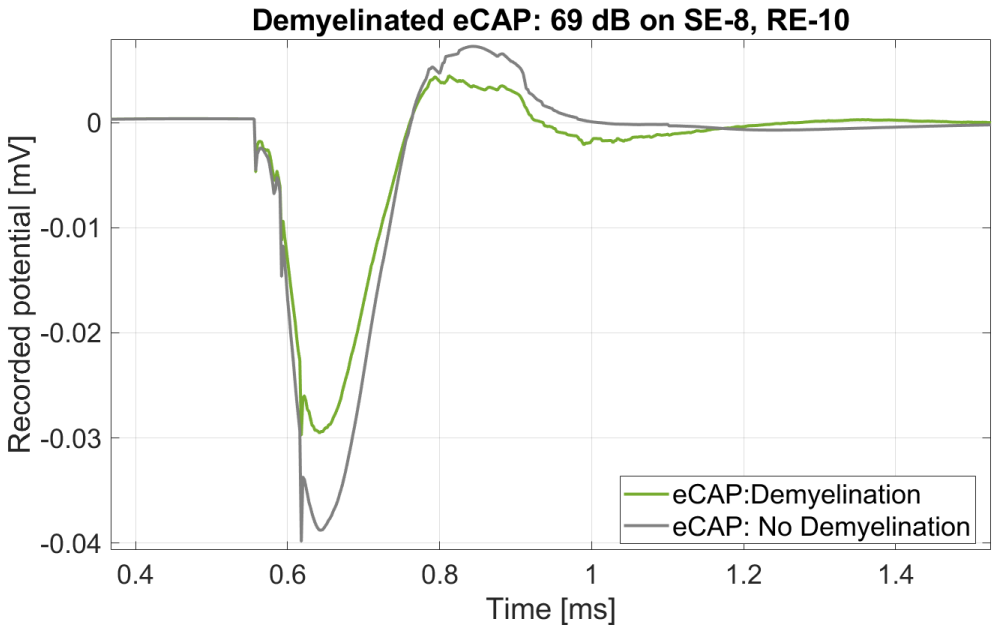


**Figure 5.28.** Healthy and demyelinated population eCAP responses measured on electrode 8. Electrode 8 was the stimulation electrode (SE) and electrode 10 was the recording electrode (RE) for this simulation.

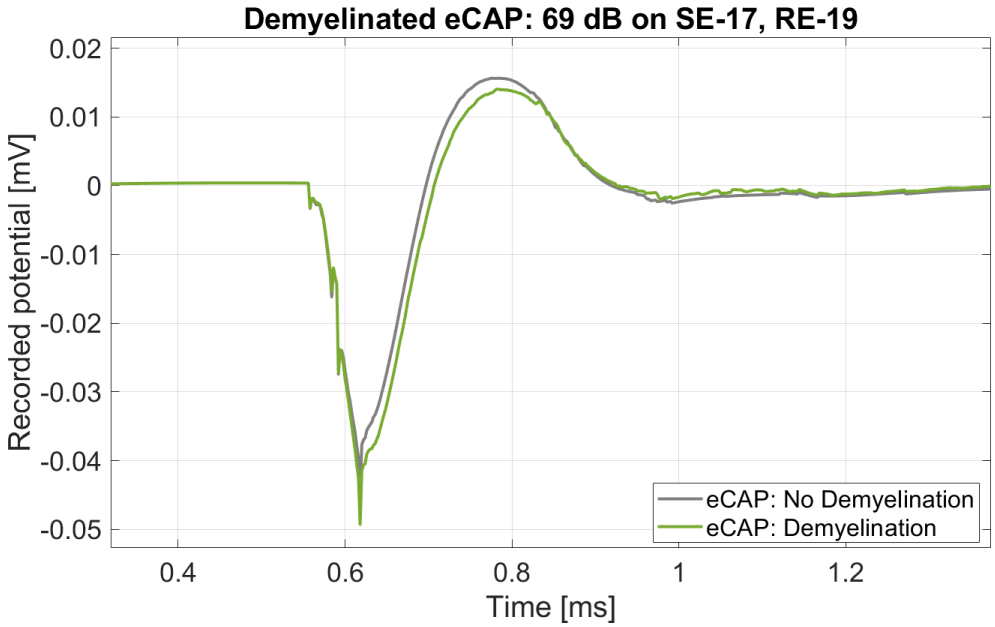


**Figure 5.29.** Healthy and demyelinated population eCAP responses measured on electrode 17. Electrode 17 was the stimulation electrode (SE) and electrode 19 was the recording electrode (RE) for this simulation.

#### 5.6.2.3 Combined damage profiles

The eCAP factors contributing to damage profile for electrode 5 indicated that the responses exhibited both reduced N1 latency and reduced eCAP amplitudes. The reduced N1 latency points towards neural degeneration of the fibres contributing to the eCAP. The reduced amplitude may be indicative of fibre loss in the area of the neural population that contributes to the eCAP response. A simulation of the eCAP response measured by electrode 5 from a population with fibre loss is shown in figure 5.30. The modelled neuronal population with fibre loss produced an eCAP waveform that shows the expected decrease in eCAP amplitude.

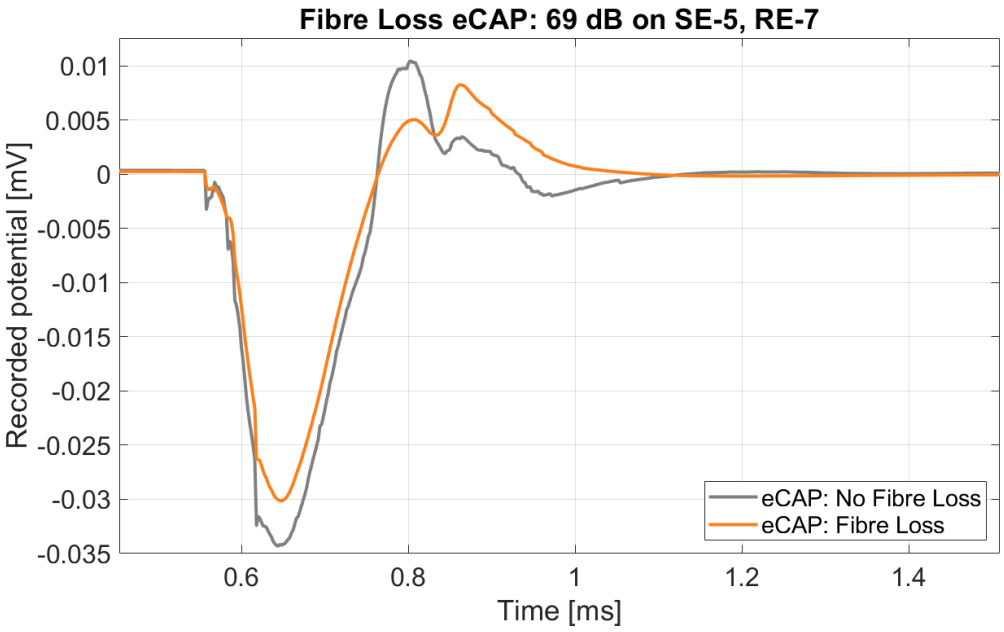


**Figure 5.30.** eCAP responses generated by a healthy population and population with fibre loss measured on electrode 5. Electrode 5 was the SE and electrode 7 was the RE for this simulation.

A simulation of the eCAP response measured by electrode 5 from a population with a combination of fibre loss and fibre degeneration is shown in figure 5.31. Half of the nerve fibres in the population were excluded as a result of fibre loss and the fibres that were included were degenerated. The modelled neuronal population with combination damage produced an eCAP waveform that shows the expected decrease in eCAP amplitude but does not show the expected reduction in N1 latency. This result suggests that the neural fibres contributing to electrode 5's eCAP response may have less fibre loss than the 50% used in this model and might also have more fibres with neural degeneration than this population.

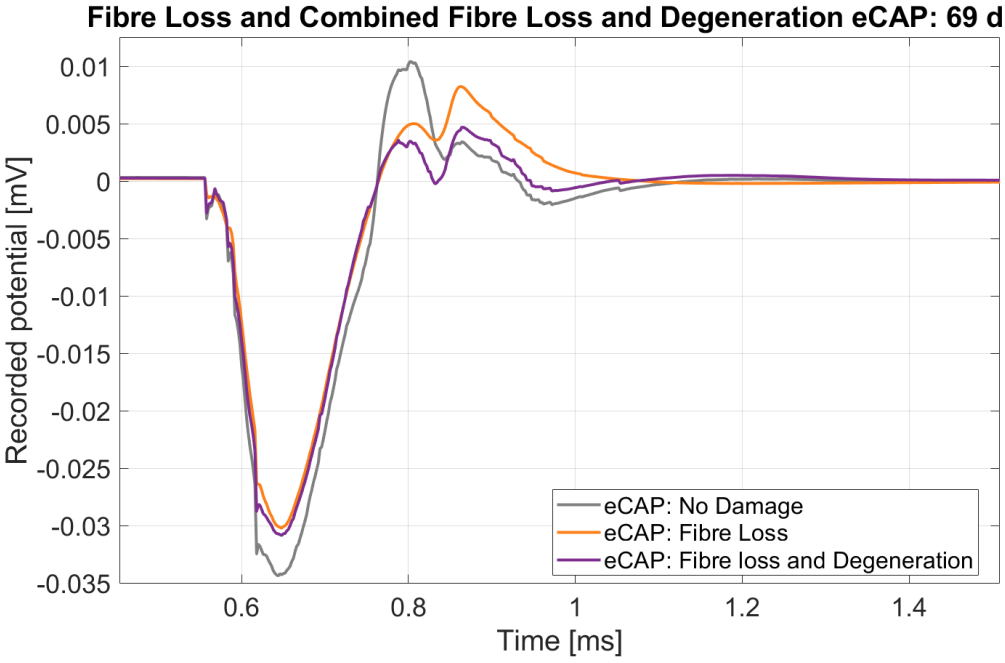


**Figure 5.31.** eCAP responses generated by a healthy population, a population with fibre loss and a population with combined fibre loss and fibre degeneration measured on electrode 5. Electrode 5 was the SE and electrode 7 was the RE for this simulation.

The implications of electrode 5 displaying characteristics of both degeneration and fibre loss are discussed in section 6.3.1.

### 5.6.3 Compiled model responses

For these model predictions, the electrodes grouped in the figures are the same as those represented in the figures containing the clinical eCAPs measured at each relevant stimulation levels. In figures 5.32 and 5.33 the same electrodes were used to stimulate the modelled nerve fibres as were grouped in the compiled clinical results measured at 145 CL, namely electrodes 20, 21 and 22 (The inset image on the figures below is figure 5.8).

The figures below illustrate the effects of eCAP waveforms relative to one another. This section only includes one compilation to illustrate the effect of neural damage to the electrodes identified in the damage profile. Several more compiled figures for other electrodes, which contain the same electrode waveforms as the clinical compilations, are included in the addendum.

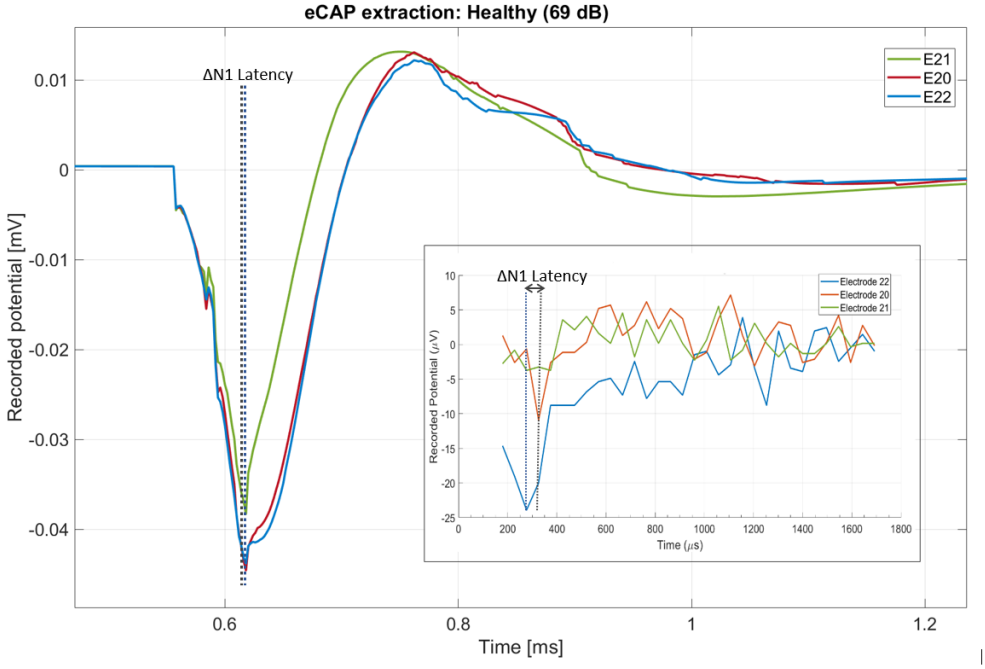


**Figure 5.32.** eCAPs of Electrodes 20, 21 and 22 with healthy neural population.

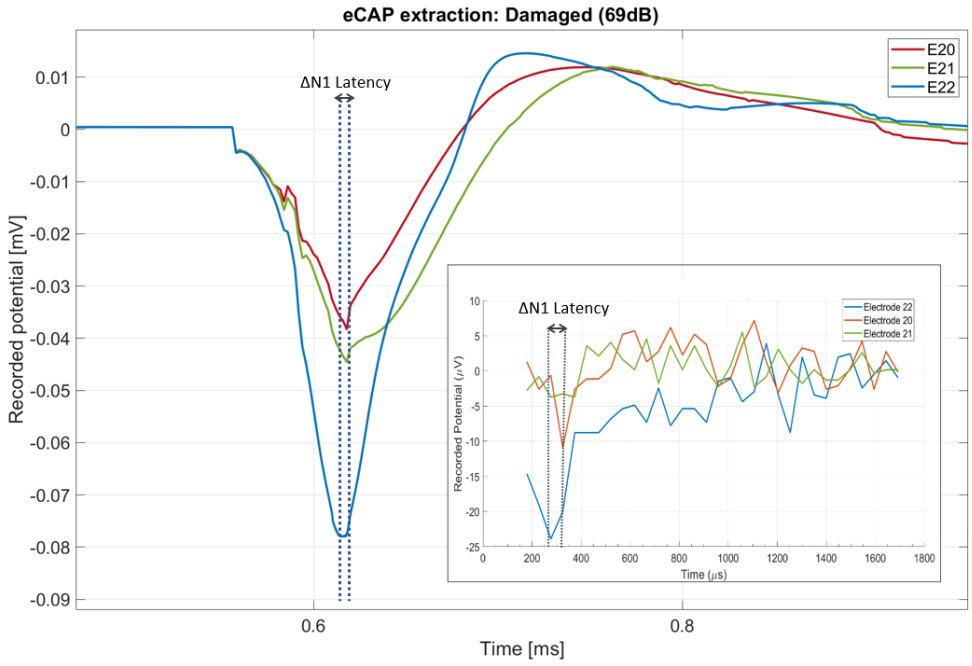


**Figure 5.33.** eCAPs of Electrodes 20, 21 and 22 with damage applied to the neural population in accordance with the damage profile.

The compiled figures show that the predicted response of the damaged neural population reflect the increase in N1 latency delay seen on the measured response for electrode 22 slightly better than the healthy model predictions. This suggests that the damage profile used in this study appears to allow the user-specific model to generate moderately more realistic electrophysiological results by applying user-specific damage to the ANFs.

### 5.6.4 Comparison of clinical responses and model prediction

#### 5.6.4.1 N1 latency

The clinical and modelled eCAP N1 latency values for all electrodes are shown below. Figure 5.34 shows clinical eCAP N1 latency values, while figure 5.35 shows the healthy and damaged ANF model predictions of eCAP N1 latency values. The N1 values for the clinical measurements are interpolated or extrapolated values well above T level, near saturation. The model eCAP waveforms were generated at 69dB, which is also near saturation for the predicted eCAPs. The trends of these values can be compared between these images.

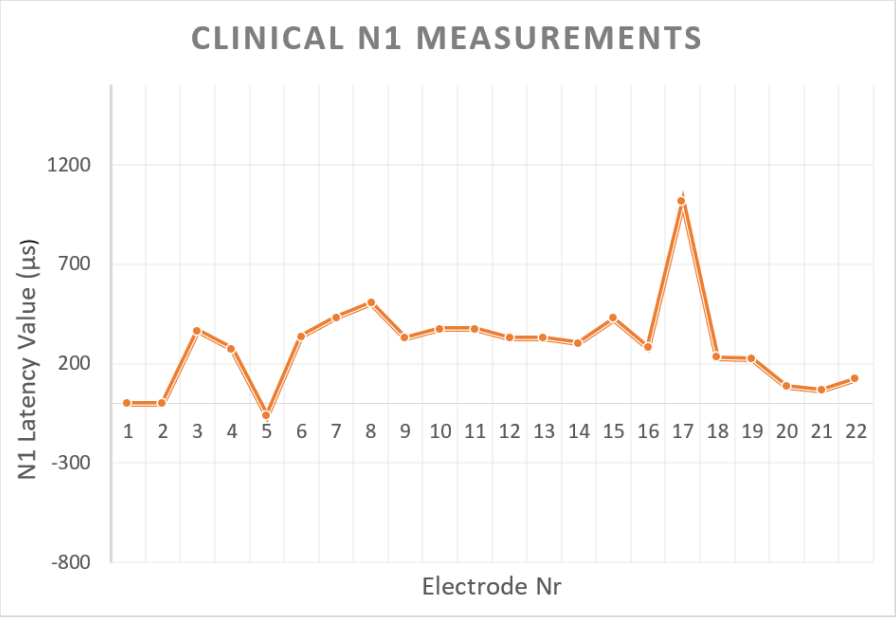


**Figure 5.34.** N1 values of clinically measured eCAPs.

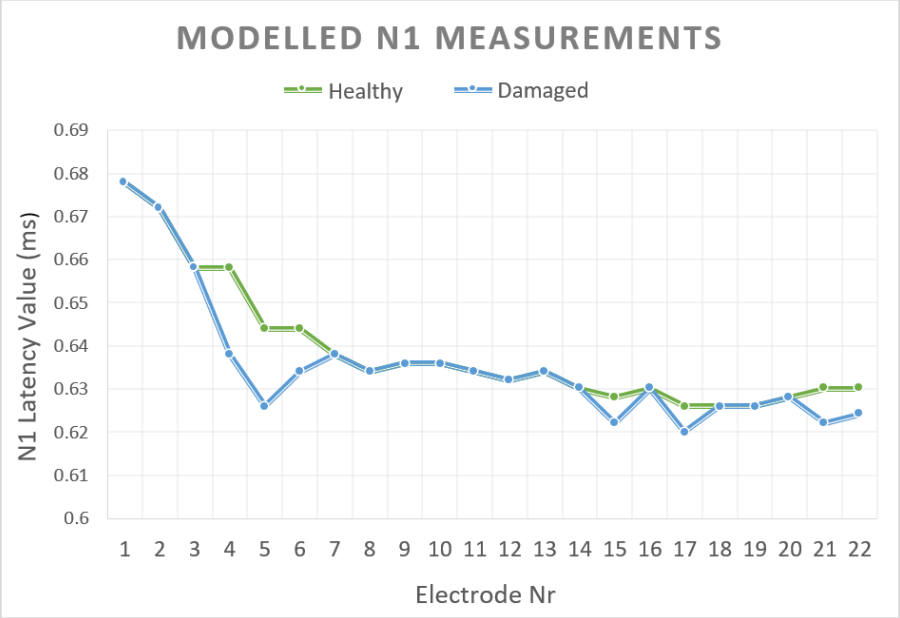


**Figure 5.35.** N1 Values of modelled eCAPs from healthy (green) and damaged (blue) neural populations.

The predicted latencies for some electrodes by the damaged neural model (blue) are in better agreement with the measured clinical values (orange) than the latencies predicted by the healthy model (green). This can be seen by the decrease in values that occurred between electrodes 4 and 6 and the reduced N1 latency values of electrodes 21 and 22 in both data sets. However, the increased latency measured for electrode 17 could not be predicted by the model.

### 5.6.5 Electrode-to-modiolus distance measurements

The distance between each electrode and the modiolus of the cochlea was measured on the CT scans used to construct the 3D cochlear model. The resulting measurements are shown in the figure below.

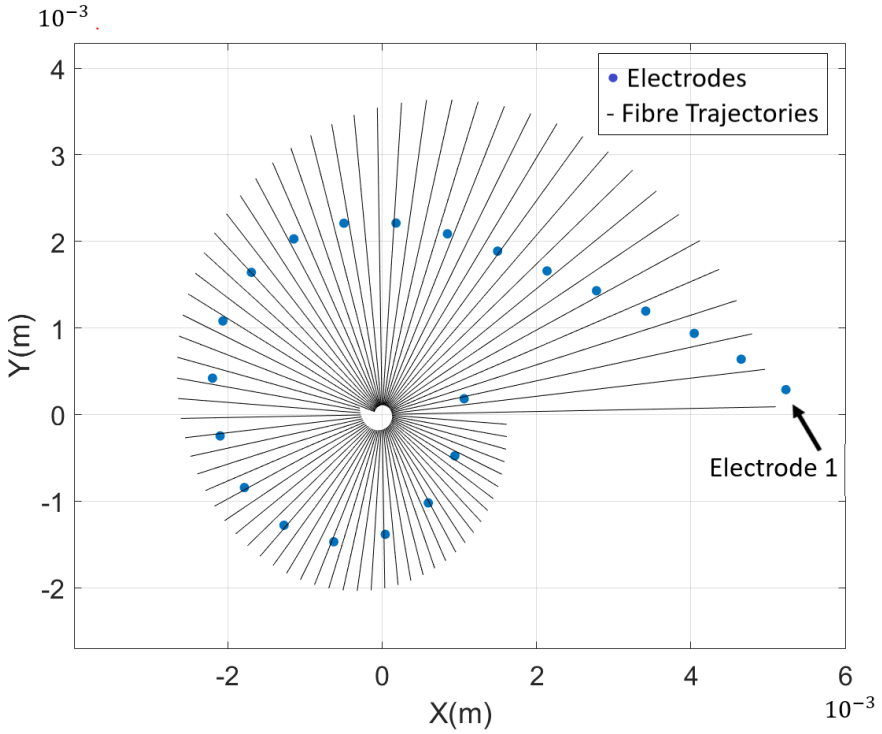


**Figure 5.36.** Placement of electrodes relative to fibre trajectories in person-specific ANF model.

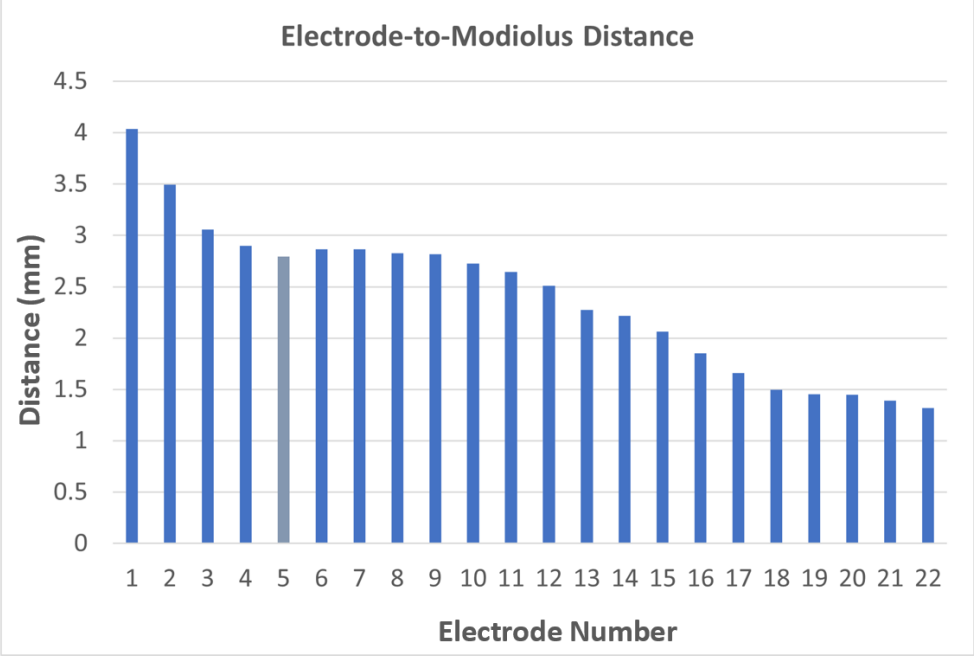


**Figure 5.37.** Electrode-to-modiolus distance measurements.

Electrode 1 is located at the most basal end of the cochlea and electrode numbers ascending to the cochlear apex, as shown in figure 5.36. According to distance values represented by figure 5.37, the

electrodes along the electrode array, starting from the most basal, are positioned increasingly closer to the modiolus. The only deviation from this pattern is that electrode 5 is slightly closer to the modiolus than the adjacent electrodes. This may suggest that the positioning of electrode 5 could be responsible for the irregular fibre firing patterns and low threshold values of the electrode.

## 5.7 CHAPTER SUMMARY

In this chapter, a summarised overview of the results obtained during the clinical measurement session is presented and discussed. The data analysis techniques used to interpret the limited electrophysiological data are also outlined in this chapter. The latter half of the chapter presents several results obtained using the combined user-specific cochlear and ANF models. These results include the fibre firing pattern for the threshold levels of each electrode along the cochlea, providing insights into the fibres that contribute to electrophysiological measurements on each electrode, and the effect of electrode placement on the firing patterns elicited by the electrodes. A comparison of modelled eCAP responses generated by healthy and damaged ANF models is presented. Compiled modelled eCAP results allow more direct comparison of the relation between eCAP waveforms measured on different electrodes, as seen in clinical waveform compilation figures. N1 latency figures as well as threshold values for both the model and clinical measurements was also included in this chapter.

# CHAPTER 6 DISCUSSION

## 6.1 CHAPTER OVERVIEW

This chapter discusses the previous chapter's results and reviews the findings of this study. The clinical eCAP and eABR measurements obtained during the clinical measurement session are discussed in section 6.2. This section also includes the conclusions drawn from the data. Section 6.3 reviews the eCAP results obtained by both the healthy and damaged user-specific models. In section 6.4 proposed improvements to the procedures used in this study are discussed. Section 6.5 contains summaries of the answers to the research questions posed in chapter 1. Potential future work is proposed in section 6.6.

## 6.2 CLINICAL ELECTROPHYSIOLOGICAL MEASUREMENTS

The eCAP waveforms measured by the AutoNRT algorithm and the eABR waveforms that were measured during the clinical session were presented in sections 5.2 and 5.4. The analysis of these clinical results is discussed in this section.

### 6.2.1 AutoNRT (eCAP) measurements

The AutoNRT measurements taken during the clinical experiment were used to determine possible auditory neural damage. The stimulation levels for the eCAPs measurements taken by the AutoNRT algorithm were determined by the 'ascending and descending series' steps, which in turn resulted in the eCAP measurements for the various electrodes to be conducted at the varying stimulation levels. Changes in stimulation levels have a direct effect on the latencies and amplitudes of eCAPs, hence eCAPs must be generated at the same stimulation levels to compare their latency and amplitude values. This exploratory study assumed that all other variables and parameters, which may affect the eCAP characteristics, are constant. Other factors which may possibly influence eCAP amplitudes and

latencies include, for example, the effect of stimulation in the apical region compared to the basal region of the cochlea on eCAP waveforms.

The analysis of the eCAP amplitudes and latencies was hampered by the varying stimulation levels of the measured eCAPs. To overcome this, the original eCAP measurements were extracted from the CustomSound software and transformed to the equivalent eCAPs at the same stimulation levels using Matlab. This allowed eCAPs at the same stimulation level to be grouped for comparison which made it possible to compare the latencies and amplitudes of the eCAPs in the figures directly.

The clinical eCAP readings contained a high level of noise, which may lead to indeterminate latency and amplitude measurements, in some instances impacting the accuracy of the neural damage predictions. For example, comparing the N1 and P1 values of the compiled original eCAP measurements at 208 CL and 211 CL, shown in table 6.1, illustrates that the measurement noise and stimulation level affect the latencies and amplitudes. At 208 CL stimulation, electrode 3 has a shorter latency than electrode 8 (325.40 µs vs 374.20 µs), while the opposite is true at 211 CL stimulation (374.20 µs vs 326.40 µs). This may affect the reliability of the conclusions about the positions of possible neural damage mechanisms drawn from the data. A possible solution to this issue would be to collect several eCAP measurements for the user over multiple clinical sessions and average the results to reduce the effect of noise from individual responses. Another possible solution would be to investigate the effect of various stimulus paradigms used to elicit eCAP responses on the noise of the measured eCAP responses using the Advanced NRT functionality to identify the stimulation paradigm that produces the response with the lowest noise level.

| Electrode | N1 peak values | P1 peak values |
|---|---|---|
| 3 | 325.40, -6.50 | 520.60, 17.40 |
| 8 | 374.20, -10.57 | 667.00, 8.94 |
| 11 | 374.20, -15.29 | 618.20, 19.84 |
| 9 | 325.40, -15.45 | 520.60, 12.36 |
| 10 | 374.20, -7.81 | 618.20, 22.93 |

| Electrode | N1 peak values | P1 peak values |
|---|---|---|
| 3 | 374.20, -11.87 | 520.60, 18.86 |
| 8 | 326.40, -17.73 | 569.40 15.94 |
| 11 | 374.20, -26.02 | 667.00, 12.03 |
| 9 | 325.40, -17.40 | 618.20, 15.77 |
| 10 | 374.20, -16.75 | 618.20, 27.16 |

**Table 6.1.** N1 and P1 coordinates at (left) 208 and (right) 211 CL stimulation. Each column contains the latency ($\mu$s) and amplitude ($\mu$V) values for the specified peak, separated by a comma.

### 6.2.2 Clinical eABR measurements

To explore the feasibility of using clinically measured eABR measurements to support conclusions drawn from eCAP measurements, eABR measurements were obtained for a subset of electrodes. The equipment that was available uses a delayed recording method to remove the stimulus artefact from the data. Unfortunately, this resulted in only wave V being captured in the measured responses. Changing the eABR measurement equipment would be necessary to capture the full waveform. Furthermore, experimenting with alternative locations of the surface electrodes may improve the quality of the eABR measurements.

## 6.3 DAMAGE SIMULATION IN PERSON-SPECIFIC NEURAL MODELS.

A user-specific auditory ANF model that reflected different aspects of neural damage was added to the user-specific VC model to evaluate the effect of damage on predicted eCAP characteristics. The damage profiles of the ANF populations neighbouring each electrode in the model were determined by analysing the clinical eCAP measurements.

While it was shown that the neural model can predict expected changes in eCAP latencies and amplitudes caused by specific types of neural damage, the predictions from the model do not always reflect clinical trends. The primary reason for this is the use of the AutoNRT approach to measuring the responses, which resulted in latency and amplitude values being ambiguous at times. A more sophisticated eCAP measuring protocol (i.e. Advanced NRT) will have to be used to improve the efficacy of the clinical measurements as a basis for the determination of neural damage. The damage profile was generated using a best approximation derived from both the grouped clinical eCAP waveforms and the interpolated and extrapolated data points with prediction bands.

The measured and modelled electrophysiological measurements in this study cannot be directly compared as they could not be conducted at the same stimulation levels. This is a result of the constraints of the AutoNRT algorithm as discussed in section 4.2.1 and the simplified representation of the user's auditory neural fibres used in the model. In contrast to the approximately 30 000 nerve fibres found in humans, the neural model only included nerve fibres every five degrees along the cochlea. In this study, the latencies, amplitudes, and other characteristics of the relevant electrode's eCAP measurements were compared to those of other electrodes, with all measurements taken at a single stimulation level. Future studies could enable direct comparison of the measured and modelled

eCAP value by selecting the stimulation level at which clinical eCAPs are measured to be equal to a stimulation level at which the neural model functions. The neural model can also be expanded by adding more neural fibres at smaller intervals along the cochlea and by including realistic fibre densities along the length of the neural array.

### 6.3.1 Predicted eCAPs

The healthy and damaged eCAP responses of neural fibres in proximity to individual electrodes to which damage was applied are shown in section 5.6.2. Figures 5.22 to 5.27 illustrate the eCAP responses to degeneration of the relevant fibres. The responses demonstrate the expected reduced N1 latency at stimulation levels near saturation. The responses also exhibited larger amplitudes, an observation which is not explicitly mentioned in the available literature. This phenomenon might be explained by the stimulation point of the degenerated fibres being much closer to the soma due to dendritic degradation, resulting in reduced latency and increased amplitude, analogous to the effect of an increase in stimulation intensity. Section 5.6.2 also includes the eCAP graphs of healthy and demyelinated neural fibres contributing to the responses to stimulation with electrodes 8 and 17. The expected reduction in amplitude, as well as a slight delay in the latency of peak N1 was observed in the demyelinated results (see figures 5.29 and 5.28). The small latency delay shown in the demyelinated results suggest that degeneration will again be the dominant determining factor of latency when combined degeneration and demyelination are applied to a fibre population. This is consistent with the findings from the simplified neural population model implemented in Chapter 3.

The damage profile that was utilised to determine which damage mechanisms affected neural fibres contributing to specific electrodes revealed that neurons excited by electrode 5 displayed both degeneration and fibre loss characteristics. It is possible for a CI user to have both fibre loss and degeneration of the remaining fibres contributing to an electrode's response. In this case, however, possible fibre loss on electrode 5 was not included in the damage profile applied to the full electrode array. The CI user in this study has exceptionally good functionality from their implant, which may suggest that a high degree of fibre loss is unlikely. The combined fibre loss and degeneration simulation also suggested that the population's fibre loss could likely be limited to a small portion of the population. The effects of fibre loss on the eCAP response for electrode 5 was examined separately and the results are shown in figure 5.30. The inclusion of fibre loss in this user's damage profile should be investigated further by evaluating alternative eCAP characteristics such as input-output function slopes and relative

refractory periods using Advanced NRT measurements. These measurements could be used to validate all potential damage mechanisms identified by the eCAP latencies and amplitudes in this study.

## 6.4 PROPOSED PROCEDURAL IMPROVEMENTS

Conducting the clinical eCAP measurements using Advanced NRT will allow for much greater control over the stimulation and recording parameters. Advanced NRT measurements allow the user to set a number of parameters, including the number of sweeps, measurement window, recording electrode, current levels, pulse widths, and recording delays, can be adjusted (Hughes 2006). This additional control would allow the effects of different stimulation patterns, such as bipolar stimulation, on eCAPs to be explored which might lead to better responses or less noise in the results. It would also be possible to conduct all the clinical eCAP measurements at the same stimulation level, enabling a more accurate comparison among all electrodes and eliminating the need for interpolation of the data points. Direct comparison of the clinical results and model predictions will be possible if the stimulation level is set to the same level used in the person-specific auditory nerve population model.

Alternative eABR measuring equipment could be considered to provide clinical eABR measurements with fewer obscured waveforms, so that additional damage mechanism markers may be observed. Experimenting with various electrode configurations and trigger settings in the clinical measuring setup may also contribute to more informative measurement results.

## 6.5 DISCUSSION OF RESEARCH QUESTIONS

The study's primary objectives have prompted investigation into the following research questions:

**Is it possible to evaluate a single AN model as well as a simple population AN model as predictors of neural response to ANF damage by using expected characteristics of SFAP and eCAP responses to damage as reported in the literature?**

The expected eCAP responses to various damage mechanisms from multiple sources of literature were analysed and summarised in table 3.1. Both a single fibre and a population model were implemented in Matlab, and the different possible damage mechanisms were applied to the neural models. The single fibre model illustrated the expected responses, although the responses could not be classified as eCAPs, since they were not compound action potentials. The single fibre model could also not

be used to examine the electrophysiological response to fibre loss as the model only contains one fibre. The simplified semicircle population model also illustrated the expected eCAP responses to fibre degeneration, demyelination, degeneration and fibre loss. The person-specific neural model also predicted the expected eCAP responses when the damage profile was applied, although this did not necessarily reflect clinical observations. Therefore, it was possible to evaluate a single AN model as well as a simple population AN model as predictors of neural response to ANF damage by using the expected characteristics of SFAP and eCAP responses to damage.

**Can electrophysiological responses be used to identify or differentiate between damage mechanisms affecting ANFs?**

A damage configuration for each damage mechanism was applied to the population model to investigate the possible effects of the damage on the outcome of the eCAP simulations. The damage configurations were based on literature and categorised as degeneration, demyelination or neural fibre loss. The effects of each mechanism could be distinguished from the model-predicted eCAP responses. The clinical eCAP measurements obtained from the CI user were also analysed to identify the various damage mechanisms. It was possible to differentiate between the three damage mechanisms examined in this study. The possible sites along the cochlea that the various damage mechanisms might be affecting could also be pinpointed with the help of the eCAP measurements. However, as noted, a more sophisticated Advanced NRT eCAP measurement protocol is required to improve the derivation of damage parameters from the data.

**How successful is the person-specific compound volume conduction (VC) and computational ANF model in predicting the amplitude and latency characteristics of measured outcomes?**

The ANF model implemented in this study was capable of reflecting the expected relative amplitude and latency changes in eCAP responses to the different damage mechanisms applied to the model, as shown in section 5.6.2. The eCAP N1 latency results for the electrode array, depicted in figure 5.35, more closely resembled the N1 latency trends found in the clinical results after the clinically identified damage was applied to the neural population in the user-specific model than the healthy model result for some electrodes, e.g. electrode 5. However, this was not true for all electrodes and some sections of the trend shown by the clinical N1 latency values were not reflected by the model's predicted latency

values. More comprehensive clinical measurements would allow for a more conclusive damage profile, possibly enabling the model to predict measured outcomes more accurately.

**Can a compound ANF model, which incorporates ANF damage provide insight regarding the effect of electrode placement on eCAP characteristics?**

The compound volume conduction (VC) and computational ANF models used in this study included the locations of all electrodes from the implanted array. This suggests that comparing the eCAP predictions of the healthy and damaged models may provide a means of determining whether an eCAP characteristic is affected by electrode placement or ANF damage mechanisms. Referring to figure 5.35, the healthy model's N1 latency values do not exhibit the trends which are reflected by the clinical data (shown in figure 5.34). This is a possible indication that the electrode placement had no effect and could suggest that the trends of the latency values in the clinical data may be a result of damage mechanisms rather than electrode placement. However, the model did not provide sufficient evidence that electrode placement did not affect the eCAP predictions for the CI user in the manner indicated by clinical eCAP characteristics. Consequently, the results of this study are inconclusive regarding the effect of electrode placement on eCAP characteristics. Nevertheless, the effects of the two different electrode configurations used for the single nerve fibre and simplified population models (shown in figure 3.13) highlighted the importance of including realistic electrode placement in user-specific models as the placement had a notable impact the generated eCAP responses.

## 6.6 FUTURE WORK

This study suggests that it is possible to investigate mechanisms of ANF damage using electrophysiological measurements and apply the deduced damage to a user-specific combined cochlear and AN model. Modelled eCAP predictions generated by a population containing the deduced neural fibre damage appear to follow expected trends from the literature. The damaged model appears to generate some predictions that are more reflective of the measured user data, such as the decrease in N1 latency at electrode 5 observed in the measured data and reflected by the damaged model predictions. The model did not reflect the measured data for all electrodes. Future work that could improve the modelled eCAP predictions may include the following.

- Follow-up clinical measurement sessions with the user, using Advanced NRT and improved eABR measurements, would allow for more eCAP and eABR data to be collected which

could be used for more comprehensive data analysis and verification of the user's neural damage profile.

- Validation of the approach may be extended to a larger CI user population to test whether the outcomes of this study can be generalised. Examination of multiple CI user's clinical data may be used to compile more comprehensive data sets and to fine-tune the relative limits outside which latency or amplitude values may indicate damage.

- Examine the potential relationship between the slope of the amplitude growth function (AGF) of the eCAPs and the user's neural survival as suggested by Gärtner et al. (2021).

- Investigate the effect of the modification of the pulse duration (PD) and interphase gap (IPG) of the stimulation on the eCAP and eABR measurements and the correspondence to neural survival as suggested by Prado-Guitierrez et al. (2006).

- Investigate additional characteristics of the eCAPs measurements which may correlate with ANF survival. These characteristics include slopes of input-output functions and pulse polarity as suggested by He, Shahsavarani et al. (2018) and Undurraga, Wieringen et al. (2010).

- Investigate the effect of including the physiological density distribution as presented by Spoendlin and Schrott (1989) in the ANF population model on eCAP prediction.

# CHAPTER 7 CONCLUSION

## 7.1 SUMMARY OF STUDY

In the first phase of this study, literature sources pertaining to existing electrophysiological measurements that have been used to identify and differentiate auditory neural damage were evaluated. eCAPS and eABR measurements were subsequently chosen for this research. Conclusions from literature regarding the characteristics of the response of eCAP and eABR measurements to different damage mechanisms were compiled to reference templates and tables. The three primary neural damage mechanisms that were identified for this study are ANF degeneration, demyelination, and fibre loss.

The neural model implemented in this study was evaluated as a predictor of eCAP responses to different types of ANF damage as anticipated from the literature. The ANF model is based on a Hodgkin-Huxley-based human compartmental ANF model developed by Rattay, Lutter and Felix (2001) which was scaled in accordance with the model by Kalkman, Briaire, Dekker et al. (2014), previously implemented by Badenhorst, Hanekom and Hanekom (2017). The model was adapted to allow demyelination and degeneration of the model's neural fibres. Fibre degeneration and demyelination mechanisms were applied to both a single-fibre model and a simplified population model. Fibre loss was only applied to the simplified population model. Both models exhibited the expected responses to the various mechanisms.

Clinical eCAP and eABR measurements were taken during an experimental measurement session with a CI user. The clinical data was analysed for possible indications of neural damage on all electrodes. The potential damage predictions to the ANFs were divided into sections corresponding to the electrodes, as the electrophysical results are compound measures of all fibres that contribute to a recorded response.

The ANF model was subsequently integrated with a 3D user-specific model of the CI user's cochlea.[1] The resulting user-specific compound model allowed investigation of the effects of damage mechanisms on modelled eCAPs with realistic neural fibre and electrode placement.

The clinical eABR measurements were limited and only allowed insight into the behaviour of wave V, which greatly limited the conclusions that could be drawn from these results.

The clinical eCAP responses were distributed across multiple stimulation levels and contained copious amounts of noise, necessitating the use of data analysis techniques to determine the outlier values used to generate a damage profile for the CI user.

The damage profile was used as reference to apply the different damage mechanisms to the relevant nerve fibres in the user-specific model. Figures containing the eCAP waveforms predicted by both the healthy and damaged neural models for affected electrodes were generated to visualise the impact of the damage on the eCAP responses. Figures were also generated using the model which showed multiple electrode's eCAP responses overlaid to illustrate how neural damage affected the waveforms of different electrodes in relation to one another. These figures mirror those compiled from the clinical measurements which contained waveforms generated at the same stimulus level.

N1 latency values were plotted for each electrode from the clinical measurements as well as the healthy ANF models, and the damaged ANF models. The trends of these values were examined. The N1 latency values from the damaged model better reflected the general trend of the clinically measured N1 latency values than the values from the healthy model.

All the eCAP responses predicted by the model which included damaged fibres, more closely followed some of the trends found in the clinical measurements than the healthy model. The simulated results, however, still contained some discrepancies when compared to the behaviour of the clinical eCAP measurements, indicating that other factors may influence the electrophysiological responses or that the damage profile used in the study could contain some inaccuracies due to limited data or extensive interpolation.

This study has shown promising results indicating that electrophysiological responses may potentially be used to identify the type and location of ANF damage. The data used in this study presented various

[1] The cochlear model was developed by another master's student in the Bioengineering research group, Joshua Thiselton.

limitations and further examination of this study's proposed use of electrophysiological measurements with more robust data sets would be advised to determine whether the findings of this study can be generalized.

## 7.2 FINAL CONCLUSION

In summary, the following can be concluded from this study:

- Damage mechanisms could be identified using electrophysiological response characteristics identified from literature.
- The person-specific ANF model used in this study is suitable to predict the expected damage responses.
- These damage mechanisms could be identified from clinical measurements and applied to a user-specific neural model to investigate the influence of ANF damage on eCAPs.

# BIBLIOGRAPHY

ABBAS, P. J. and BROWN, C. J. (2015). 'Assessment of responses to cochlear implant stimulation at different levels of the auditory pathway'. *Hearing Research* 322, 67–76.

AGRAWAL, V. and NEWBOLD, C. (2012). 'Computer modelling of the cochlea and the cochlear implant: a review'. *Cochlear Implants International* 13 (2), 113–23.

ALGARÍN, C. et al. (2003). 'Iron Deficiency Anemia in Infancy: Long-Lasting Effects on Auditory and Visual System Functioning'. *Pediatric Research* 53 (2), 217–223.

ALONSO, J. E. et al. (2021). 'Cochlear Meniere's: A Distinct Clinical Entity With Isolated Cochlear Hydrops on High-Resolution MRI?' *Frontiers in Surgery* 8, Article 680260.

ALVAREZ, I. et al. (Sept. 2008). 'An improved masker-probe method for stimulus artifact reduction in electrically evoked compound action potentials'. *Journal of Neuroscience Methods* 175, 143–7.

BADENHORST, W., HANEKOM, T. and HANEKOM, J. J. (2017). 'Analysis of a purely conductance-based stochastic nerve fibre model as applied to compound models of populations of human auditory nerve fibres used in cochlear implant simulations'. *Biological Cybernetics* 111 (5), 439–458.

EL-BADRY, M. M., DING, D. L. et al. (2007). 'Physiological effects of auditory nerve myelinopathy in chinchillas'. *European Journal of Neuroscience* 25 (5), 1437–1446.

EL-BADRY, M. and MCFADDEN, S. (Sept. 2009). 'Evaluation of inner hair cell and nerve fiber loss as sufficient pathologies underlying auditory neuropathy'. *Hearing Research* 255 (1-2), 84–90.

BARBEE, C. M. et al. (2018). 'Effectiveness of Auditory Measures for Detecting Hidden Hearing Loss and/or Cochlear Synaptopathy: A Systematic Review'. *Seminars in Hearing* 39 (2), 172–209.

BARTHOLOMEW, R. A. et al. (2020). 'Labyrinthine concussion: Historic otopathologic antecedents of a challenging diagnosis'. *Laryngoscope Investigative Otolaryngology* 5 (2), 267–277.

BAUDHUIN, J. L., HUGHES, M. L. and GOEHRING, J. L. (2016). 'A Comparison of Alternating Polarity and Forward Masking Artifact-Reduction Methods to Resolve the Electrically Evoked Compound Action Potential'. *Ear and Hearing* 37 (4), 247–255.

BHATTACHARYYA, N. (Jan. 2021). *Auditory Brainstem Response Audiometry*. URL: https://emedicine.medscape.com/article/836277-overview#showall (visited on 26/02/2021).

BIERER, J. and FAULKNER, K. (2010). 'Identifying cochlear implant channels with poor electrode-neuron interface: partial tripolar, single-channel thresholds and psychophysical tuning curves'. *Ear and Hearing* 31 (2), 247–258.

BIESHEUVEL, J. D., BRIAIRE, J. J. and FRIJNS, J. H. M. (2018). 'The Precision of eCAP Thresholds Derived From Amplitude Growth Functions'. *Ear Hear* 39 (4), 701–711.

BLACK, R. C. and CLARK, G. M. (1980). 'Differential electrical excitation of the auditory nerve'. *Journal of the Acoustical Society of America* 67 (3), 868–874.

BOHNE, B. and HARDING, G. (Aug. 2000). 'Degeneration in the cochlea after noise damage: Primary versus secondary events'. *The American journal of otology* 21, 505–509.

BOTROS, A. and PSARROS, C. (2010). 'Neural Response Telemetry Reconsidered: II. The Influence of Neural Population on the ECAP Recovery Function and Refractoriness'. *Ear and Hearing* 31 (3), 380–391.

BRIAIRE, J. and FRIJNS, J. (2006). 'The consequences of neural degeneration regarding optimal cochlear implant position in scala tympani: A model approach'. *Hearing Research* 214 (1), 17–27.

BRIAIRE, J. J. and FRIJNS, J. H. M. (2005). 'Unraveling the electrically evoked compound action potential'. *Hearing Research* 205 (1), 143–156.

BROCHIER, T., MCKAY, C. and CARLYON, R. (2021). 'Interpreting the Effect of Stimulus Parameters on the Electrically Evoked Compound Action Potential and on Neural Health Estimates'. *Journal of the Association for Research in Otolaryngology* 22 (1), 81–94.

BROCHIER, T., GUÉRIT, F. et al. (2021). 'Evaluating and Comparing Behavioural and Electrophysiological Estimates of Neural Health in Cochlear Implant Users'. *Journal of the Association for Research in Otolaryngology* 22 (1), 67–80.

BROWN, C. J., ABBAS, P. J. and GANTZ, B. (1990). 'Electrically evoked whole-nerve action potentials: data from human cochlear implant users'. *The Journal of the Acoustical Society of America* 88 (3), 1385–1391.

BUCHMAN, C. A. et al. (2006). 'Auditory neuropathy characteristics in children with cochlear nerve deficiency'. *Ear Hear* 27 (4), 399–408.

BURAN, B. et al. (2020). 'Optimizing Auditory Brainstem Response Acquisition Using Interleaved Frequencies'. *Journal of the Association for Research in Otolaryngology*, 225–242.

BUSS, E. et al. (2018). 'Effects of Cochlear Implantation on Binaural Hearing in Adults With Unilateral Hearing Loss'. *Trends in Hearing* 22, Article 2331216518771173.

CAKIR, A., DWYER, R. and NOBLE, J. (2017). 'Evaluation of a high-resolution patient-specific model of the electrically stimulated cochlea'. *Journal of Medical Imaging (Bellingham, Wash.)* 4 (2), Article 025003.

CALDAS, F. et al. (2016). 'Analysis of electrically evoked compound action potential of the auditory nerve in children with bilateral cochlear implants'. *Brazilian Journal of Otorhinolaryngology* 82 (2), 123–130.

CARLYON, R. et al. (2021). 'Using Interleaved Stimulation to Measure the Size and Selectivity of the Sustained Phase-Locked Neural Response to Cochlear Implant Stimulation'. *Journal of the Association for Research in Otolaryngology* 22 (2), 141–159.

CARVALHO, B. et al. (2020). 'Neural Recovery Function of the Auditory Nerve in Cochlear Implant Surgery: Comparison between Prelingual and Postlingual Patients'. *International Archives of Otorhinolaryngology* 24 (4), 444–449.

CDC (June 2021). *Preventing Noise-Induced Hearing Loss | Centers for Disease Control and Prevention*. URL: https://www.cdc.gov/ncbddd/hearingloss/noise.html (visited on 24/02/2022).

CHEN, D. M. D., PHILLIPS, C. and D., D. M. (2015). 'Imaging the patient with hearing loss'. *Applied Radiology* 44 (10), 10–19.

CHRISTOV, F. et al. (2016). 'ECAP analysis in cochlear implant patients as a function of patient's age and electrode-design'. *European Annals of Otorhinolaryngology, Head and Neck Diseases* 133, (Suppl. 1), S1–S3.

CINAR, B. C. et al. (2019). 'Cochlear Nerve Hypoplasia: Audiological Characteristics in Children and Adults'. *Audiol Neurootol* 24 (3), 147–153.

CLEMMENS, C. S. et al. (2013). 'Unilateral cochlear nerve deficiency in children'. *Otolaryngol Head Neck Surg* 149 (2), 318–25.

COHEN, G. M., PARK, J. C. and GRASSO, J. S. (1990). 'Comparison of demyelination and neural degeneration in spiral and Scarpa's ganglia of C57BL/6 mice'. *Journal of Electron Microscopy Technique* 15 (2), 165–72.

COHEN, L. T., RICHARDSON, L. et al. (2003). 'Spatial spread of neural excitation in cochlear implant recipients: comparison of improved ECAP method and psychophysical forward masking'. *Hearing Research* 179 (1), 72–87.

COLLETTI, V. et al. (2005). 'Auditory Brainstem Implant (ABI): New Frontiers in Adults and Children'. *Otolaryngology - Head and Neck Surgery* 133 (1), 126–138.

*COMSOL Multiphysics*® (2020). Computer Program. Version 6.0. Stockholm, Sweden.

*Custom sound® EP* (2021). Version 6.0.

DANG, K. et al. (2015). 'In situ validation of a parametric model of electrical field distribution in an implanted cochlea'. In: 7th International IEEE/EMBS Conference on Neural Engineering (NER), 22–24 Apr 2015. Montpellier, France: IEEE, 667–670.

DAVIS, T. J. et al. (2016). 'Relationship Between Electrode-to-Modiolus Distance and Current Levels for Adults With Cochlear Implants'. *Otology and Neurotology* 37, 31–37.

DEKKER, D. M. T., BRIAIRE, J. J. and FRIJNS, J. H. M. (2014). 'The impact of internodal segmentation in biophysical nerve fiber models'. *Journal of Computational Neuroscience* 37 (2), 307–315.

DEPREZ, H. et al. (2017). 'Characterization of cochlear implant artifacts in electrically evoked auditory steady-state responses'. *Biomedical Signal Processing and Control* 31, 127–138.

DHANASINGH, A. et al. (2020). 'Literature Review on the Distribution of Spiral Ganglion Cell Bodies inside the Human Cochlear Central Modiolar Trunk'. *The Journal of International Advanced Otology* 16 (1), 104–110.

DI STADIO, A. et al. (2019). 'E-ABR in Patients with Cochlear Implant: A Comparison between Patients with Malformed Cochlea and Normal Cochlea'. *The Journal of International Advanced Otology* 15 (2), 215–221.

DING, L., MCFADDEN, S. L. and SALVI, R. J. (2002). 'Calpain immunoreactivity and morphological damage in chinchilla inner ears after carboplatin'. *Journal of the Association for Research in Otolaryngology* 3 (1), 68–79.

DU, Y., WU, X. and LI, L. (2006). 'Mechanisms of bacterial meningitis-related deafness'. *Drug Discovery Today: Disease Mechanisms* 3, 115–118.

EARL, B. and CHERTOFF, M. (2009). 'Predicting Auditory Nerve Survival Using the Compound Action Potential'. *Ear and hearing* 31, 7–21.

EGGERMONT, J. J. (2019). 'Chapter 30 - Auditory brainstem response'. In: *Clinical Neurophysiology: Basis and Technical Aspects*. Ed. by K. H. LEVIN and P. CHAUVEL. Vol. 160. Handbook of Clinical Neurology. Elsevier, 451–464.

ELIADES, S. J. and TSUNADA, J. (2019). 'Chapter 25 - Marmosets in Auditory Research'. *The Common Marmoset in Captivity and Biomedical Research*. Ed. by R. MARINI et al. Academic Press, pp. 451–475.

EMERSON, L. P. et al. (2011). 'Peripheral auditory assessment in minor head injury: a prospective study in tertiary hospital'. *Indian Journal of Otolaryngology and Head and Neck Surgery* 63 (1), 45–49.

ESHRAGHI, A. A. et al. (2012). 'The Cochlear Implant: Historical Aspects and Future Prospects'. *The Anatomical Record* 295 (11), 1967–1980.

FIFER, R. C. and NOVAK, M. A. (1990). 'Myogenic influences on the electrical auditory brainstem response (EABR) in humans'. *Laryngoscope* 100 (11), 1180–1184.

FINLEY, C. C., WILSON, B. S. and WHITE, M. W. (1990). 'Models of Neural Responsiveness to Electrical Stimulation'. *Cochlear Implants: Models of the Electrically Stimulated Ear*. Ed. by J. M. MILLER and F. A. SPELMAN. New York, NY: Springer New York, pp. 55–96.

FRANKENHAEUSER, B. and HUXLEY, A. F. (1964). 'The action potential in the myelinated nerve fibre of Xenopus laevis as computed on the basis of voltage clamp data'. *The Journal of Physiology* 171 (2), 302–315.

FRIJNS, J. H. M., SNOO, S. L. de and SCHOONHOVEN, R. (1995). 'Potential distributions and neural excitation patterns in a rotationally symmetric model of the electrically stimulated cochlea'. *Hearing Research* 87 (1), 170–186.

FURMAN, A. C., KUJAWA, S. G. and LIBERMAN, M. C. (2013). 'Noise-induced cochlear neuropathy is selective for fibers with low spontaneous rates'. *Journal of Neurophysiology* 110 (3), 577–86.

GAN, J. et al. (2021). 'Current Understanding of Hearing Loss in Sporadic Vestibular Schwannomas: A Systematic Review'. *Frontiers in Oncologyl* 11, Article 687201.

GANESAN, P. et al. (2018). 'Ototoxicity: A Challenge in Diagnosis and Treatment'. *Journal of Audiology and Otology* 22 (2), 59–68.

GÄRTNER, L. et al. (2021). 'Correlation of Electrically Evoked Compound Action Potential Amplitude Growth Function Slope and Anamnestic Parameters in Cochlear Implant Patients-Identification of Predictors for the Neuronal Health Status'. *Life (Basel, Switzerland)* 11 (3), Article 203.

GEE, A. H. et al. (2021). 'Practicable assessment of cochlear size and shape from clinical CT images'. *Scientific Reports* 11 (1), Article 3448.

GOEHRING, T. et al. (2019). 'A Site-Selection Strategy Based on Polarity Sensitivity for Cochlear Implants: Effects on Spectro-Temporal Resolution and Speech Perception'. *Journal of the Association for Research in Otolaryngology* 20 (4), 431–448.

GOLDWYN, J. H., BIERER, S. M. and BIERER, J. A. (2010). 'Modeling the electrode-neuron interface of cochlear implants: effects of neural survival, electrode placement, and the partial tripolar configuration'. *Hearing Research* 268 (1-2), 93–104.

GORGA, M. P., WORTHINGTON, D. W. et al. (1985). 'Some Comparisons between Auditory Brain Stem Response Thresholds, Latencies, and the Pure-Tone Audiogram'. *Ear and Hearing* 6 (2), 105–112.

GORGA, M. P., JOHNSON, T. A. et al. (2006). 'Using a combination of click- and tone burst-evoked auditory brain stem response measurements to estimate pure-tone thresholds'. *Ear and Hearing* 27 (1), 60–74.

GREENE, J. and AL-DHAHIR, M. (Jan. 2022). *Acoustic Neuroma*. `https://www.ncbi.nlm.nih.gov/books/NBK470177/`.

GU, J. W. et al. (2012). 'Brainstem auditory evoked potentials suggest a role for the ventral cochlear nucleus in tinnitus'. *Journal of the Association for Research in Otolaryngology* 13 (6), 819–33.

GUEDES, M. C. et al. (2007). 'Influence of evoked compound action potential on speech perception in cochlear implant users'. *Brazilian Journal of Otorhinolaryngology* 73 (4), 439–45.

HAN, J. J. et al. (2019). 'A Predictive Model for Cochlear Implant Outcome in Children with Cochlear Nerve Deficiency'. *Scientific Reports - Nature* 9 (1), Article 1154.

HANEKOM, T. (2001). 'Three-Dimensional Spiraling Finite Element Model of the Electrically Stimulated Cochlea'. *Ear and Hearing* 22 (4), 300–315.

HANEKOM, T. and HANEKOM, J. J. (2016). 'Three-dimensional models of cochlear implants: A review of their development and how they could support management and maintenance of cochlear implant performance'. *Network* 27 (2-3), 67–106.

HE, S., ABBAS, P. J. et al. (2016). 'Temporal Response Properties of the Auditory Nerve in Implanted Children with Auditory Neuropathy Spectrum Disorder and Implanted Children with Sensorineural Hearing Loss'. *Ear and Hearing* 37 (4), 397–411.

HE, S., CHAO, X. et al. (2020). 'Recommendations for Measuring the Electrically Evoked Compound Action Potential in Children With Cochlear Nerve Deficiency'. *Ear Hear* 41 (3), 465–475.

HE, S., SHAHSAVARANI, B. S. et al. (2018). 'Responsiveness of the Electrically Stimulated Cochlear Nerve in Children With Cochlear Nerve Deficiency'. *Ear and Hearing* 39 (2), 238–250.

HE, S., TEAGLE, H. F. B. and BUCHMAN, C. A. (2017). 'The Electrically Evoked Compound Action Potential: From Laboratory to Clinic'. *Frontiers in Neuroscience* 11, Article 00339.

HE, S., XU, L. et al. (2020). 'The Effect of Interphase Gap on Neural Response of the Electrically Stimulated Cochlear Nerve in Children With Cochlear Nerve Deficiency and Children With Normal-Sized Cochlear Nerves'. *Ear Hear* 41 (4), 918–934.

HERRMANN, D. P. et al. (2021). 'Effects of electrical pulse polarity shape on intra cochlear neural responses in humans: Triphasic pulses with anodic and cathodic second phase'. *Hearing Research* 412, Article 108375.

HESHMAT, A. et al. (2020). 'Dendritic Degeneration of Human Auditory Nerve Fibers and Its Impact on the Spiking Pattern Under Regular Conditions and During Cochlear Implant Stimulation'. *Frontiers in Neuroscience* 14, Article 599868.

HICKOX, A. E. and LIBERMAN, M. C. (2014). 'Is noise-induced cochlear neuropathy key to the generation of hyperacusis or tinnitus?' *Journal of Neurophysiology* 111 (3), 552–564.

HODGKIN, A. L. and HUXLEY, A. F. (1952). 'A quantitative description of membrane current and its application to conduction and excitation in nerve'. *The Journal of Physiology* 117 (4), 500–544.

HONRUBIA, V., STRELIOFF, D. and SITKO, S. T. (1976). 'Physiological Basis of Cochlear Transduction and Sensitivity'. *Annals of Otology, Rhinology and Laryngology* 85 (6), 697–710.

HUGHES, M. L. (Nov. 2006). *Fundamentals of clinical ECAP measures in cochlear implants part 2: Measurement techniques and tips*. URL: http://www.audiologyonline.com/articles/fundamentals-clinical-ecap-measures-in-965-965 (visited on 12/06/2021).

HUGHES, M. L., CHOI, S. and GLICKMAN, E. (2018). 'What can stimulus polarity and interphase gap tell us about auditory nerve function in cochlear-implant recipients?' *Hearing research* 359, 50–63.

HUGHES, M. L., CASTIONI, E. E. et al. (2012). 'Temporal response properties of the auditory nerve: Data from human cochlear-implant recipients'. *Hearing Research* 285 (1), 46–57.

ISAACSON, J. E. and VORA, N. M. (2003). 'Differential diagnosis and treatment of hearing loss'. *American Family Physician* 68 (6), 1125–1132.

ITO, T. et al. (June 2004). 'Cochlear nerve demyelination causes prolongation of wave I latency in ABR of the myelin deficient (MD) rat'. *Hearing Research* 191, 119–24.

JAHN, K. N. and ARENBERG, J. G. (2019). 'Polarity sensitivity in pediatric and adult cochlear implant listeners'. *Trends in hearing* 23, Article 2331216519862987.

JERGER, J. and JOHNSON, K. (1988). 'Interactions of age, gender, and sensorineural hearing loss on ABR latency'. *Ear and Hearing* 9 (4), 168–176.

JI, F. et al. (June 2014). 'NRT test in auditory neuropathy patients with cochlear implants'. *Acta oto-laryngologica* 134, 1–13.

JOHNSTONE, B. M., JOHNSTONE, J. R. and PUGSLEY, I. D. (1966). 'Membrane resistance in endolymphatic walls of the first turn of the guinea-pig cochlea'. *The Journal of the Acoustical Society of America* 40 (6), 1398–404.

JOSHI, S., DAU, T. and EPP, B. (2017). 'A Model of Electrically Stimulated Auditory Nerve Fiber Responses with Peripheral and Central Sites of Spike Generation'. *Journal of the Association for Research in Otolaryngology* 18 (2), 323–342.

KAJI, R. (2003). 'Physiology of conduction block in multifocal motor neuropathy and other demyelinating neuropathies'. *Muscle and Nerve* 27 (3), 285–296.

KALKMAN, R. K., BRIAIRE, J. J., DEKKER, D. M. et al. (2014). 'Place pitch versus electrode location in a realistic computational model of the implanted human cochlea'. *Hearing Research* 315, 10–24.

KALKMAN, R. K., BRIAIRE, J. J. and FRIJNS, J. H. M. (2016). 'Stimulation strategies and electrode design in computational models of the electrically stimulated cochlea: An overview of existing literature'. *Network: Computation in Neural Systems* 27 (2-3), 107–134.

KASBEKAR, A. V. et al. (2019). 'Intraoperative Monitoring of the Cochlear Nerve during Neurofibromatosis Type-2 Vestibular Schwannoma Surgery and Description of a "Test Intracochlear Electrode"'. *J Neurol Surg Rep* 80 (1), e1–e9.

KAZAHAYA, K. and SINGH, D. J. (2007). 'CHAPTER 1 - Congenital Malformations of the Head and Neck'. In: *Pediatric Otolaryngology*. Ed. by R. F. WETMORE and L. M. BELL. The Requisites in Pediatrics. Philadelphia: Mosby, 1–22.

KEMP, D. T. (2002). 'Otoacoustic emissions, their origin in cochlear function, and use'. *British Medical Bulletin* 63 (1), 223–241.

KOCHHAR, A., HILDEBRAND, M. S. and SMITH, R. J. H. (2007). 'Clinical aspects of hereditary hearing loss'. *Genetics in Medicine* 9 (7), 393–408.

KOHRMAN, D. C. et al. (2020). 'Hidden Hearing Loss: A Disorder with Multiple Etiologies and Mechanisms'. *Cold Spring Harbor Perspectives in Medicine* 10 (1), Article 035493.

KUJAWA, S. G. and LIBERMAN, M. C. (Nov. 2009). 'Adding Insult to Injury: Cochlear Nerve Degeneration after "Temporary" Noise-Induced Hearing Loss'. *Journal of Neuroscience* 29 (45), 14077–14085.

KURABI, A. et al. (2017). 'Cellular mechanisms of noise-induced hearing loss'. *Hearing Research* 349, 129–137.

KUTZ, J. W. et al. (2006). 'Clinical Predictors for Hearing Loss in Children With Bacterial Meningitis'. *Archives of Otolaryngology–Head and Neck Surgery* 132 (9), 941–945.

LAI, W. K. and DILLIER, N. (2000). 'A Simple Two-Component Model of the Electrically Evoked Compound Action Potential in the Human Cochlea'. *Audiology and Neurotology* 5 (6), 333–345.

LANDRY, T. G. et al. (2011). 'Spiral ganglion neuron survival and function in the deafened cochlea following chronic neurotrophic treatment'. *Hearing Research* 282 (1-2), 303–313.

LEE, K. Y. (2013). 'Pathophysiology of age-related hearing loss (peripheral and central)'. *Korean Journal of Audiology* 17 (2), 45–49.

LEE, S. et al. (2020). 'Simpler and effective radiological evaluations for modiolar proximity of a slim modiolar cochlear implant electrode'. *Scientific Reports* 10 (1), Article 17714.

LEGATT, A. D. (2018). 'Electrophysiology of Cranial Nerve Testing: Auditory Nerve'. *Journal of Clinical Neurophysiology* 35 (1), 25–38.

LEUWER, R. and MÜLLER, J. (2005). 'Restoration of hearing by hearing aids: conventional hearing aids - implantable hearing aids - cochlear implants - auditory brainstem implants'. *GMS Current Topics in Otorhinolaryngology, Head and Neck Surgery* 4, Article 03.

LIBERMAN, M. C. (2017). 'Noise-induced and age-related hearing loss: New perspectives and potential therapies'. *F1000Research* 6, Article 927.

LIBERMAN, M. C. and KUJAWA, S. G. (2017). 'Cochlear synaptopathy in acquired sensorineural hearing loss: Manifestations and mechanisms'. *Hearing Research* 349, 138–147.

LONG, P. et al. (2018). 'Myelin development, plasticity, and pathology in the auditory system'. *Developmental Neurobiology* 78 (2), 80–92.

LOW, P. A. and MCLEOD, J. G. (1977). 'Refractory period, conduction of trains of impulses, and effect of temperature on conduction in chronic hypertrophic neuropathy'. *Journal of Neurology, Neurosurgery and Psychiatry* 40 (5), 434–47.

MACHEREY, O. et al. (Apr. 2007). 'A Dual-Process Integrator–Resonator Model of the Electrically Stimulated Human Auditory Nerve'. *Journal of the Association for Research in Otolaryngology* 8, 84–104.

MALHERBE, T., HANEKOM, T. and HANEKOM, J. (2015). 'Constructing a three-dimensional electrical model of a living cochlear implant user's cochlea'. *International Journal for Numerical Methods in Biomedical Engineering* 32, Article 2751.

MANGADO, N. et al. (2015). 'Automatic Model Generation Framework for Computational Simulation of Cochlear Implantation'. *Annals of Biomedical Engineering* 44, 2453–2463.

MATHERS, C., SMITH, A. and CONCHA, M. (Jan. 2000). 'Global burden of hearing loss in the year 2000'. *Global Burden of Disease* 18, 1–30.

MEENDERINK, S. W. F., LIN, X. and DONG, W. (2021). 'Using electrocochleography to detect sensory and neural damages in a gerbil model'. *Scientific Reports* 11 (1), Article 19557.

MILLER, C. A. et al. (1998). 'Electrically evoked compound action potentials of guinea pig and cat: responses to monopolar, monophasic stimulation'. *Hearing Research* 119 (1), 142–154.

MUDRY, A. and MILLS, M. (2013). 'The early history of the cochlear implant: a retrospective'. *JAMA Otolaryngology – Head and Neck Surgery* 139 (5), 446–453.

NADOL J. B., J. (1997). 'Patterns of neural degeneration in the human cochlea and auditory nerve: implications for cochlear implantation'. *Otolaryngology Head and Neck Surgery* 117 (3 Pt 1), 220–8.

NELSON, K. R., GILMORE, R. L. and MASSEY, A. (1988). 'Acoustic nerve conduction abnormalities in Guillain-Barré syndrome'. *Neurology* 38 (8), 1263–1263.

NOGUEIRA, W. et al. (2016). 'Validation of a Cochlear Implant Patient-Specific Model of the Voltage Distribution in a Clinical Setting'. *Frontiers in Bioengineering and Biotechnology* 4, Article 00084.

OLUSANYA, B. O., DAVIS, A. C. and HOFFMAN, H. J. (2019). 'Hearing loss: Rising prevalence and impact'. *Bulletin of the World Health Organization* 97 (10), Article 646.

ORZAN, E. et al. (2021). 'Correlation of cochlear aperture stenosis with cochlear nerve deficiency in congenital unilateral hearing loss and prognostic relevance for cochlear implantation'. *Scientific Reports* 11 (1), Article 3338.

PARKINS, C. W. and COLOMBO, J. (1987). 'Auditory-nerve single-neuron thresholds to electrical stimulation from scala tympani electrodes'. *Hearing Research* 31, 267–285.

PFINGST, B. E., DE HAAN, D. R. and HOLLOWAY, L. A. (1991). 'Stimulus features affecting psychophysical detection thresholds for electrical stimulation of the cochlea. I: Phase duration and stimulus duration'. *The Journal of the Acoustical Society of America* 90 (4), 1857–1866.

PFINGST, B. E., ZHOU, N. et al. (2015). 'Importance of cochlear health for implant function'. *Hearing research* 322, 77–88.

PISONI, D. B. et al. (2017). 'Three challenges for future research on cochlear implants'. *World Journal of Otorhinolaryngology - Head and Neck Surgery* 3 (4), 240–254.

POURJAVID, A. et al. (Sept. 2011). 'Amplitude Changes of the Electrically Evoked Compound Action Potential in Children with Cochlear Implants: Preliminary Results'. *Iranian journal of pediatrics* 21, 390–394.

PRADO-GUITIERREZ, P. et al. (May 2006). 'Effect of interphase gap and pulse duration on electrically evoked potentials is correlated with auditory nerve survival'. *Hearing Research* 215 (1-2), 47–55.

QUANDT, F. N. and DAVIS, F. A. (1992). 'Action potential refractory period in axonal demyelination: a computer simulation'. *Biological Cybernetics* 67 (6), 545–52.

RAMEKERS, D. et al. (2014). 'Auditory-nerve responses to varied inter-phase gap and phase duration of the electric pulse stimulus as predictors for neuronal degeneration'. *Journal of the Association for Research in Otolaryngology* 15 (2), 187–202.

RAMPP, S. et al. (2017). 'Towards an optimal paradigm for intraoperative auditory nerve monitoring with auditory steady state responses'. *Journal of Clinical Monitoring and Computing* 31 (1), 123–134.

RANCE, G. and STARR, A. (2015). 'Pathophysiological mechanisms and functional hearing consequences of auditory neuropathy'. *Brain* 138 (11), 3141–3158.

RATTAY, F., LUTTER, P. and FELIX, H. (2001). 'A model of the electrically excited human cochlear neuron. I. Contribution of neural substructures to the generation and propagation of spikes'. *Hearing Research* 153 (1-2), 43–63.

RISI, F. (2018). 'Considerations and Rationale for Cochlear Implant Electrode Design - Past, Present and Future'. *The Journal of International Advanced Otology* 14 (3), 382–391.

S. ABDELSALAM, N. M. and OMAR, A. P. (2015). 'Electric auditory brainstem response (E-ABR) in cochlear implant children: Effect of age at implantation and duration of implant use'. *Egyptian Journal of Ear, Nose, Throat and Allied Sciences* 16 (2), 145–150.

SAGERS, J. E. et al. (2017). 'Human Cochlear Histopathology Reflects Clinical Signatures of Primary Neural Degeneration'. *Scientific Reports* 7 (1), Article 4884.

SCHAETTE, R. and MCALPINE, D. (2011). 'Tinnitus with a normal audiogram: physiological evidence for hidden hearing loss and computational model'. *Journal of Neuroscience* 31 (38), 13452–7.

SCHEPERLE, R. A. (2017). 'Suprathreshold compound action potential amplitude as a measure of auditory function in cochlear implant users'. *Journal of Otology* 12 (1), 18–28.

SCHVARTZ-LEYZAC, K. C. and PFINGST, B. E. (2016). 'Across-site patterns of electrically evoked compound action potential amplitude-growth functions in multichannel cochlear implant recipients and the effects of the interphase gap'. *Hearing Research* 341, 50–65.

SCHWARZ, J. R. and EIKHOF, G. (1987). 'Na currents and action potentials in rat myelinated nerve fibres at 20 and 37° C'. *Pflügers Archiv : European Journal of Physiology* 409 (6), 569–577.

SHARMA, D. K. (2017). 'Audiological Assessment in Meniere's Disease'. *Up to Date on Meniere's Disease*. Ed. by F. B. JR. Rijeka: IntechOpen. Chap. 6.

SHEARER, A. E., HILDEBRAND, M. S. and SMITH, R. J. H. (1993). 'Hereditary Hearing Loss and Deafness Overview'. *GeneReviews*. Ed. by M. P. ADAM et al. Seattle (WA): University of Washington, Seattle Copyright © 1993-2021, University of Washington, Seattle. GeneReviews is a registered trademark of the University of Washington, Seattle. All rights reserved.

SHEPHERD, R. K., ROBERTS, L. A. and PAOLINI, A. G. (2004). 'Long-term sensorineural hearing loss induces functional changes in the rat auditory nerve'. *European Journal of Neuroscience* 20 (11), 3131–40.

SHEPHERD, R., HATSUSHIKA, S. and CLARK, G. (1993). 'Electrical stimulation of the auditory nerve: The effect of electrode position on neural excitation'. *Hearing Research* 66 (1), 108–120.

SHIBATA, S. B. et al. (2011). 'Nerve maintenance and regeneration in the damaged cochlea'. *Hearing Research* 281 (1-2), 56–64.

SHINN, J. B. and MUSIEK, F. E. (2007). 'The auditory steady state response in individuals with neurological insult of the central auditory nervous system'. *Journal of the American Academy of Audiology* 18 (10), 826–45.

ŠIŠKOVÁ, Z. et al. (2014). 'Dendritic Structural Degeneration Is Functionally Linked to Cellular Hyperexcitability in a Mouse Model of Alzheimer's Disease'. *Neuron* 84 (5), 1023–1033.

SKIDMORE, J. et al. (2020). 'Prediction of the Functional Status of the Cochlear Nerve in Individual Cochlear Implant Users Using Machine Learning and Electrophysiological Measures'. *Ear and Hearing* 42 (1), 180–192.

SKOE, E. and TUFTS, J. (2018). 'Evidence of noise-induced subclinical hearing loss using auditory brainstem responses and objective measures of noise exposure in humans'. *Hearing Research* 361, 80–91.

SMIT, J., HANEKOM, T. and HANEKOM, J. J. (2008). 'Predicting action potential characteristics of human auditory nerve fibres through modification of the Hodgkin-Huxley equations'. *South African Journal of Science* 104, 284–292.

SMIT, J. E., HANEKOM, T. and HANEKOM, J. J. (2009). 'Modelled temperature-dependent excitability behaviour of a single ranvier node for a human peripheral sensory nerve fibre'. *Biological Cybernetics* 100 (1), 49–58.

SNEL-BONGERS, J. et al. (2013). 'Threshold Levels of Dual Electrode Stimulation in Cochlear Implants'. *Journal of the Association for Research in Otolaryngology* 14 (5), 781–790.

SPOENDLIN, H. and SCHROTT, A. (1989). 'Analysis of the human auditory nerve'. *Hearing Research* 43 (1), 25–38.

STAMPER, G. C. and JOHNSON, T. A. (2015). 'Auditory function in normal-hearing, noise-exposed human ears'. *Ear and Hearing* 36 (2), 172–84.

STARR, A., PICTON, T. and KIM, R. (Jan. 2001). 'Pathophysiology of auditory neuropathy'. *Auditory Neuropathy: A New Perspective on Hearing Disorders*, 67–82.

STARR, A., PICTON, T. W., SININGER, Y. et al. (1996). 'Auditory neuropathy'. *Brain* 119 (Pt 3), 741–53.

STRAHL, S. B. et al. (2016). 'Assessing the Firing Properties of the Electrically Stimulated Auditory Nerve Using a Convolution Model'. *Advances in Experimental Medicine and Biology* 894, 143–153.

STRELIOFF, D. (1973). 'A computer simulation of the generation and distribution of cochlear potentials'. *The Journal of the Acoustical Society of America* 54 (3), 620–629.

STYPULKOWSKI, P. H. and VAN DEN HONERT, C. (1984). 'Physiological properties of the electrically stimulated auditory nerve I. Compound action potential recordings'. *Hearing Research* 14 (3), 205–223.

TAGOE, T. et al. (2014). 'Auditory nerve perinodal dysmyelination in noise-induced hearing loss'. *Journal of Neuroscience* 34 (7), 2684–8.

TEJANI, V. D., ABBAS, P. J. and BROWN, C. J. (2017). 'Relationship Between Peripheral and Psychophysical Measures of Amplitude Modulation Detection in Cochlear Implant Users'. *Ear and Hearing* 38 (5), 268–284.

TONG, Y. C. et al. (1990). 'A digital computer model of electrical stimulation in the human cochlea for auditory prosthesis research'. In: 6th International Conference on Biomedical Engineering, 6–8 Dec 1990. Singapore, 169–172.

UNDURRAGA, J. A., CARLYON, R. P. et al. (2013). 'The polarity sensitivity of the electrically stimulated human auditory nerve measured at the level of the brainstem'. *Journal of the Association for Research in Otolaryngology* 14 (3), 359–77.

UNDURRAGA, J. A., WIERINGEN, A. van et al. (2010). 'Polarity effects on neural responses of the electrically stimulated auditory nerve at different cochlear sites'. *Hearing Research* 269 (1), 146–161.

VERBIST, B. M. (2012). 'Imaging of sensorineural hearing loss: a pattern-based approach to diseases of the inner ear and cerebellopontine angle'. *Insights Imaging* 3 (2), 139–53.

VERHULST, S., ALTOÈ, A. and VASILKOV, V. (2018). 'Computational modeling of the human auditory periphery: Auditory-nerve responses, evoked potentials and hearing loss'. *Hearing Research* 360. Computational models of the auditory system, 55–75.

VERHULST, S., BHARADWAJ, H. M. et al. (2015). 'Functional modeling of the human auditory brainstem response to broadband stimulation'. *The Journal of the Acoustical Society of America* 138 (3), 1637–59.

VERHULST, S., JAGADEESH, A. et al. (2016). 'Individual Differences in Auditory Brainstem Response Wave Characteristics: Relations to Different Aspects of Peripheral Hearing Loss'. *Trends in Hearing* 20, Article 2331216516672186.

VIANA, L. M. et al. (2015). 'Cochlear neuropathy in human presbycusis: Confocal analysis of hidden hearing loss in post-mortem tissue'. *Hearing Research* 327, 78–88.

WAN, G. and CORFAS, G. (2017). 'Transient auditory nerve demyelination as a new mechanism for hidden hearing loss'. *Nature Communications* 8, Article 14487.

WANG, B., GUO, X. et al. (2022). 'Evaluation of auditory pathway by EABR before cochlear implantation and the postoperative effect analysis'. *European Archives of Oto-Rhino-Laryngology*, Article 07458–9.

WANG, J. and PUEL, J. L. (2020). 'Presbycusis: An Update on Cochlear Mechanisms and Therapies'. *Journal of Clinical Medicine* 9 (1), Article 218.

WERMESKERKEN, G. K. van, OLPHEN, A. F. van and GRAAMANS, K. (2009). 'Imaging of electrode position in relation to electrode functioning after cochlear implantation'. *European Archives of Oto-Rhino-Laryngology* 266 (10), 1527–31.

WILSON, B. S. and DORMAN, M. F. (2008). 'Cochlear implants: A remarkable past and a brilliant future'. *Hearing Research* 242 (1), 3–21.

WINSTON A.K.and Stoner, R. (2013). 'ABR: An illustration of auditory dysfunction through clinical cases, presented in partnership with Rush University'. AudiologyOnline, Article 12179.

WŁODARCZYK, K. and SKARŻYŃSKI, P. H. (2020). 'Difficulties with magnetic resonance imaging in patients with cochlear implants: a review'. *Journal of Hearing Science* 10 (1), 21–23.

WOLFE, J. (2020). *Cochlear implants: audiologic management and considerations for implantable hearing devices*. San Diego, CA, USA: Plural Publishing, 6–24.

WONG, K. et al. (2019). 'Auditory Brainstem Implants: Recent Progress and Future Perspectives'. *Frontiers in Neuroscience* 13, Article 00010.

XING, Y. et al. (2012). 'Age-related changes of myelin basic protein in mouse and human auditory nerve'. *PLOS One* 7 (4), Article 0034500.

XU, L. et al. (2020). 'The Effect of Pulse Polarity on Neural Response of the Electrically Stimulated Cochlear Nerve in Children With Cochlear Nerve Deficiency and Children With Normal-Sized Cochlear Nerves'. *Ear and Hearing* 41, 1306–1319.

YAMAZAKI, H. et al. (2015). 'Usefulness of MRI and EABR Testing for Predicting CI Outcomes Immediately After Cochlear Implantation in Cases With Cochlear Nerve Deficiency'. *Otology and neurotology* 36 (6), 977–984.

YE, H. B. et al. (2012). 'Bilirubin induces auditory neuropathy in neonatal guinea pigs via auditory nerve fiber damage'. *Journal of Neuroscience Research* 90 (11), 2201–13.

ZAHNERT, T. (2011). 'The differential diagnosis of hearing loss'. *Deutsches Ärzteblatt International* 108 (25), 433–43.

ZHANG, C. et al. (2017). 'Auditory function and inner ear pathology in Guinea pigs with peripheral nerve demyelination'. *International Journal of Clinical and Experimental Medicine* 10, 11937–11944.

ZHOU, N. and PFINGST, B. E. (2014). 'Relationship between multipulse integration and speech recognition with cochlear implants'. *The Journal of the Acoustical Society of America* 136 (3), Article 1257.

ZHOU, R., ABBAS, P. J. and ASSOULINE, J. G. (1995). 'Electrically evoked auditory brainstem response in peripherally myelin-deficient mice'. *Hearing Research* 88 (1-2), 98–106.

# ADDENDUM A ADDENDUM: ADDITIONAL DATA

## A.1 COMPLETE INTERPOLATED DATA SETS

All the data points that were interpolated for the N1 and P1 peaks to 5.5dB above T level are shown below. These are the data sets that the prediction bands were applied to in order to identify outlier values. Outlier values were used to identify which electrodes were in immediate proximity to damaged neural fibres, as indicated by outlier eCAP characteristics such as relatively low or high amplitudes and latencies compared to the majority of the values.

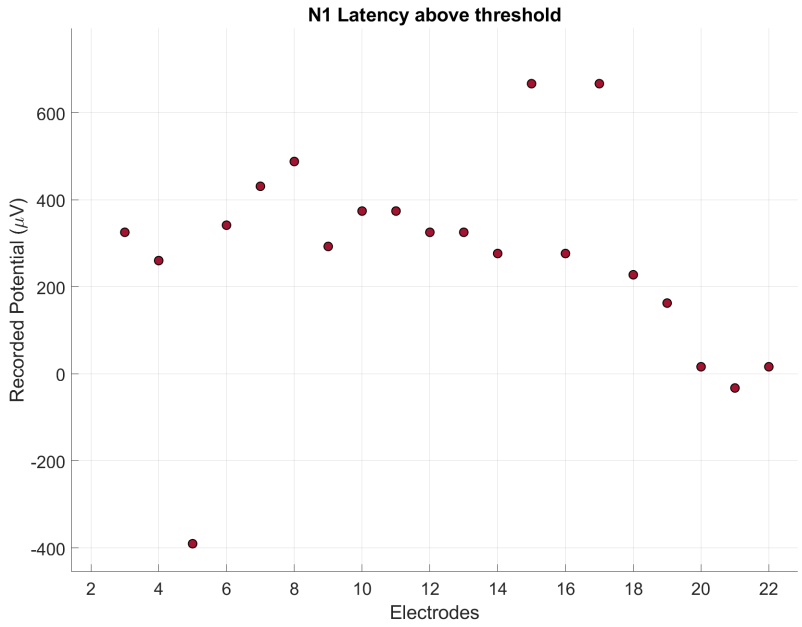


**(a)**

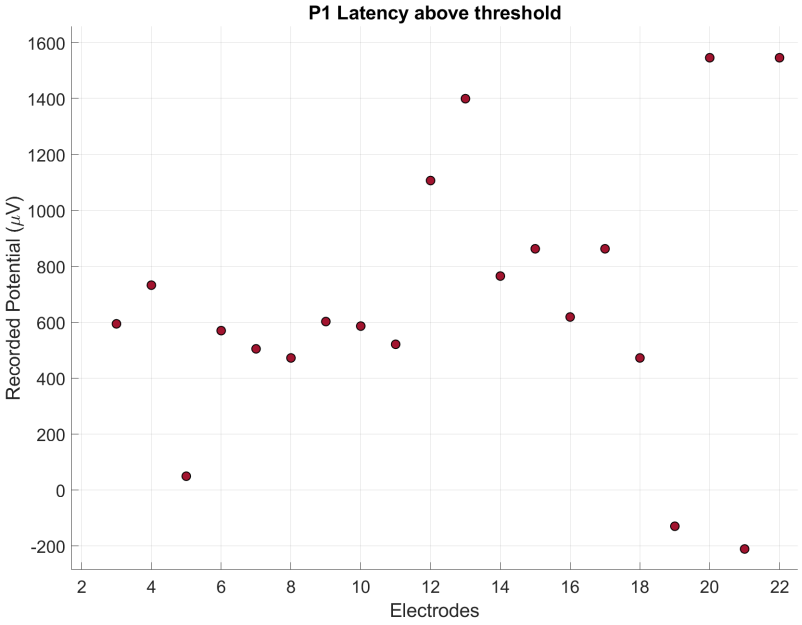


**(b)**

**Figure A.1.** (a) N1 and (b) P1 latency above threshold.

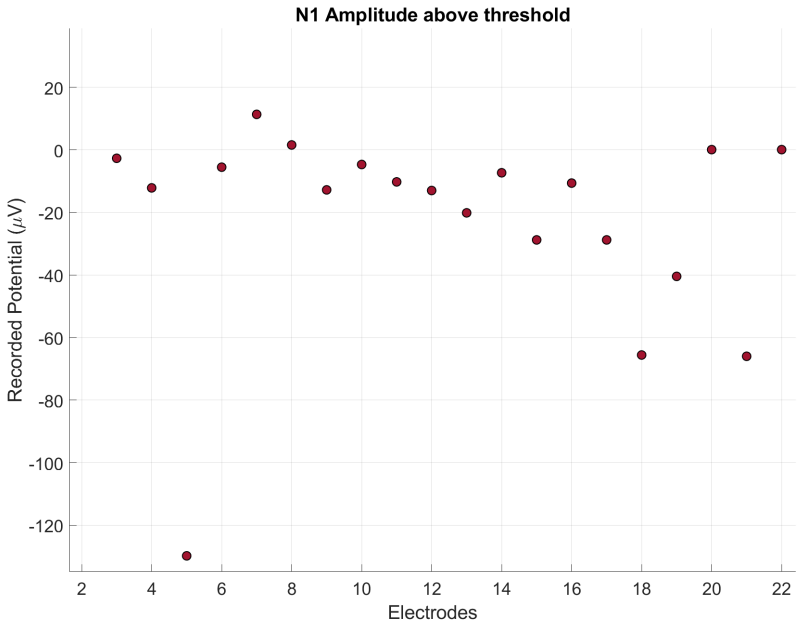


**(a)**

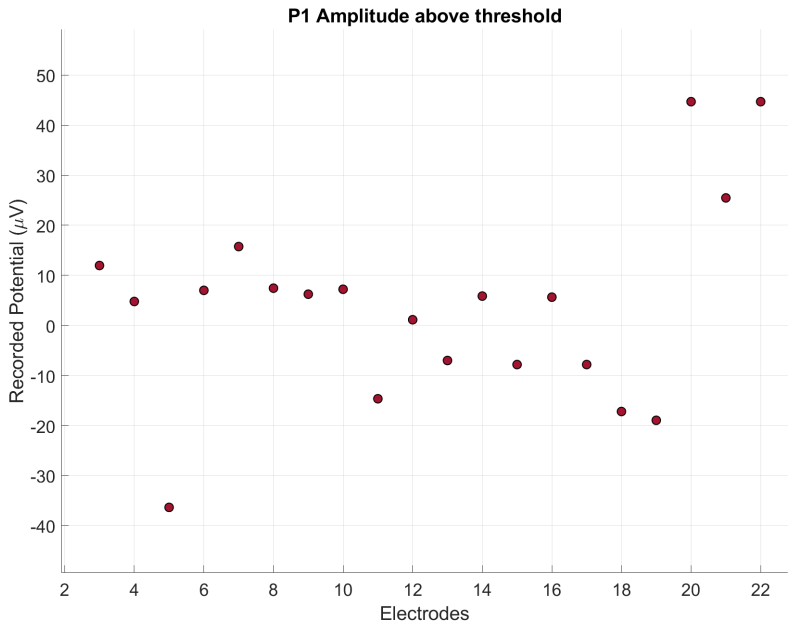


**(b)**

**Figure A.2.** (a) N1 and (b) P1 amplitude above threshold.

All the data points that were interpolated for the N1 and P1 peaks to 5.5dB above comfort level are shown below.

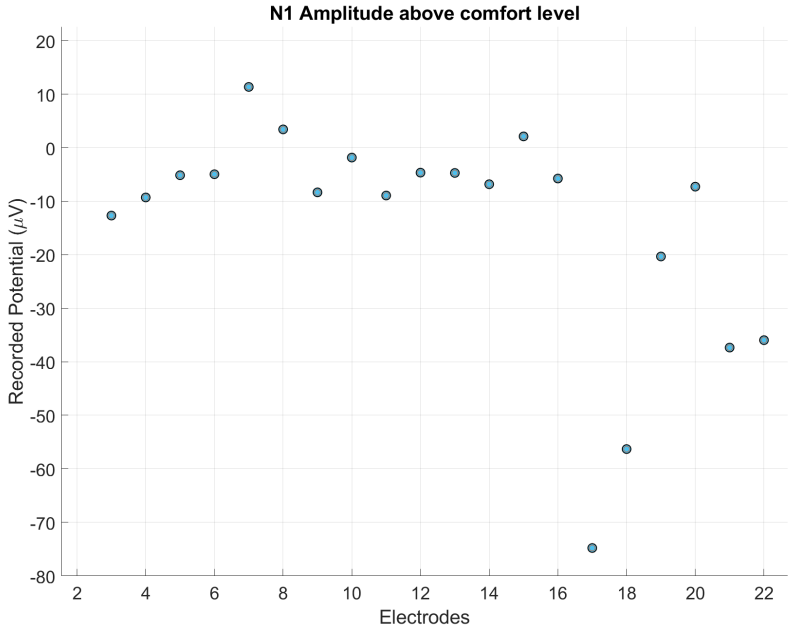


**(a)** N1 Ampl

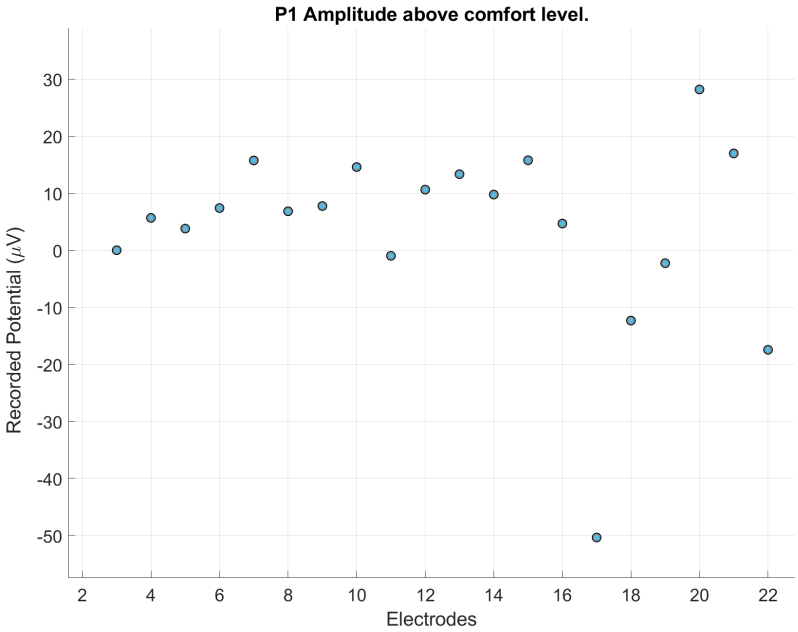


**(b)** P1 Ampl

**Figure A.3.** (a) N1 and (b) P1 amplitude above comfort level.

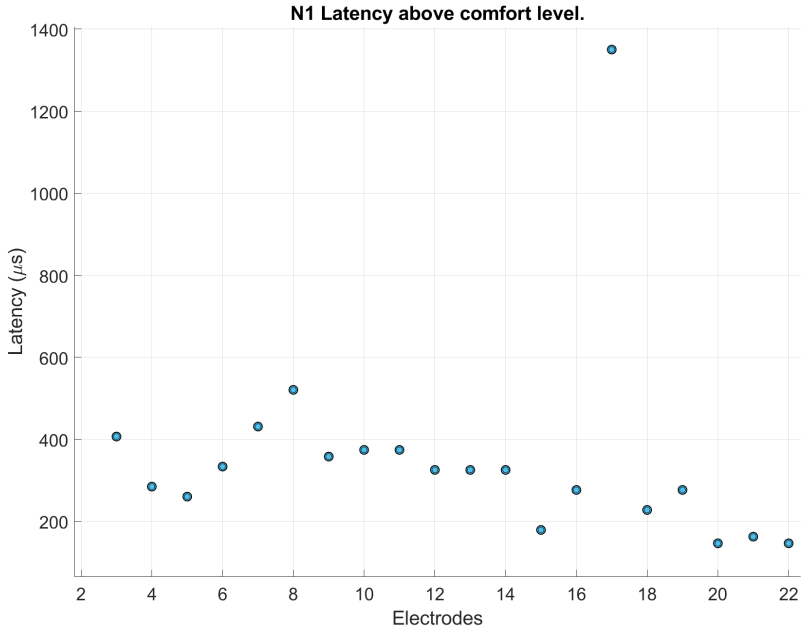


**(a)** N1 Lat

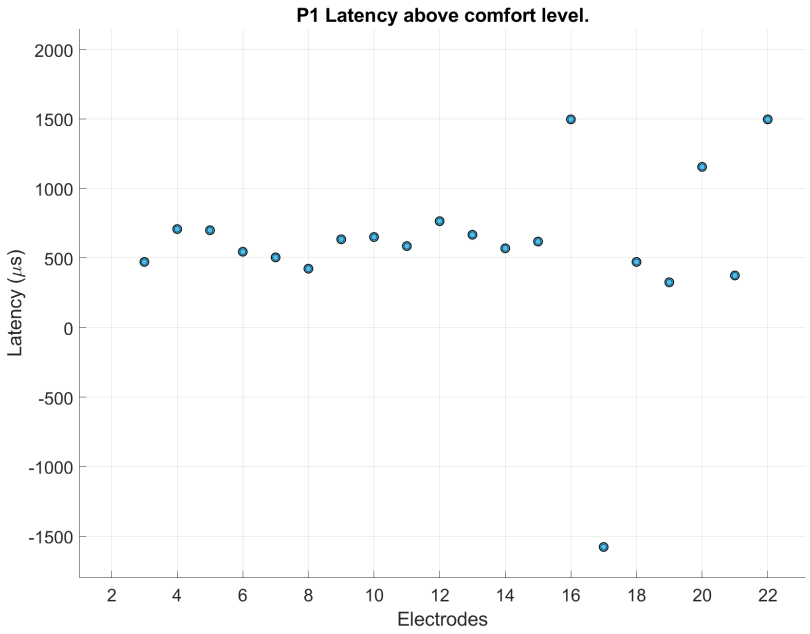


**(b)** P1 Lat

**Figure A.4.** (a) N1 and (b) P1 latency above comfort level.

## A.2 ADDITIONAL EABR MEASUREMENTS

| Trace | ms | µV |
|---|---|---|
| 1L1 | 3.13 | 1.653 |
| 1L2 | 4.33 | 0.908 |
| 1L3 | 4.20 | 0.633 |
| Average | 3.89 | 1.06 |

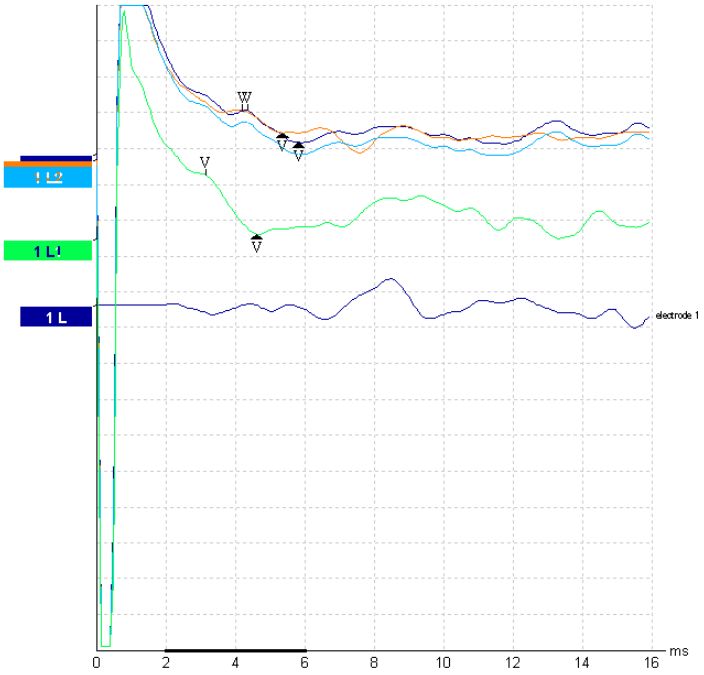


**Figure A.5.** eABR response to stimulation on electrode 1 with the peak values recorded in the table on the left.

| Trace | ms | µV |
|---|---|---|
| 1L | 3.33 | 1.169 |
| 1L1 | 3.80 | 1.001 |
| 1L3 | 2.60 | 8.985 |
| 1L4 | 3.40 | 1.262 |

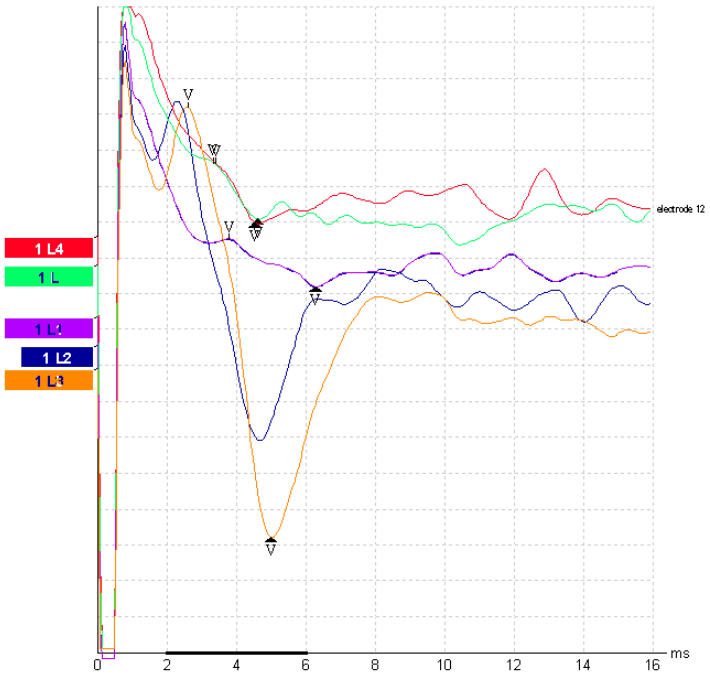


**Figure A.6.** eABR response to stimulation on electrode 12 with the peak values recorded in the table on the left.

| Trace | ms | µV |
|---|---|---|
| 1L | 3.27 | 1.330 |
| 1L1 | 2.47 | 10.82 |
| 1L3 | 3.00 | 1.294 |

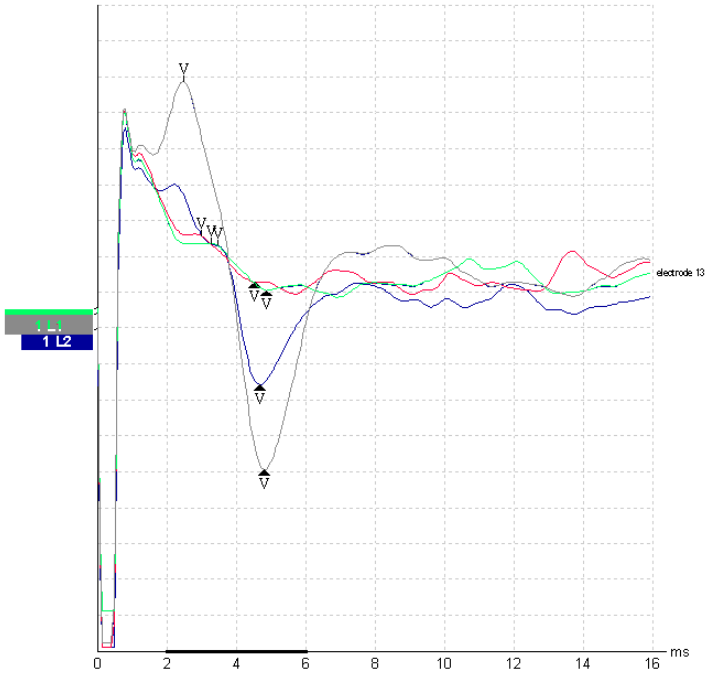


**Figure A.7.** eABR response to stimulation on electrode 13 with the peak values recorded in the table on the left.

| Trace | ms | µV |
|---|---|---|
| 1L1 | 3.53 | 0.743 |
| 1L (Cursor) | 2.53 | 1.502 |

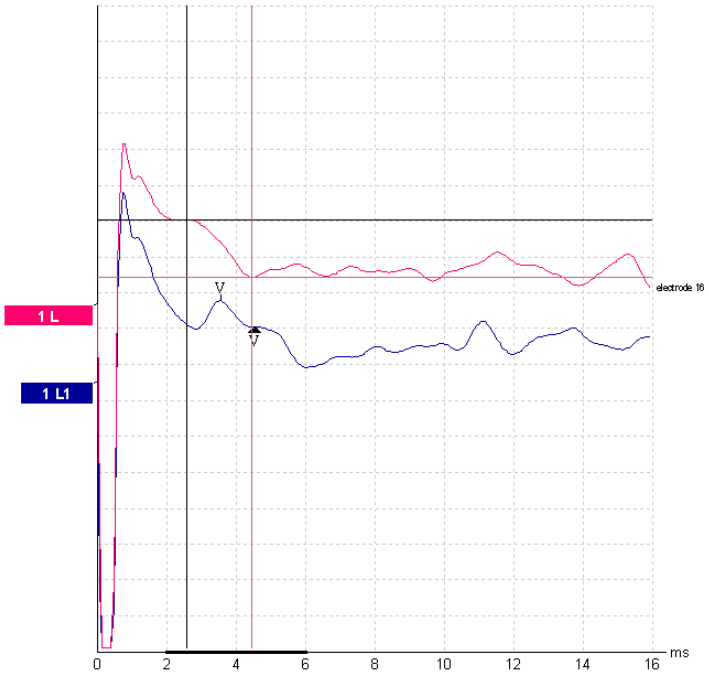


**Figure A.8.** eABR response to stimulation on electrode 16 with the peak values recorded in the table on the left.

| Trace | ms | µV |
|---|---|---|
| 1L | 3.40 | 0.740 |
| 1L1 | 3.47 | 0.892 |

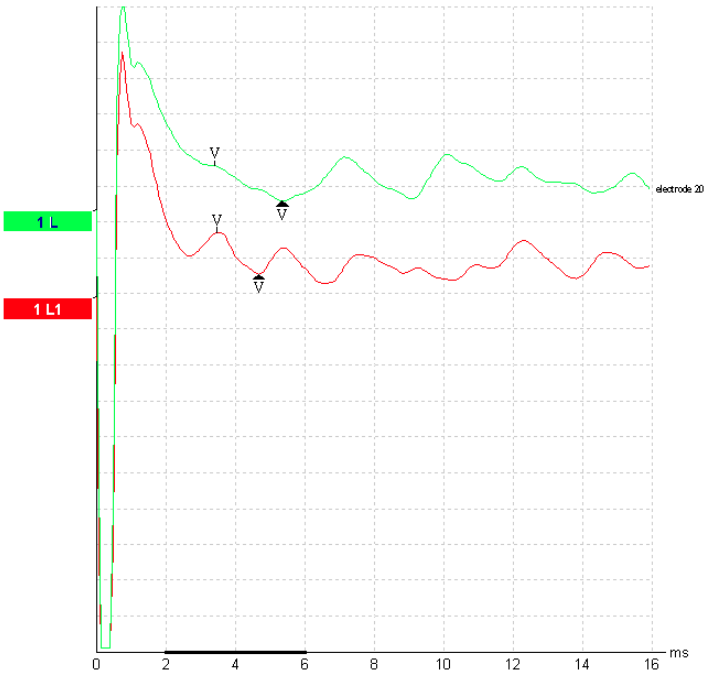


**Figure A.9.** eABR response to stimulation on electrode 20 with the peak values recorded in the table on the left.

| Trace | ms | µV |
|---|---|---|
| 1L | 3.60 | 0.476 |
| 1L3 | 3.13 | 0.982 |

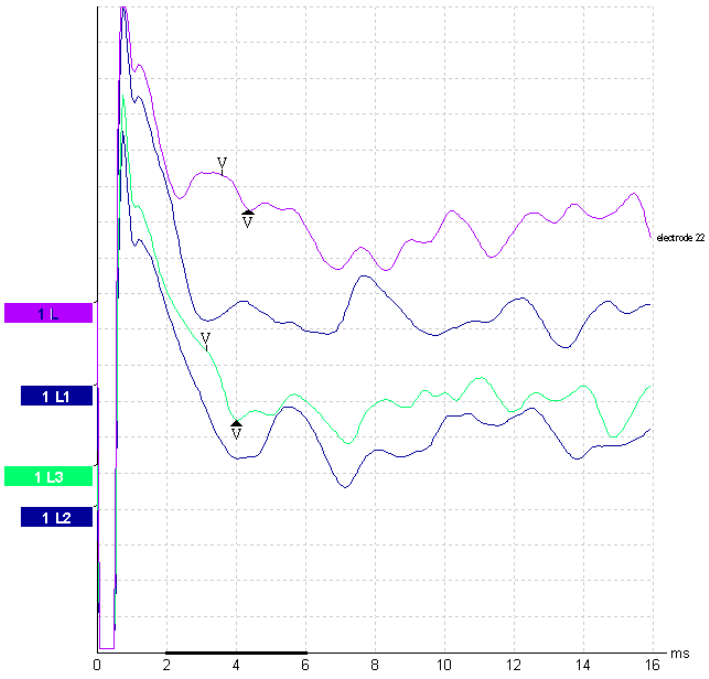


**Figure A.10.** eABR response to stimulation on electrode 22 with the peak values recorded in the table on the left.

### A.3 ADDITIONAL COMPILED ECAP SIMULATION RESULTS

The figures included in this section illustrate the model results of various electrodes, grouped to correlate with the clinically measured eCAPs at singular stimulation levels.

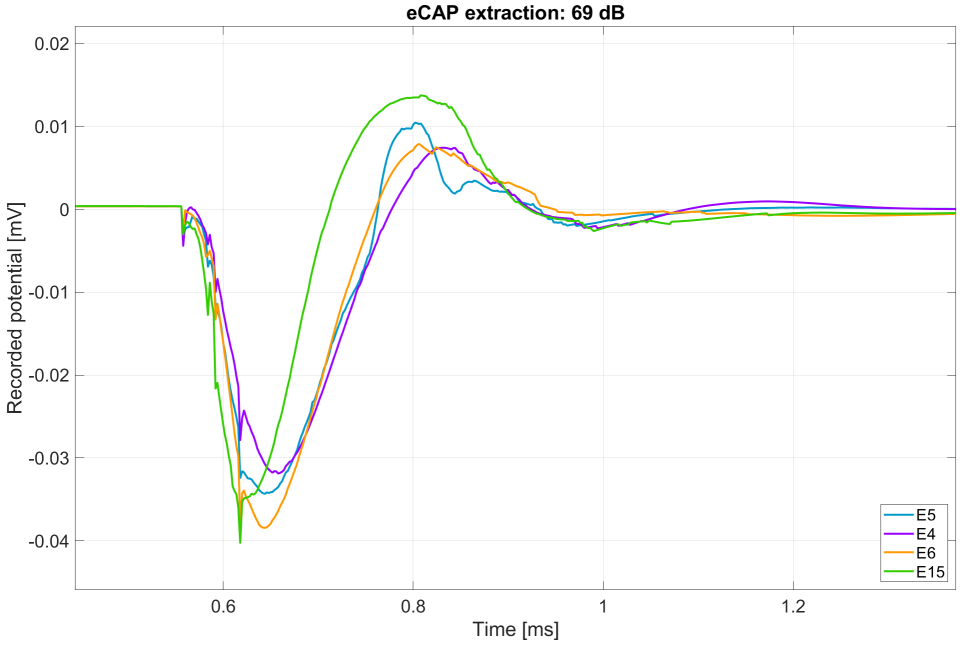


**Figure A.11.** eCAPs of electrodes 4, 5, 6 and 15 with healthy neural population.

The electrodes grouped in figure A.11 are the same as those represented in the figure containing the clinical eCAPs measured at 178 CL.

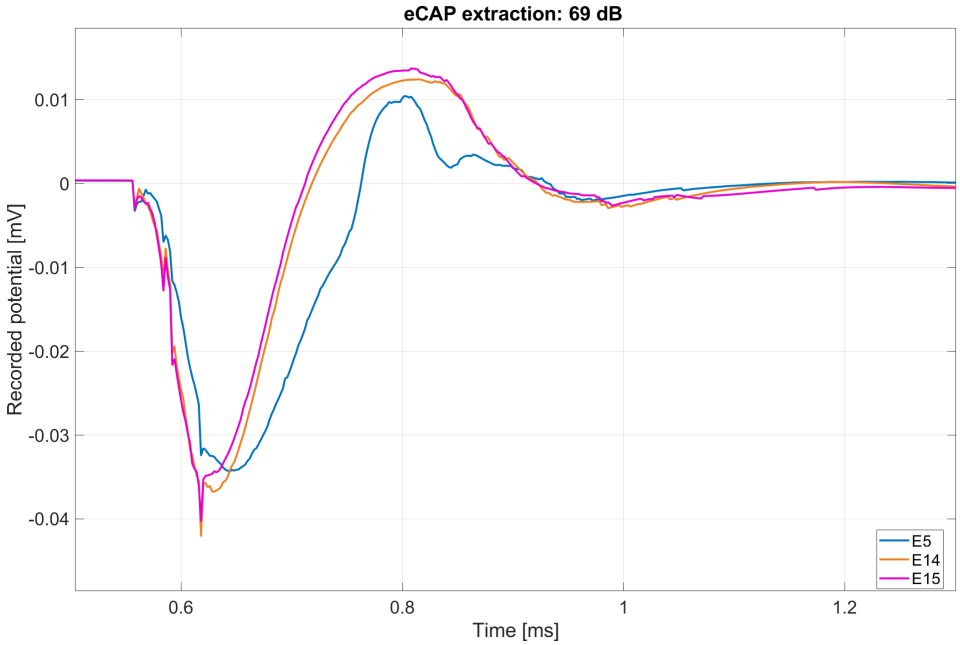


**Figure A.12.** eCAPs of electrodes 5, 14 and 15 with healthy neural population.

The electrodes grouped in figure A.12 are the same as those represented in the figure containing the clinical eCAPs measured at 181 CL.

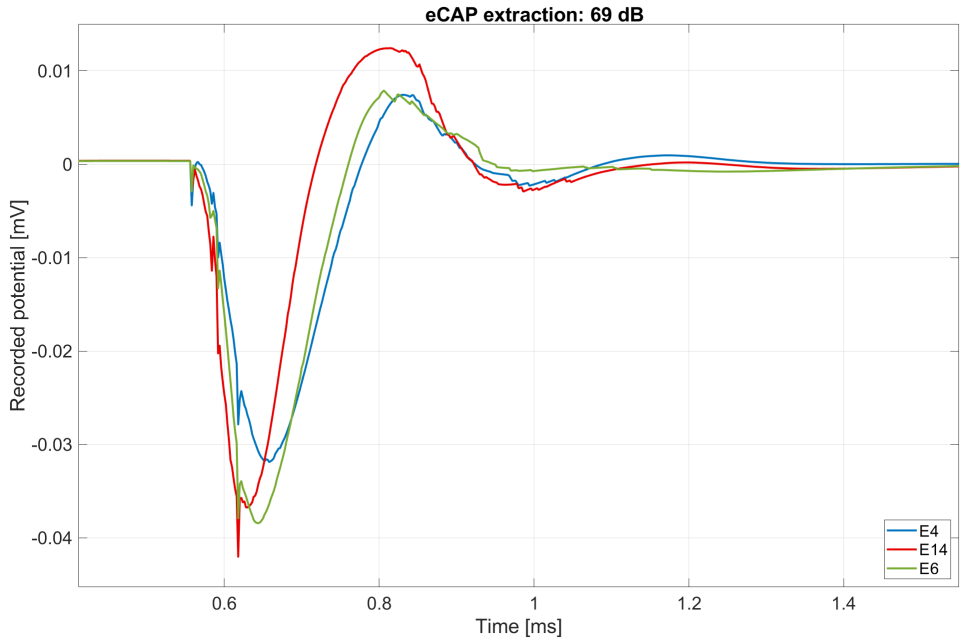


**Figure A.13.** eCAPs of electrodes 4, 6 and 14 with with a healthy neural population.

The electrodes grouped in figure A.13 are the same as those represented in the figure containing the clinical eCAPs measured at 184 CL.

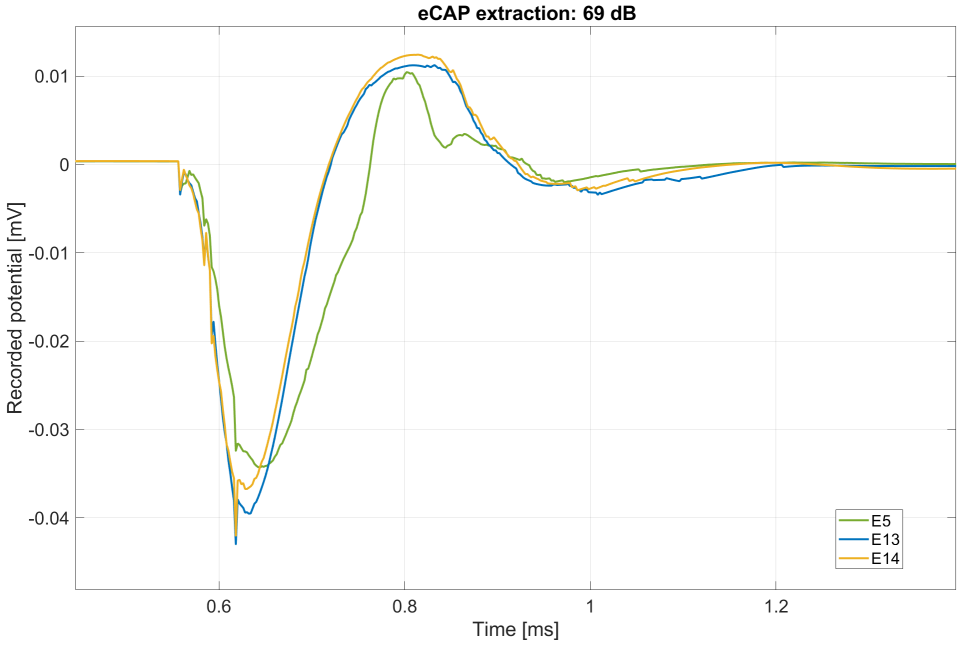


**Figure A.14.** eCAPs of electrodes 5, 13 and 14 with with a healthy neural population.

The electrodes grouped in figure A.14 are the same as those represented in the figure containing the clinical eCAPs measured at 187 CL.

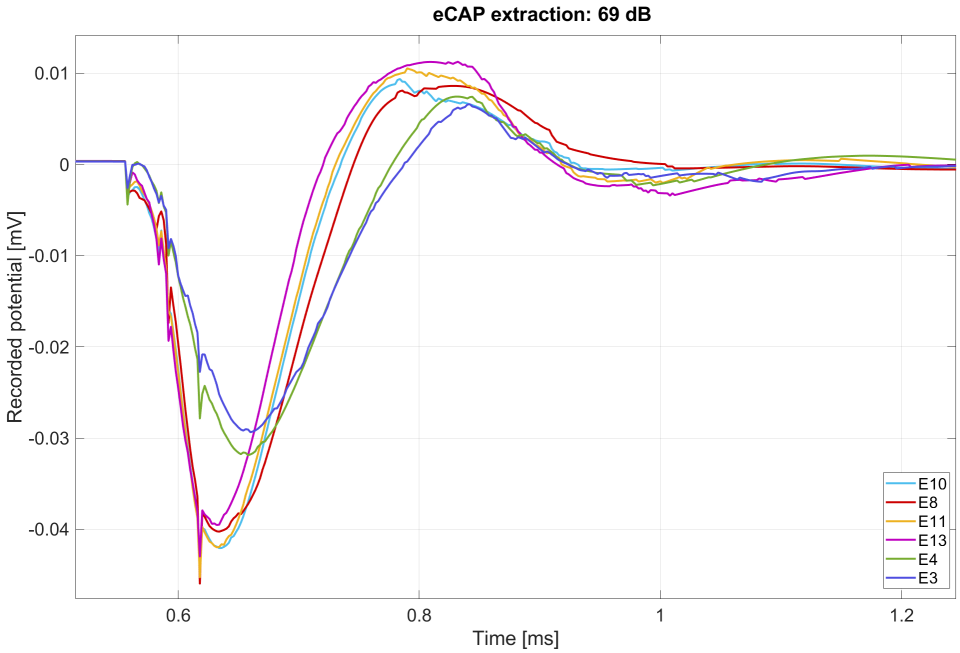


**Figure A.15.** eCAPs of electrodes 3, 4, 8, 10, 11 and 13 with with a healthy neural population.

The electrodes grouped in figure A.15 are the same as those represented in the figure containing the clinical eCAPs measured at 199 CL.

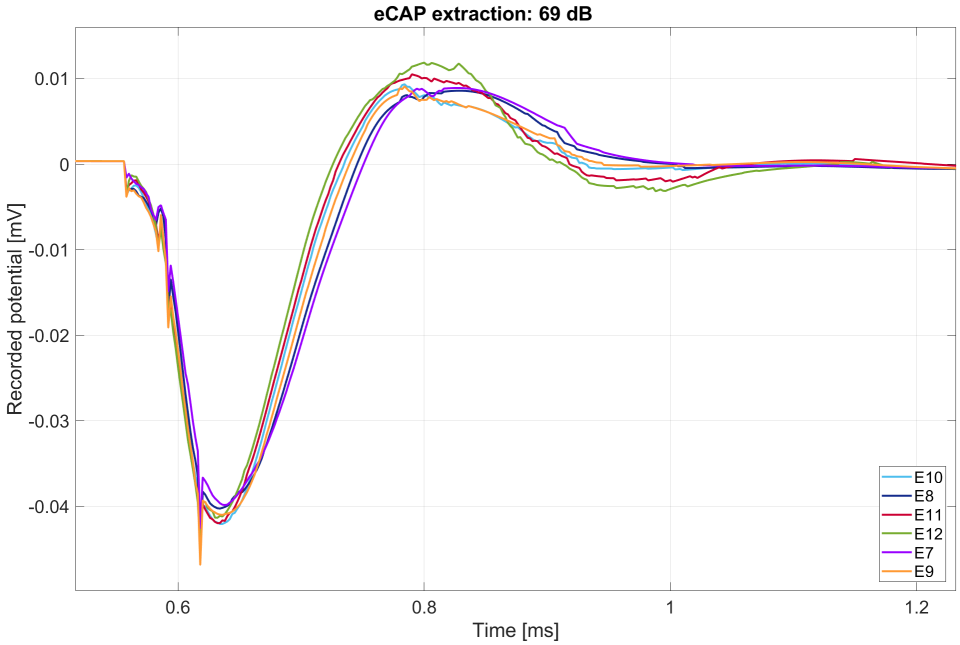


**Figure A.16.** eCAPs of electrodes 7 through 12 with with a healthy neural population.

The electrodes grouped in figure A.16 are the same as those represented in the figure containing the clinical eCAPs measured at 202 CL.

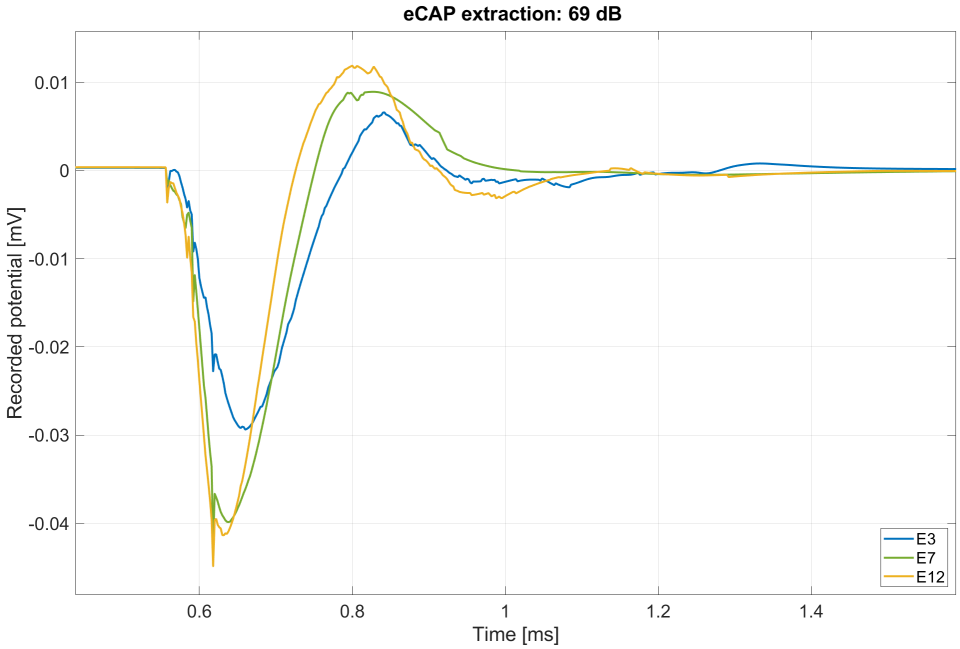


**Figure A.17.** eCAPs of electrodes 3, 7 and 12 with with a healthy neural population.

The electrodes grouped in figure A.17 are the same as those represented in the figure containing the clinical eCAPs measured at 205 CL.

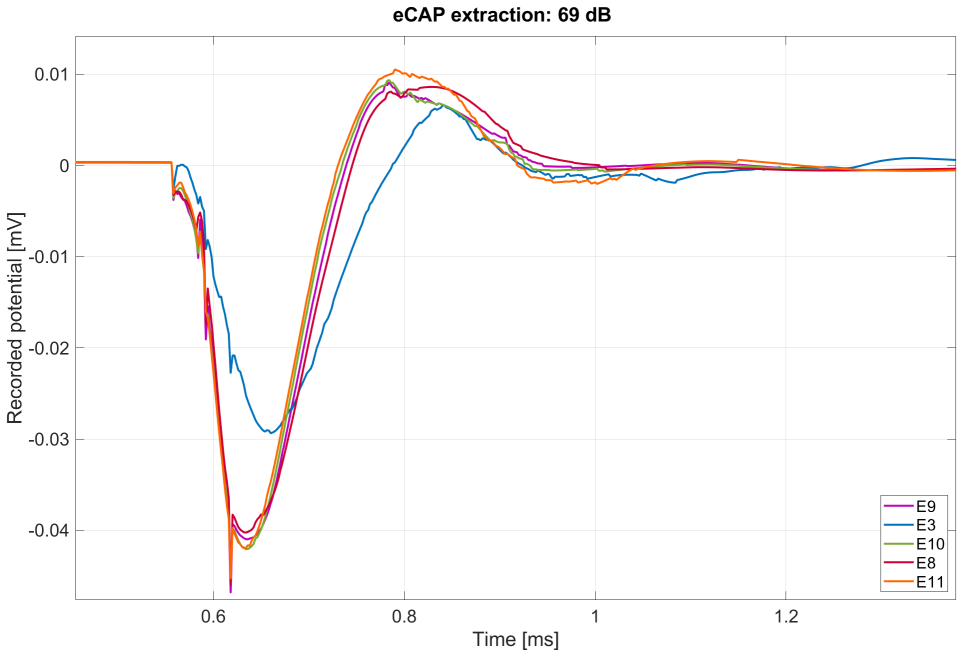


**Figure A.18.** eCAPs of electrodes 3, 8, 9, 10 and 11 with with a healthy neural population.

The electrodes grouped in figure A.18 are the same as those represented in the figure containing the clinical eCAPs measured at 208 CL.

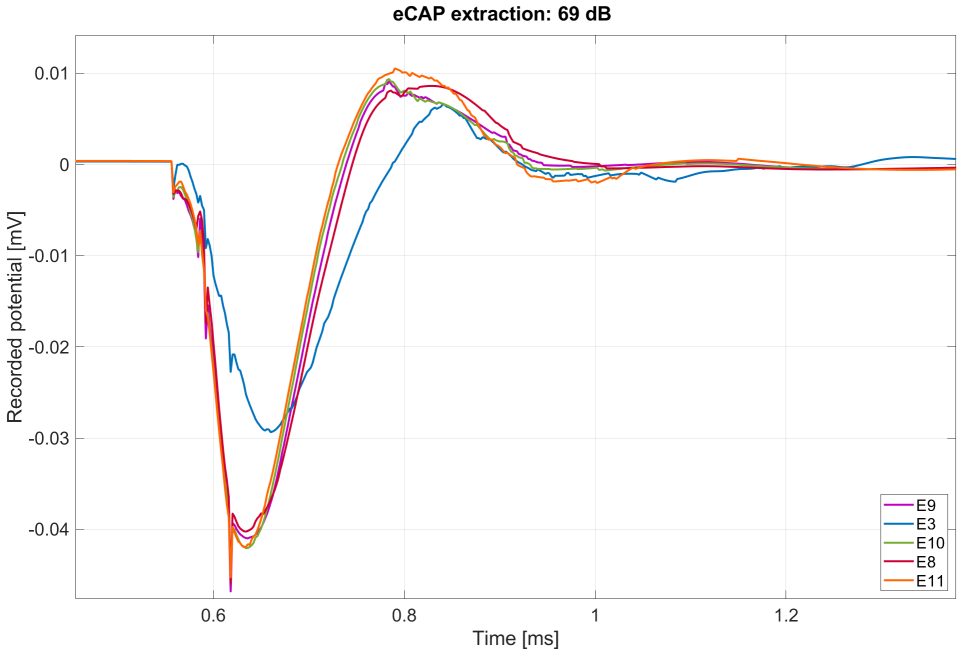


**Figure A.19.** eCAPs of electrodes 3, 8, 9, 10 and 11 with a healthy neural population.

The electrodes grouped in figure A.19 are the same as those represented in the figure containing the clinical eCAPs measured at 211 CL.

## A.4 COMPARISON OF ECAP RESPONSES TO DAMAGED AND HEALTHY NEURAL MODELS USING COMPILED FIGURES

The following figures were chosen for damage simulation because they comprised many eCAP traces for electrodes with damage indicated by the damage profile.

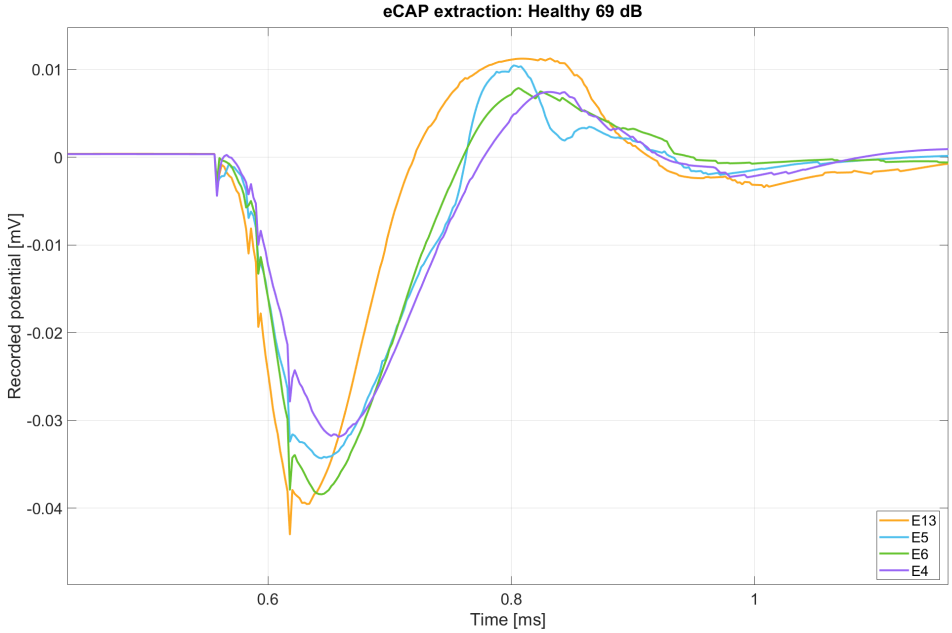


**Figure A.20.** eCAPs of electrodes 4, 5, 6 and 13 with a healthy neural population.

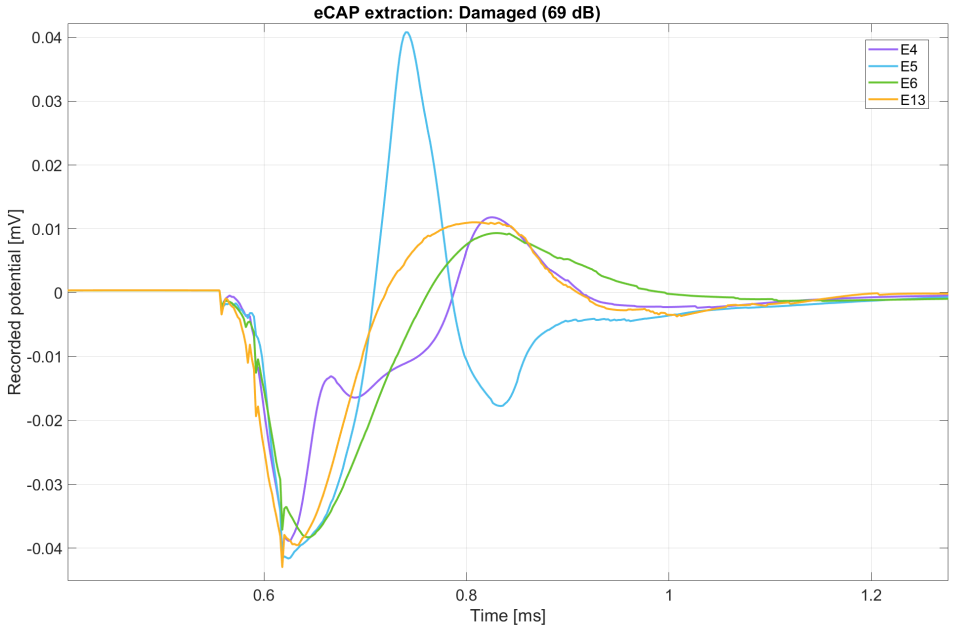


**Figure A.21.** eCAPs of electrodes 4, 5, 6 and 13 with damage applied to neural population.

The electrodes grouped in figures A.21 and A.20 are the same as those represented in the figure containing the clinical eCAPs measured at 190 CL.

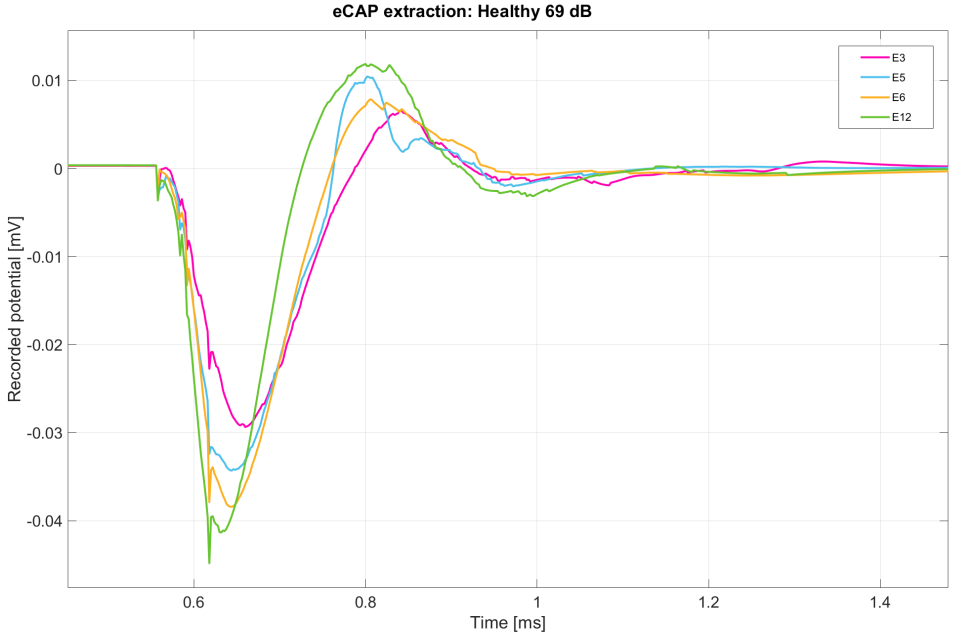


**Figure A.22.** eCAPs of electrodes 3, 5, 6 and 12 with a healthy neural population.

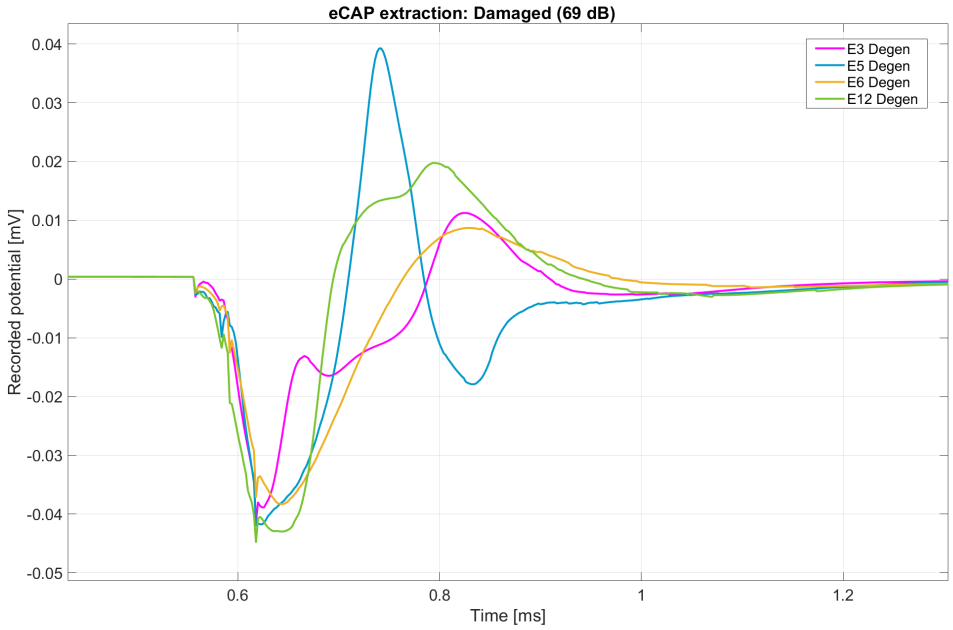


**Figure A.23.** eCAPs of electrodes 3, 5, 6 and 12 with damage applied to neural population.

The electrodes grouped in figures A.23 and A.22 are the same as those represented in the figure containing the clinical eCAPs measured at 193 CL.